DETERMINATION OF THE DENSITY OF LOCALIZED STATES IN WELL CHARACTERIZED THIN FILMS OF HYDROGENATED AMORPHOUS SILICON PREPARED BY GLOW DISCHARGE

BY

DEVI SHANKER MISRA

DEPARTMENT OF PHYSICS
INDIAN INSTITUTE OF TECHNOLOGY, KANPUR

MAY, 1984

DETERMINATION OF THE DENSITY OF LOCALIZED STATES IN WELL CHARACTERIZED THIN FILMS OF HYDROGENATED AMORPHOUS SILICON PREPARED BY GLOW DISCHARGE

A Thesis Submitted
in Partial Fulfilment of the Requirements
for the Degree of

DOCTOR OF PHILOSOPHY

BY

DEVI SHANKER MISRA

to the

DEPARTMENT OF PHYSICS
INDIAN INSTITUTE OF TECHNOLOGY, KANPUR

MAY, 1984

CERTIFICATE

This is to certify that the work presented in this thesis entitled 'DETERMINATION OF THE DENSITY OF LOCALIZED STATES IN WELL CHARACTERIZED THIN FILMS OF HYDROGENATED AMORPHOUS SILICON PREPARED BY GLOW DISCHARGE' by Devi Shanker Misra has been carried out under my supervision and it has not been submitted elsewhere for a degree.

May 1984

S.C. Agarwal
Department of Physics
Indian Institute of Technology
Kanpur, India

ACKNOWLEDGEMENT

It is a great pleasure to express my gratitude to Dr. S.C. Agarwal for his constant encouragement, inspiration and guidance throughout the course of this work. I am also thankful to him for patiently going through this manuscript and his valuable suggestions during the preparation of the manuscript.

My sincere thanks are due to Profs. H. Fritzsche, W. Paul, S. Guha, T.M. Srinivasan, R. Sharan, A. Mansingh and K.L. Bhatia for various helpful discussions at different stages of this work.

I am also thankful to Prof. R.M. Singru, Head, Physics Department, I.I.T. Kanpur and Dr. A.N. Dixit, Head, Physics Department, Christ Church College, Kanpur for encouraging me and taking a keen interest in the progress of my research work.

It is also a great pleasure to thank Drs. R.R. Arya, P.N. Dixit, A. Kumar, V.A. Singh and K.L. Narasimhan for various helpful discussions and suggestions at different stages of this work. I also thank Mr. Shailendra Kumar and Mr. Vijay Kumar for various helpful discussions.

My sincere thanks are due to my friends Drs. A.K. Sinha, Mukul Misra, B.P. Singh, Gyanesh Chandra, Mohd. Rafat and Messrs K.J. Mookerjee, Ajit Mohan, S. Major and G.P. Bagaria

and many others who helped me in more than one ways and made my stay at I.I.T. Kanpur a memorable pleasure.

I am thankful to Mr. J.S. Sharma and his associates in Physics Workshop, Mr. J.N. Sharma and his associates in Glass Blowing Shop and Mr. S.D. Sharma and his associates in Low Temperature Laboratory. I am also thankful to Mr. Sampat Singh and his associates for running Liquid Nitrogen Plant efficiently and providing Liquid Nitrogen to me timely. I thank Mr. R.K. Jain and Mr. K.V. Rajgopalan for running IR spectrophotometer. I also appreciate the services rendered to me by Mr. Beni Prasad of my laboratory.

I thank Mr. K.N. Islam for his excellent meticulous and patientful typing, Mr. B.K. Jain for tracing the figures and Mr. H.K. Panda and L.S. Rathaur for cyclostyling this thesis.

The work carried out here would not have been possible without the emotional support and constant encouragement from my family. I wish to express my profound regards to my parents and my eldest brother.

Devi Shanker Misra

CONTENTS

LIST OF FIGURES

Figure | Page

Figure		Page

Nomenclature of various parts of the dc glow discharge system (ref. Fig. 2.1)

A - Main Cylinder (SiH_4+Ar), B - Auxiliary Cylinder, V - Valve at Main Cylinder, PG - Pressure Gauge, D1-D5 - Diaphragm Valves, N - Needle Valve, S1-S3 - SS Flanges, GT - Glass Tube, H - Heater & Substrate Holder, SU - Substrates, GR - Grid, CP - Ceramic Posts, SH - Shield, HT - High Tension, AL - Anode, TC - Thermocouple, H1 - Heater Current L ads, G - Reaction Chamber, GS1, GS2 - Graded Seals, Q - Quartz U-tube, F - Furnace, T1, T2 - Liq. N_2 Traps, ND1, ND2 - Dewars, MIV - Solenoid Valve, RP - Rotary Pump.

LIST OF TABLES

SYNOPSIS

Devi Shanker Misra
Ph.D.
Department of Physics
Indian Institute of Technology, Kanpur
April 1984

Determination of the Density of Localized States in Well Characterized Thin Films of Hydrogenated Amorphous Silicon Prepared by Glow Discharge.

The discovery by Spear and LeComber that thin films of hydrogenated amorphous silicon (a-Si:H) prepared by glow discharge of silane gas can be doped, has led to an enormous increase in the activity in the area of amorphous semiconductors. The ability to dope, makes a-Si:H an interesting material not only from the devices point of view but also from the point of view of fundamental studies. Among the many useful devices made are the a-Si:H based solar cells, which appear to be very promising towards the development of a low cost alternative source of energy. These technological advances are hampered by problems which require a more complete understanding of the physical processes in this material, before they can be handled. One of the most well known of these is the light induced degradation of a-Si:H observed first by

Staebler and Wronski in 1977. An exposure to sunlight for a few hours changes many major characteristics of a-Si:H including dark conductivity, activation energy and trapping parameters. The effect is reversible upon annealing. Clearly, as a first step towards tackling such problems, a knowledge of the electronic structure of a-Si:H is necessary. Fortunately, such studies which are of fundamental interest to physicists, have been more fruitful on a-Si:H than the other amorphous semiconductors. Consequently, a large number of attempts have been made to obtain the distribution of localized states in a-Si:H.

Spear and his collaborators were the first to report the distribution of the density of localized states (DOS) in a-Si:H. Using field effect measurements, they found about 10^{16} - 10^{17} eV^{-1} cm^{-3} states near the Fermi level (E_F) in undoped a-Si:H. The results show that the DOS increases as one moves towards either of the mobility edges. They also observed a structure in DOS in the form of two peaks, one at 0.4 eV and other 1.2 eV below E_C. Since then, many attempts have been made to detect these peaks by this and other methods but their presence is as yet to be fully confirmed.

Space charge limited currents (SCLC), steady state capacitance measurements as a function of bias, C(V),

frequency, $C(\omega)$, temperature, C(T) and isothermal capacitance transient spectroscopy (ICTS) have been done on a-Si:H Schottky diodes by different groups. Steady state and transient photoconductivity and deep level transient spectroscopy (DLTS) have also been done to obtain the DOS in a-Si:H. However, the DOS obtained by different methods do not quite agree with each other. For example, using DLTS the DOS in doped a-Si:H are found to be about 1-2 order of magnitude smaller than those obtained by the field effect. Results also show a minimum in DOS at $\sim$ 0.45 eV. Interestingly this is also the position where Spear and LeComber obtain a peak in undoped a-Si:H.

Thermally stimulated currents (TSC) have also been measured in a-Si:H to determine DOS and often show pronounced structures.

In order to deduce DOS from the data of various measurements, several simplifying assumptions have to be made. For example, an assumption which is common to all the analyses is that the material is homogeneous. However, there is evidence to show that the material is actually heterogeneous on a small scale. Similarly, although the presence of surface states is not likely to affect the transient measurements, their neglect in the analysis of field effect and steady state capacitance data might lead

to discrepancies. Moreover, it may not be justified to compare the results on doped a-Si:H with those on the undoped material since the doping may change the DOS. Thus, there is a possibility that the different assumptions involved in the analyses of various experiments might be responsible for the differences in DOS. This can be verified by doing several different measurements on a given sample of a-Si:H and comparing the DOS obtained. One of the objectives of the present work is to measure DOS in a-Si:H by several methods and to find out whether it is the assumptions involved in the analyses or the differences in the samples which give rise to these discrepancies in DOS.

A glow discharge system is designed and fabricated and thin films of a-Si:H are prepared (Chapter 2). These are characterized electrically, optically and structurally and are highly photoconducting. The Staebler-Wronski effect is found to be small. Using Pd as the contact, Schottky barriers are fabricated and characterized. They show a good rectification ratio ($\sim$1000 at 1.0 V), barrier height ($\phi_B \simeq 0.8 - 0.95$ eV) and ideality factor ($n \simeq 1.2 - 1.35$).

Chapter 3 presents the DOS calculated by doing SCLC, C(V), C(ω), C(T) and ICTS measurements on these Schottky diodes. The DOS obtained from different methods are found to be in agreement with each other ($g(E_F) \sim 10^{16} - 10^{17}$ eV^{-1}cm^{-3})

CHAPTER 1

INTRODUCTION

Among the many amorphous semiconductors, hydrogenated amorphous silicon (a-Si:H) prepared by the glow discharge of the silane (SiH_4) gas is one of the most widely studied material.[1,2,3] It is one of the few amorphous materials which, when prepared under suitable preparation conditions (e.g., high substrate temperature (T_s)), can be efficiently doped[4,5] n(p) type by mixing a suitable dopant PH_3(B_2H_6) to SiH_4 (see Fig. 1.1). The doping is possible because it has a smaller density of localized states in the band gap than the other amorphous materials. It is now well recognized on the basis of the evidence provided by IR spectroscopy[6,7], nuclear experiments,[8,9,10] hydrogen evolution[8,11,12] and electron spin resonance (ESR)[13,14] that a-Si:H owes this remarkable property to the presence of hydrogen in its network. Hydrogen, not only reduces the density of states by compensating the dangling bonds but also modifies the structure possibly leading to strain relieved internal surfaces as hypothesized by Phillips.[15]

The possibility of doping has removed one of the main limitations of amorphous semiconductors and opened up an exciting new field for fundamental studies and applied developments in this material. As a result, a large number of electronic, opto-electronic and photovoltaic devices have

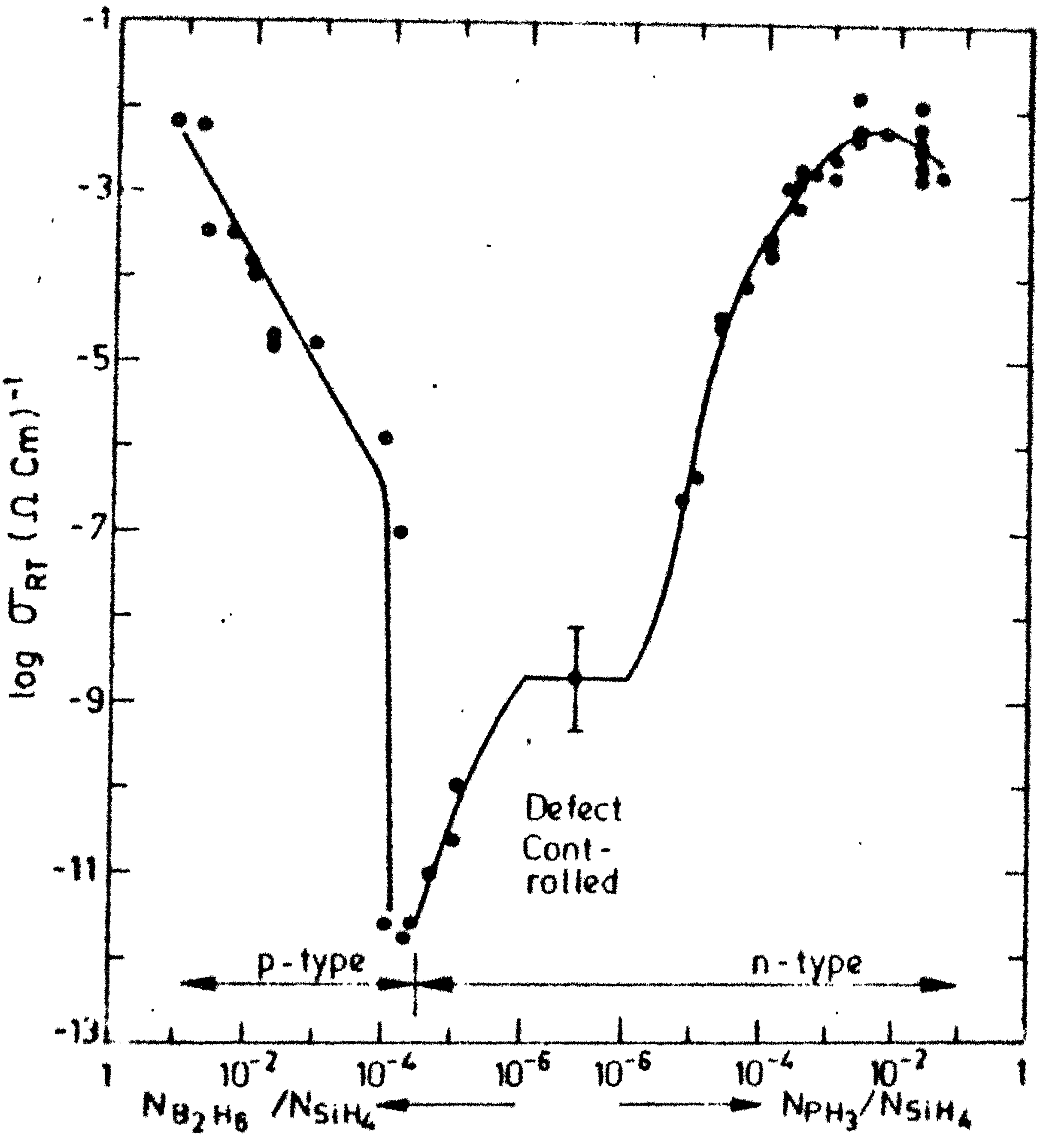

Fig.1.1 : Room temperature conductivity (σ_{dc}(300 K)) of n- and p-type amorphous Si specimens plotted as a function gaseous impurity ratio. It may be noticed that (300 K) changes by several orders of magnitude for a few parts per million impurities (ref. 4 and 5).

been fabricated using a-Si:H as the basic material.[16-24] However, these technological advances are hampered by problems which require a more complete understanding of the physics of the material. One of the most well known is the light induced changes in a-Si:H, observed by Staebler and Wronski in 1977.[25] They observed that the dark conductivity of the material decreases by several orders of magnitude when it is exposed to sun-light for a few hours. The sample returns to its original state after annealing in dark. Subsequently, a large number of studies have been done to identify the origin of this effect and it is found that the effect influences many major characteristics of a-Si:H.[26] To understand the nature of this effect and also for the improvement of the devices a detailed knowledge of the electronic structure is necessary. Therefore, several studies have been undertaken to obtain the density and distribution of localized states (DOS) in the mobility gap of a-Si:H.[1,2,27]

Spear and LeComber reported[28] the first results on the DOS in a-Si:H. They used a field effect experiment in which the Fermi level is moved by application of a high electric field through a gate insulator. The resulting change in the conductivity of the material measured using two ohmic contacts, is interpreted to obtain the DOS in the mobility gap. The DOS obtained by Spear and LeComber

is shown in Fig. 1.2. It shows a much smaller DOS ($\approx 10^{17}$ eV^{-1} cm^{-3}) near Fermi level (E_F) than the evaporated one (dashed line Fig. 1.2) which is $\approx 10^{20}$ $eV^{-1} cm^{-3}$. It is interesting to note that because of this high DOS in evaporated films (a-Si), one does not get much of a field effect. Thus, the DOS data for a-Si in Fig. 1.2 is only a lower estimate of DOS.

This method has since been used by several other authors[29,30] and gives about 10^{16} - 10^{17} eV^{-1} cm^{-3} states in undoped a-Si:H near Fermi level. The details of distribution obtained by them, however, differ. The Dundee[28] group, for example, finds two peaks in the DOS distribution (one at 0.4 eV and other 1.2 eV below the conduction band edge), which are not observed by others.[29,30] Further since the field effect measurements might be affected by the surface states, one is not sure that the DOS obtained, represent the bulk. Indeed, Goodman and Fritzsche[29] have argued that this may be quite significant, since in the field effect experiment, the current flows in a narrow channel of 50 - 100 A° width of the material adjacent to the gate. Further, the effect of strctural and compositional inhomogeneities on this narrow current path should also be considered. This will be particularly important if the grain boundaries at the interface act as potential barriers.[1] Also, the layers of a-Si:H near the interface may, in reality, be quite different from the bulk, since they are grown on

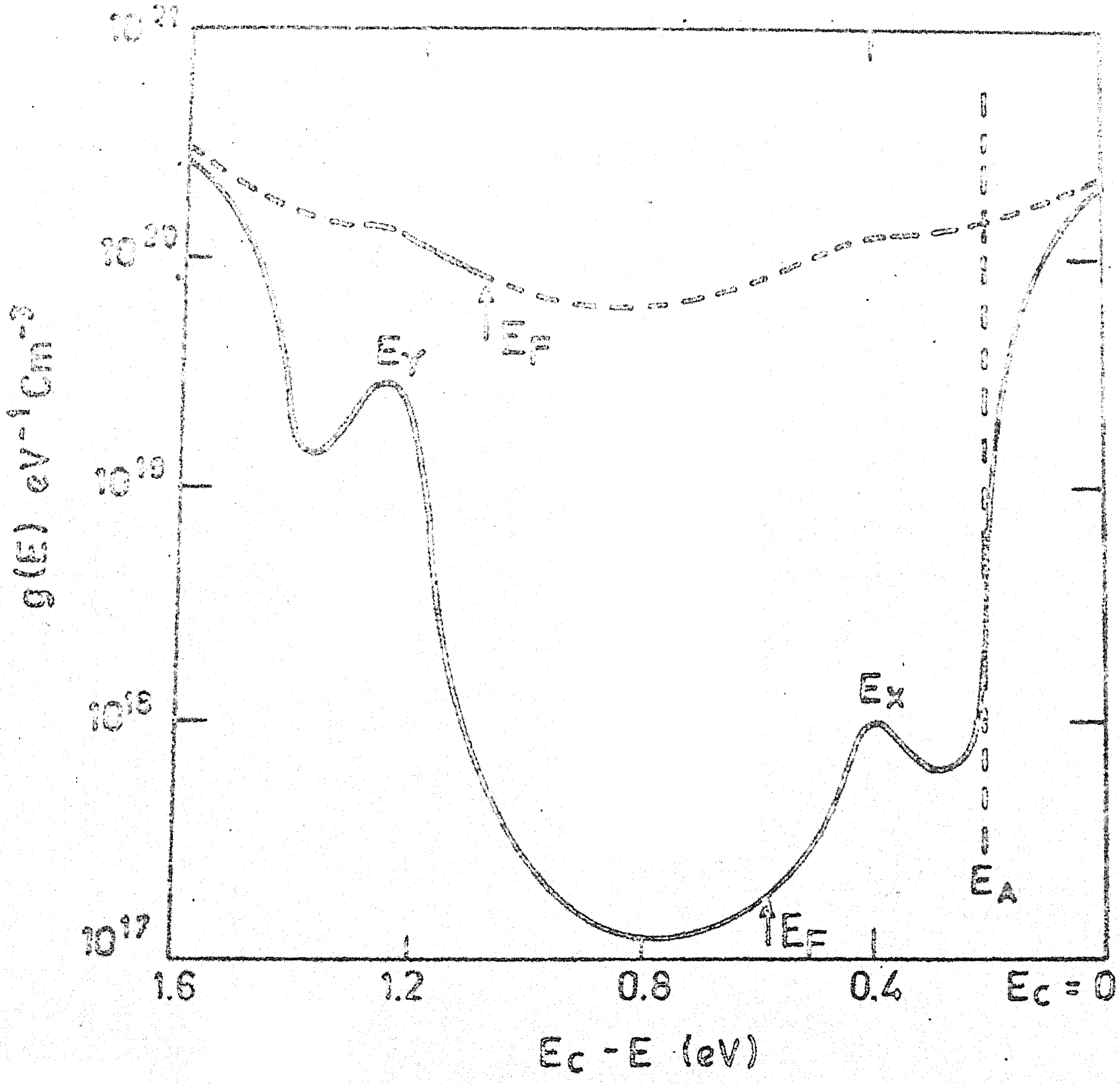

Fig. 1.? : Density of state distributions (DOS) for a-Si specimens obtained by Spear's group using field effect technique (ref. 28). Solid curve is DOS of a-Si:H sample prepared at T_s ~ 520 K and dashed curve is DOS for an evaporated Si sample. In evaporated Si sample the measurements could only be done in a small range of energy (solid portion of the dashed curve). DOS of a-Si:H sample shows two peaks; one at E_X (~ 0.4 eV below E_c) and other at E_Y (1.2 eV below E_c).

an insulator rather than the growing a-Si:H layers.[1] Although, Guha et al[31] report that the field effect on their specimen measured after heat drying, is the same at the top and the bottom surface, there is considerable evidence that at least in some cases, the surface and interface dominate the apparent bulk properties of a-Si.[32-34]

Apart from the neglect of the interface states, the analysis of the field effect data suffers from other uncertainties as well. For example, to calculate the DOS, one needs to know the field voltage at which the bands become flat. Although Weisfield and Anderson[35] have suggested a method of determining this flat band voltage (V_{FB}) from the temperature dependence of the field effect response, they assume that the band bending at the interface is independent of temperature, which may not be true. Thus the choice of V_{FB} remains rather arbitrary and may lead to errors in the calculated DOS. Further, the analysis of field effect is based on the assumption that the mobility edge follows the potential V(x) upto the surface. This implies that all the states are shifted by V(x) without any change in their localization and mobility. This may not be justified.[1]

Thus one has to look for other independent experiments to assess the extent to which the DOS obtained by the field effect experiment should be relied upon. Several workers have obtained the DOS from the measurements of steady state capacitance and conductance on a-Si:H Schottky diodes.[30,36-43]

These do not always agree with the DOS obtained from the field effect. But due to a lack of detailed theoretical understanding of the barriers, these DOS also can not be trusted fully. Besides, one neglects the surface states and structural heterogeneities and is thus open to a criticism similar to that of field effect, in this regard.

Lang et al have used the deep level transient spectroscopy (DLTS) to obtain the DOS in doped a-Si:H.[39,44] In this technique, the difference in capacitance of a Schottky diode or p-n junction is measured, at two suitable time intervals, after excitation with a light or voltage pulse, as the temperature is continuously raised.[45] This gives the dynamic response of the junction space charge region. The results show a minimum in DOS which is one to two orders of magnitude smaller than the minimum obtained by other methods. Further, the minimum in the doped samples occurs at $\approx$ 0.45 eV below the conduction band. Interestingly, this is the position where Spear and LeComber[28] report a peak in the DOS in the undoped samples. Lang et al[39] have argued that since the DLTS is not sensitive to the surface states, their results represent the true bulk DOS in a-Si:H. However, in their analysis also, the structural inhomogeneities are ignored. Although, the discrepancy is not yet fully resolved, it may be related to the fact that the doping can alter the DOS significantly. Since DLTS experiments on undoped samples are difficult to perform, this question might not be easily

answered. However, the steady state capacitance measurements by Lang et al[39], on an undoped sample, also give a DOS at the Fermi level which is much smaller than reported by others.

More recently, the space charge limited currents (SCLC) have been used to obtain the DOS in a-Si:H.[46-49] This met od has the advantage that it is not influenced by the surface states.[46] The DOS, obtained by the analysis of SCLC is usually smaller by a factor of 3 to 5 as compared to that obtained by the field effect. This has been taken to be an evidence for the contribution of the surface states in the field effect experiment.[46] But here again, one assumes that the material is homogeneous, and that the DOS does not change from place to place in the sample.

Isothermal capacitance transient spectroscopy (ICTS) has also been applied to obtain, the DOS in a-Si:H.[50] In this method, a Schottky diode or a p-n junction is used. The occupancy of the gap states is perturbed by either applying a voltage pulse or shining band gap light. After the excitation is put off, the junction capacitance is measured as a function of time, at a constant temperature. This ICTS signal is exploited to get the DOS in the gap. Using this method on samples of a-Si:H doped by different levels of P, Okushi et al[50] concluded that the DOS distribution is altered by doping. Although this method is free from the influence of surface states, the heterogeneities are neglected.

The thermally stimulated currents (TSC) technique which is very useful in obtaining information about the density and parameters of traps in crystalline semiconductors[51] has recently been applied in a-Si:H.[52-56] The TSC measurements are done in coplanar samples of a-Si:H as well as on the Schottky diodes and often show pronounced structures. However, the deduction of DOS by these results is often difficult due to (i) the presence of continuous distribution of traps (ii) a lack of detailed knowledge of recombination kinetics, in a-Si:H. Moreover, the effects of surface states and structural heterogeneities are neglected here also.

Steady state and transient photoconductivity measurements have also been done in a-Si:H to obtain the DOS[57] and it has been shown that the results can be fitted to a DOS with sum of two exponentials without any structure. Again, the surface states and the structural heterogeneities of the material are neglected in this analysis, as well.

Besides the methods described above, there are other measurements from which the DOS has been deduced, e.g., Transient current spectroscopy (TCUR)[58], Transient voltage spectroscopy[59] etc. However, for the discussion of these, we refer the interested reader to the relevant papers in the recent proceedings of the 10th International Conference on Amorphous and Liquid Semiconductors.[48] Clearly, the DOS obtained by different workers, by different methods, do not quite agree with each other. Since, in order to extract the

DOS distribution from experiments, some simplyfying assumptions have to be made, which may not be the same for all the experiments and it is possible that these are responsible for this disagreement. Alternatively, a-Si:H prepared in different laboratories might, indeed, have quantitatively different DOS, which might explain the discrepancy. With an object to decide between the two alternatives and to remove inconsistencies in DOS, various measurement techniques have been used to determine the DOS in well characterized thin films of a-Si:H prepared by dc glow discharge of SiH_4. The content of the chapters are discussed below.

Chapter 2 contains details of dc glow discharge system used for preparation of thin films of a-Si:H. The results of structural and electrical characterizations are also discussed.

The results of DOS, estimated in thin films of a-Si:H, by measuring steady state capacitance as a function of bias, C(V), frequency, $C(\omega)$, and temperature, C(T), on a-Si:H/Pd Schottky diodes are presented in Chapter 3. These are compared with the DOS obtained from Space Charge Limited Currents (SCLC) and Isothermal Capacitance Transient Spectroscopy (ICTS) on the same diodes. The assumptions used in deducing the DOS from each of the measurements have also been spelled out and the limitations pointed out.

Since, the capacitance measurements give DOS only in a small range of energy near E_F, the thermally stimulated

currents (TSC) are measured in thin films of a-Si:H to ascertain and find out structures in DOS, if any. Also, by TSC measurements, the DOS at certain energies in the band gap are estimated. These results are discussed in Chapter 4. A model, to account for the low temperature TSC peak in a-Si:H is also proposed.

The results of DOS obtained from the low temperature photoconductivity measurements on thin films of a-Si:H are presented and discussed in Chapter 5.

Finally, the results of various measurements are compared with each other, as well as with the results obtained by others, in Chapter 6.

REFERENCES

1. H. Fritzsche, Solar Energy Mater. 3 (1980) 447

2. W. Paul and D.A. Anderson, Solar Energy Mater. 5 (1981) 229

3. D.E. Carlson, Solar Energy Mater. 3 (1980) 503

4. W.E. Spear and P.G. LeComber, Solid State Commun. 17 (1975) 1193

5. W.E. Spear and P.G. LeComber, Phil. Mag. 33 (1976) 935

6. J.C. Knights, Jap. J. Appl. Phys. 18 (1979) 101; J.C.Knights and R.A. Lujan, Appl. Phys. Lett. 35 (1979) 244; J.C.Knights, J. Non Cryst. Solids 35,36 (1980) 159; J.C. Knights, Solar Cells 2 (1980) 409

7. C.C. Tsai and H. Fritzsche, Solar Energy Mater. 1 (1979) 29

8. M.H. Brodsky, M.A. Frisch, J.F. Jiegler and W.A. Lanford, Appl. Phys. Lett. 30 (1977) 561

9. W.A. Lanford, H.P. Trautvetter, J.F. Ziegler and J. Keller, Appl. Phys. Lett. 28 (1976) 566

10. M. Milleville, W. Fuhs, F.J. Demond, H. Mannsperger, G. Muller and S. Kalbitzer, Appl. Phys. Lett. 34 (1979) 173

11. A. Triska, D. Dennison and H. Fritzsche, Bull. Am. Phys. Soc. 20 (1975) 392

12. D.K. Biegelson, R.A. Street, C.C. Tsai and J.C. Knights, Phys. Rev. B20 (1979) 4839

13. R.A. Street, J.C. Knights and D.K. Biegelson, Phys. Rev. B 18 (1978) 1880

14. R.A. Street, D. Biegelson and J. Stuke, Phil. Mag. B 40 (1979) 451

15. J.C. Phillips, Phys. Rev. Lett. 42 (1979) 1151

16. K. Muraso, T. Tomata, Masahira Sakaue and T. Ogano, J. Non Cryst. Solids 59,60 (1983) 1211

17. S. Kodato, S. Nishida, M. Konagai and K. Takahasi, J. Non Cryst. Solids 59,60 (1983) 1207

18. S. Konako, F. Okumura, H. Uchida, M. Kanamori, M. Sakamoto, T. Itamo, U. Kajwara and T. Saito, J. Non Cryst. Solids 59,60 (1983) 1227

19. D.E. Carlson and C.R. Wronski, Appl. Phys. Lett. 28 (1976) 671

20. D.E. Carlson, IEEE Trans., Electron Devices 24 (1977) 449

21. H. Okamoto, Y. Nitta, T. Adachi and Y. Hamakawa, Surf. Sci. 86 (1979) 486

22. Y. Kuwano, T. Imai, M. Ohnishi, S. Nakano and T. Fakatsu, Jap. J. Appl. Phys. 19 (1980) 137

23. Y. Hamakawa, H. Okamoto and Y. Nitta, Appl. Phys. Lett. 35 (1979) 187

24. Y. Hamakawa, Thin Solid Films 108 (1983) 301

25. D.L. Staebler and C.R. Wronski, Appl. Phys. Lett. 31 (1977) 292; D.L. Staebler and C.R. Wronski, J. Appl. Phys. 51 (1980) 3262

26. For a recent review see, D. Adler, Solar Cells 9 (1983) 133

27. For a review of recent studies, J. Non Cryst. Solids 59,60 (1980)

28. W.E. Spear and P.G. LeComber, J. Non. Cryst. Solids, 8-10 (1972) 727; A. Madan, P.G. LeComber and W.E. Spear, J. Non Cryst. Solids 20 (1976) 239

29. Nancy. B. Goodman and H. Fritzsche, Phil. Mag. B42 (1980) 149

30. M. Hirose, T. Suzuki and G.H. Döhler, Appl. Phys. Lett. 34 (1979) 234

31. S. Guha, K.L. Narasimhan, R.V. Navkhandewala and S.M. Pietruszko, Appl. Phys. Lett. 37 (1980) 572

32. I. Solomon, T. Dietl and D. Kaplan, J. Phys. (Paris), 39 (1978) 1241

33. D.G. Ast and M.H. Brodsky, J. Non Cryst. Solids, 35,36 (1980) 611

34. M.H. Tanielian, M. Chatani, H. Fritzsche, V. Smid and P.D. Persans, J. Non Cryst. Solids 35,36 (1980) 576

35. R.L. Weisfield and D.A. Anderson, Phil. Mag. B44 (1981) 83

36. P. Viktorovitch and D. Jousse, J. Non Cryst. Solids 35,36 (1980) 569

37. P. Viktorovitch and G.Moddel, J. Appl. Phys. 51 (1980) 4847

38. P. Viktorovich, J. Appl. Phys. 52 (1981) 1392

39. D.V. Lang, J.D. Cohen and J.P. Harbison, Phys. Rev. 25 (1982) 5285

40. J. Beichler, W. Fuhs, H. Mell and H.M. Welsch, J. Non Cryst. Solids, 35,36 (1980) 537

41. I. Balberg, J.J. Hanak, H.A. Wiekliem and E. Gal, J. Phys. (Paris), 42 (1981) C4-459

42. A. Glade, W. Fuhs and H. Mell, J. Non Cryst. Solids, 59,60 (1983) 269

43. I. Balberg, E. Gal and B. Pratt. J. Non Cryst. Solids, 59,60 (1983) 277

44. J.D. Cohen, D.V. Lang, J.P. Harbison and A.M. Sergest, J. Phys. (Paris), 42 (1981) C4-371

45. D.V. Lang in Thermally Stimulated Relaxation in Solids, Topics in Appl. Phys. Ser. 37 ed. P. Braunlich, Springer Verlag, Heidelberg, 1979

46. K.D. Mackenzie, P.G. LeComber and W.E. Spear, Phil. Mag. 46 (1982) 377

47. W. denBoer, J. Phys. (Paris), 42 (1981) C4-451

48. E. Bhattacharya, S. Guha, K.V. Krishna and D.R. Bapat, J. Appl. Phys. 53 (1982) 6285

49. S. Ashok, A. Lester and S.J. Fonash, IEEE, Electron Dev. Lett. EDL-1 (1980) 200

50. H. Okushi, Y. Tokumaru, S. Yamasaki, H. Oheda and K. Tanaka, J. Phys. (Paris) 42 (1981) C4-613

51. Thermally Stimulated Relaxation in Solids, Topics in Appl. Phys. Series 37 ed. P. Braunlich, (Springer, Heidelberg, 1979)

52. W. Fuhs and H. Milleville, Phys. Stat. Sol. (b) 98 (1980) K29

53. A. Chenevas-Paule and J. Dijon, J. Phys. (Paris) 42 (1981) C4-605

54. M. Yamaguchi, J. Non Cryst. Solids 59,60 (1983) 425

55. N. Ibaraki and H. Fritzsche, Int. Topical Conf. on Transport and Defects in Amorphous Semiconductors, 22-24 March 1984, Bloomfield Hills, MI

56. D.S. Misra, A. Kumar and S.C. Agarwal (Accepted in Phil. Mag.)

57. C.Y. Huang, S. Guha and S.J. Hudgens, Phys. Rev. B27 (1983) 7460

58. J. Beichler, H. Mell and K. Weber, J. Non Cryst Solids 59,60 (1983) 257

59. N.M. Johnson, J. Non Cryst Solids 59,60 (1983) 265

CHAPTER 2

PREPARATION AND CHARACTERIZATION OF a-Si:H FILMS AND a-Si:H/Pd SCHOTTKY DIODES

2.1 INTRODUCTION

In a glow discharge apparatus amorphous silicon is prepared by the decomposition of silane gas, at low pressure, by applying an electric field. Both rf and dc fields have been used. Chittick et al[1] were the first to produce a-Si:H by this method and they used an rf field which was coupled inductively to the discharge chamber. However, since inductive coupling is difficult to use with a large size reaction chamber, the rf systems with capacitive coupling are, sometimes, preferred[2,3]. A dc glow discharge is also being used to deposite a-Si:H films[3,4]. Pure SiH_4 as well as SiH_4 mixed with other gases (for instance, SiH_4+Ar[5], SiH_4+H_2[4] in different proportions) have been used for the glow discharge deposition. Although, different laboratories using different variants of this method have succeeded in making a-Si:H films of good quality having a small number of localized states, the deposition parameters which yield such good films are not yet fully known. It can, however, be said that in all the cases a high substrate temperature[2] ($T_s \simeq 300°C$) is necessary for producing films of good quality. Some of the other parameters which are considered to help in obtaining films of good quality are (i) low power[6] (ii) high flow rate[6].

A dc glow discharge system is designed and fabricated in our laboratory and highly photoconducting films of good quality are produced.

2.2 DESIGN CONSIDERATIONS

The physical properties of SiH_4 are listed in Table 2.1[7]. It is a corrosive and inflammable gas and burns at room temperature with a cold blue flame when it comes in contact with air. The glow discharge apparatus should, therefore, be free from leaks. Our system has a leak rate $\lesssim 10^{-6}$ torr ls^{-1} which is quite low[8]. Also the metallic parts of the system are made of stainless steel.

Table 2.1 : Physical properties of silane[7]

Molecular weight	32.12
Specific volume at 70°F, 1 atm	12.1 cu.ft/lb
Boiling point at 1 atmos.	-112°C
Freezing point at 1 atmos.	-185°C
Density, Gas at 20°C	1.44 g/liter
Specific gravity, liquid at -185°C	0.68
Critical temperature	-4°C
Critical pressure	702.7 psi
Viscosity at 15°C	112.4 micropoises

2.3 GLOW DISCHARGE APPARATUS

The glow discharge apparatus is shown in Fig. 2.1. It has three main parts, (i) Gas handling system, (ii) Reaction chamber (iii) Evacuation system.

(i) Gas handling system

This consists of a main cylinder (A, containing a mixture of 3% SiH_4 + 97% Argon at a pressure $\approx$ 1500 psi) an auxiliary cylinder (B) with a pressure gauge (PG), a port having diaphragm valves and a needle valve (N). Prior to the SiH_4 discharge the gas mixture is transferred from the main cylinder (A) to auxiliary cylinder (B) at a pressure $\approx$ 15 psi to minimize the danger and to be able to control the flow of the gas, to a better degree, through the needle valve, N. (This can also be achieved using a SiH_4 gas regulator which was not available).

(ii) Reaction chamber

A thick walled ($\approx$ 7 mm thick) pyrex glass cylinder of diameter $\approx$ 16 cm (O.d) and length $\approx$ 20 cm is used as a reaction chamber. An aluminium plate (AL) of $\approx$ 10 cm diameter is used as the anode and an aluminium grid (GR) at a distance of $\approx$ 2.5 cm as the cathode. The grid helps in overcoming the difficulties associated with the charging of the glass substrates during the discharge. The substrates (SU) are kept about 1 cm below the grid on a stainless steel plate (H) which is grounded and can be heated to 500°C, with

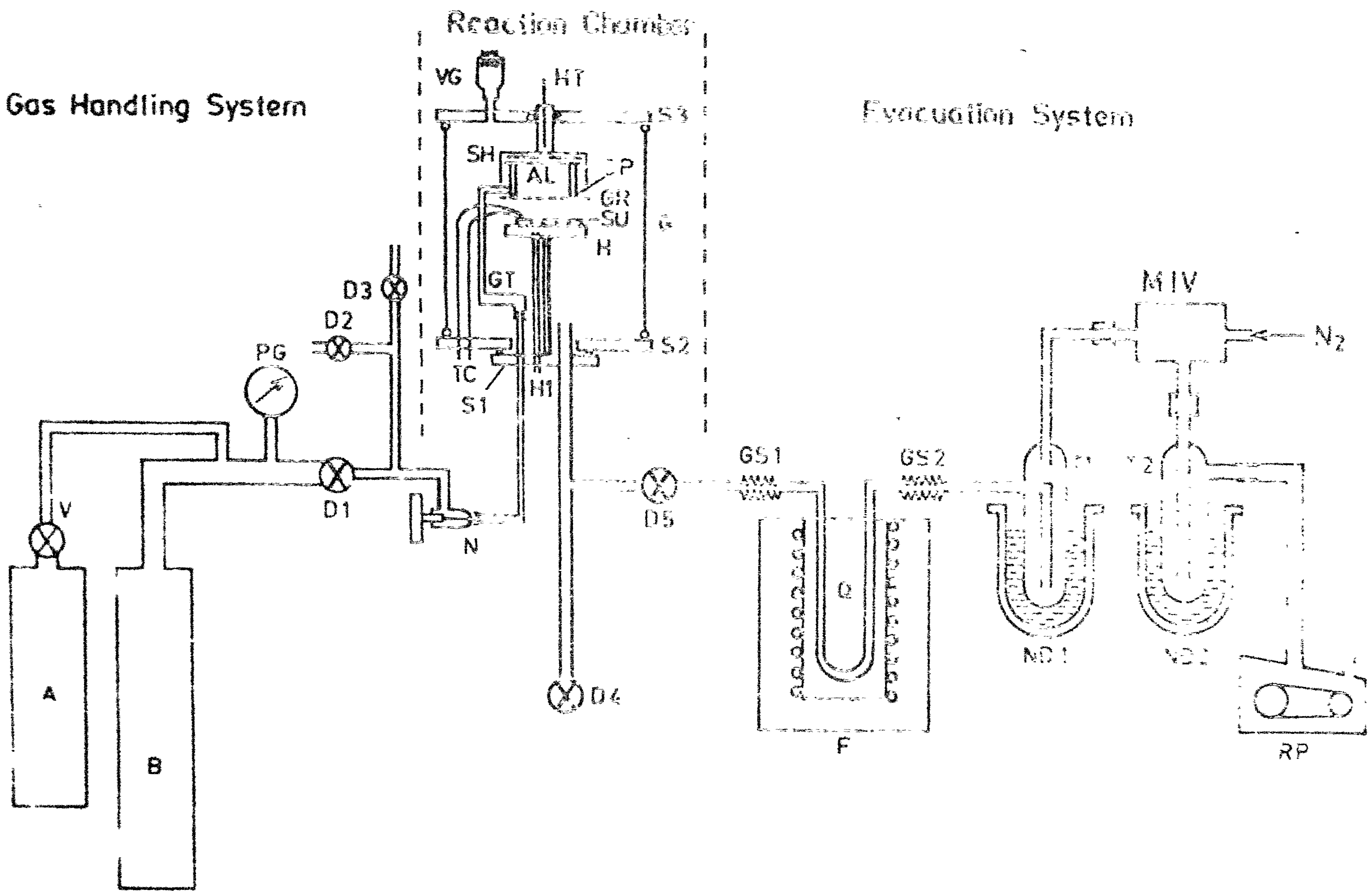

Fig. 2.1 : dc glow discharge system (for nomenclature of various parts, see List of Figures)

the help of an internal heater. The temperature of the substrates (T_s) is measured by mounting a chromel alumel thermocouple on a dummy substrate, loaded on the plate (H). The pressure is monitored using a thermocouple gauge (VG).

(iii) Evacuation system

The evacuation system consists of a 2 stage rotary pump (speed $\approx$ 200 l/min.), a high temperature furnace (F) and a magnetic isolation cum air admittance valve (MIV). Any SiH_4 gas which might escape the electric discharge, gets decomposed in the furnace, following the reaction[9]

$$SiH_4 \xrightarrow{1000^\circ C} Si + 2H_2$$

The system is constantly pumped during the operation. The isolation valve, MIV, placed between furnace and rotary pump, is connected in such a way that during an emergency, such as a sudden power failure, the pump is isolated and the system is flooded with dry nitrogen gas.

2.4 SUBSTRATES

The substrates used for the electrical and optical properties are 0.5 mm thick Corning 7059 glass slides of size 1.25 cm x 1.25 cm. For IR spectroscopy and electron microscopy, the polished high resistivity silicon wafers and carbon coated grids, respectively, are used.

2.4.1 Substrates Cleaning Procedure

(i) 7059 glass substrates

The 7059 glass substrates are first washed in a detergent solution, rinsed in deionized water and then are cleaned, ultrasonically, in acetone. Finally, they are vapour degreased in isopropyl alcohol.

(ii) Silicon wafer cleaning

After washing in a detergent solution as described above, the Si wafers are given an etch in 15% solution of electronic grade hydrofluoric acid and rinsed in deionized water. Then, they are ultrasonically cleaned in acetone and finally degreased in vapours of isopropyl alcohol.

(iii) Electron microscopy grids

Copper grids having predeposited carbon coating are washed in acetone and vapour degreased in isopropyl alcohol.

2.4.2 Evaporation of Contacts

About 1 μm thick nichrome is evaporated through a suitable mask onto the clean 7059 substrates using an oil-diffusion pumped vacuum coating unit with a liquid nitrogen trap having a base pressure $\approx 10^{-6}$ torr. The thickness is measured using a quartz crystal thickness monitor (Edwards FTM 3).

In the gap cell configuration (Fig. 2.2(a)) two coplanar nichrome strips are evaporated, onto a clean 7059

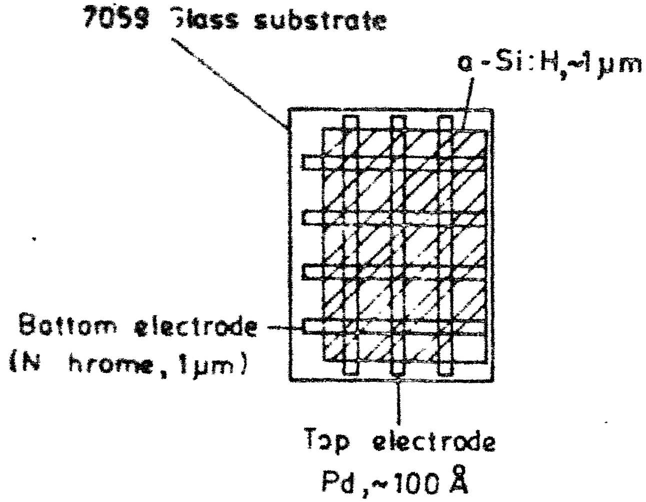

Fig.2.2(c) : Sandwich configuration with nichrome as bottom and Pd top contacts

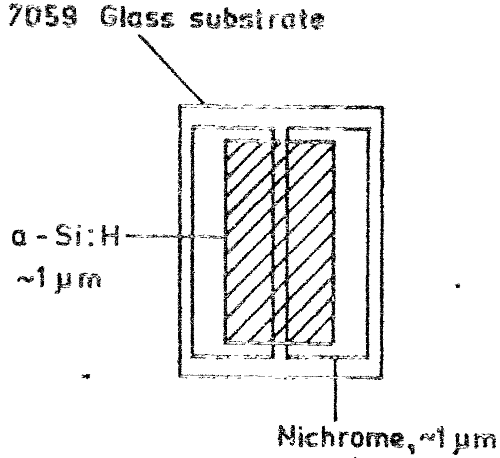

Fig.2.2(a) : Coplanar electrode geometry with nichrome on bottom.

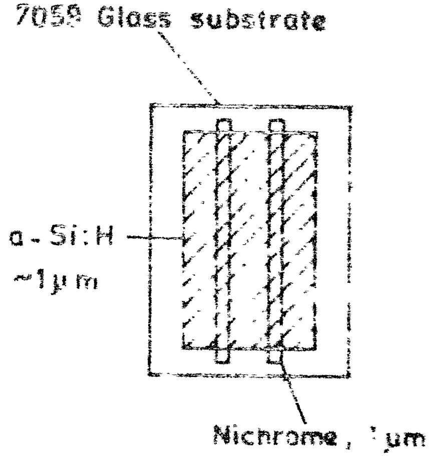

Fig.2.2(b) : Coplanar electrode geometry with nichrome on top

glass substrates, with a separation $\approx$ 1.0 mm. In some cases two nichrome strips with a separation $\approx$ 2.0 mm are used at the top of a-Si:H films (Fig. 2.2(b)), without any significant change in the results.

In the sandwich configuration (Fig. 2.2(c)) the bottom contact is made by evaporation of nichrome strips ($\approx$ 1.0 mm wide and $\approx$ 2.0 mm separation).

2.4.3 SiH_4 Decomposition Procedure

The substrates are loaded on the stainless steel plate (H) in the reaction chamber (see Fig. 2.1).

(i) Initial pumping

The system is evacuated using the rotary pump RP (Fig. 2.1). Liquid nitrogen is filled in dewars ND1 and ND2 to avoid contamination of walls of reaction chamber by back streaming of oil vapours. Pressure in the system reaches $\approx 10^{-2}$ torr in about half an hour.

(ii) Flushing

Hydrogen gas is introduced into the system through the valve D3 and the system is flushed with hydrogen, several times.

(iii) Baking of the system

At $\approx 10^{-2}$ torr, the reaction chamber is heated to $>350\,°C$ by putting on the substrate heater. The furnace (F)

is brought to ~ 1000°C and the other parts of the system are baked using heat lamps and heating tapes. Baking is continued for about 20 hr after which the pressure becomes $\simeq 5\times10^{-3}$ torr (at high temperature).

(iv) Cleaning by hydrogen discharge

The hydrogen gas is introduced through D3 and a constant flow is maintained at a pressure $\approx$ 1 torr in the reaction chamber. To strike the glow discharge, a high voltage is applied between the anode, AL (H.T.) and the cathode, GR. A stable discharge is obtained when a current limiting resistance of 40 KΩ is used in series and $\approx$ 700 V is applied. The discharge of hydrogen is kept on for one hour, for the cleaning of the reaction chamber.

(v) Glow discharge of SiH_4

After the hydrogen discharge, all heating is stopped except the furnace and the substrate heater. The pressure in the system becomes $\approx 10^{-3}$ torr. The substrate temperature is brought to the desired value using the variac controlling the substrate heater. This is usually $T_s \approx 300°C$. SiH_4+Ar mixture from cylinder A is transferred to B at a pressure $\approx$ 15 psi. and then A is isolated for the rest of operation. The gas mixture is introduced in the reaction chamber and a constant flow is maintained at a pressure $\approx$ 1 torr by controlling the needle valve N. A high voltage ($\approx$ 730 V) is applied, between the anode AL, the cathode GR and the

series resistance $\sim$ 40 KΩ to strike the discharge. It takes about 4 hr to obtain $\approx$ 1 μm thick a-Si:H films. The parameters, associated with the deposition of good quality films are summarized in Table 2.2.

Table 2.2 : Deposition parameters

Sl. No.	Deposition parameters	Values
1.	Substrate temperature (T_s)	580 K
2.	Pressure	1 torr
3.	Distance between anode and screen	2.5 cm
4.	D.C. voltage	460 V
5.	Discharge current	6.3 mA
6.	Power density	40 mW/cm^2
7.	Deposition rate	1 A°/s

2.4.4 Preparation of Schottky Diodes

For the preparation of Schottky diodes, the surface of a-Si:H with nichrome back contact (section 2.4.2) is first etched with 10% electronic grade hydrofluoric acid. Then the samples are rinsed in deionized water, vapour degreased in isopropyl alcohol and heat dried at $\approx$ 150°C for 2 hr in a vacuum $\approx 10^{-6}$ torr. The top contact of Pd of $\approx$ 100 A° (see Fig. 2.2(c)) thickness is deposited by thermal evaporation at a pressure $\approx 10^{-6}$ torr and substrate temperature $\approx$ 150°C.

2.5 STRUCTURAL CHARACTERIZATION

2.5.1 Electron Microscopy

Copper electron microscopy grids coated with carbon are used for deposition of about 500 A° thick a-Si:H films for transmission electron microscopy. A Philips (PM 300) electron microscope is used. A typical electron diffraction micrograph of a-Si:H deposited at $T_s \approx$ 580 K is presented in Fig. 2.3. The micrograph shows diffused rings characteristic of the amorphous nature of the samples.[10]

2.5.2 IR Spectroscopy

1 μm thick films of a-SiH are prepared on single crystalline Si wafers for IR spectroscopy. The transmittance is measured between 200 and 2500 cm^{-1} using a Perkin Elmer 580 spectrophotometer. Typical results for two samples prepared at $T_s \approx$ 300 K and 580 K are presented in Fig. 2.4 (curves (a) and (b) respectively). Absorption bands corresponding to various modes of vibration of Si-H and Si-O etc.[11] are observed and listed in Fig. 2.4.

IR spectra of the samples deposited at 300 K have absorption peaks corresponding to $Si\text{-}H_2$, $(Si\text{-}H_2)_n$ etc. While in the samples deposited at 580 K, a peak appears at 2000 cm^{-1} which corresponds to Si-H (stretching mode), whereas other peaks related with $Si\text{-}H_2$, Si-O etc. can hardly be seen. Thus, the hydrogen is present mostly as monohydride in films deposited at 580 K. Also, the intensity of peaks

Fig.2.3 : Electron diffraction micrograph of a-Si:H deposited at 580 K

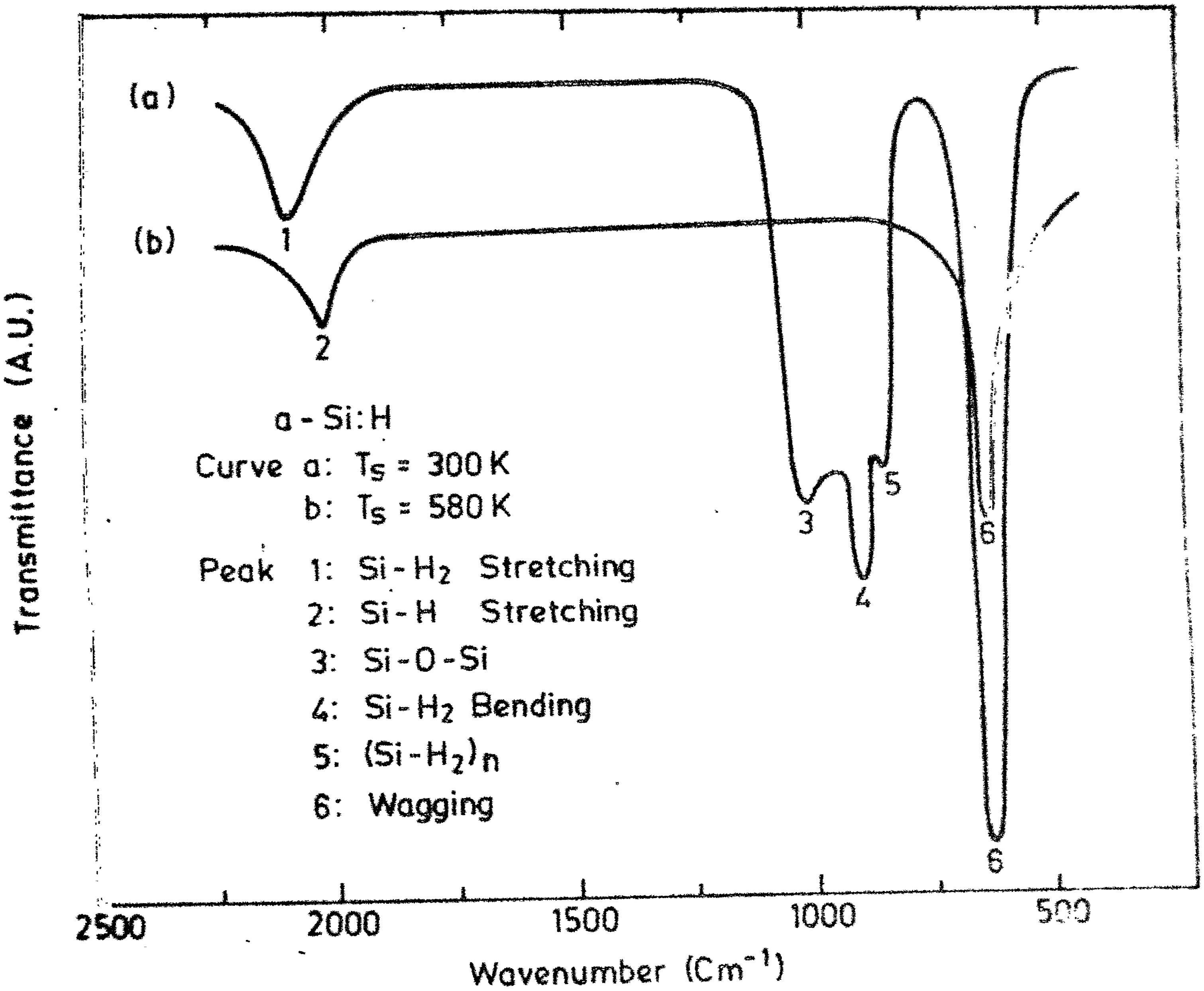

Fig.2.4 : IR spectra of a-Si:H (a) sample deposited at T_s = 300 K and (b) sample deposited at T_s = 580 K

reduces in samples deposited at 580 K which implies that the concentration of hydrogen is lower in samples deposited at 580 K than those deposited at 300 K. These results are in agreement with the literature[11,12].

2.6 OPTICAL CHARACTERIZATION

This consists of measurement of optical transmission in the wavelength (λ) range 500 nm - 2500 nm and gives thickness and optical gap of the samples.

2.6.1 Optical Gap and Thickness Measurements

Optical transmission measurements at 300 K are carried out on a-Si:H films deposited on 7059 glass at 580 K, using a Varian Cary 17D spectrophotometer, to determine the optical gap. The absorption coefficient is calculated following the analysis of Cody et al[13] using the relation which is true in high absorption region ($\alpha D \gg 1$).

$$T_M = C \, |\tilde{t}_{12}|^2 \, |\tilde{t}_{23}|^2 \, e^{-\alpha D} \qquad (1)$$

where T_M is measured transmittance, C is = 0.96 for 7059 glass, $\tilde{t}_{12}$ and $\tilde{t}_{23}$ are functions of refractive index (n) of a-Si:H and D is film thickness.

$|\tilde{t}_{12}|^2$ and $|\tilde{t}_{23}|^2$ are calculated using the refractive index data of a-Si:H films reported by Cody et al[13]. This is not likely to cause much error since $|\tilde{t}_{12}|^2$ and $|\tilde{t}_{23}|^2$ are not dominant terms as compared to exponential term. The film thickness D is calculated from the interference

fringes observed in the transmittance data in the wavelength range 900 nm - 1400 nm, using,

$$\left[\frac{n_2(\lambda_2)}{\lambda_2} - \frac{n_1(\lambda_1)}{\lambda_1}\right] D = \frac{1}{2} \tag{2}$$

where λ_1 and λ_2 are wavelengths corresponding to two adjacent maxima and n_1 and n_2 are refractive indices at λ_1 and λ_2. Since the refractive index in 900 - 1400 nm range is approximately 3.5 and is constant,[13] it is assumed that $n_1(\lambda_1) = n_2(\lambda_2) = 3.5$.

Using D from Eq. (2), α is calculated for different photon energies (E). A resultant plot of $(\alpha E)^{1/2}$ vs E for a typical sample is shown in Fig. 2.5. It is fitted to a straight line following the relation[14]

$$(\alpha E)^{1/2} \propto (E-E_G) \tag{3}$$

The intercept on E axis in Fig. 2.5 gives the optical gap E_G to be 1.8 ± 0.1 eV, for the samples at T_s 580 K, in agreement with the literature[3,13,15].

2.7 ELECTRICAL CHARACTERIZATION

Electrical characterization of the samples is done by measuring room temperature dark conductivity (σ_{dc}(300 K)), photoconductivity (σ_{ph}(300 K)) and σ_{dc} as a function of temperature. Samples are also characterized for light induced changes[16,17] (Staebler-Wronski effect, S-W effect).

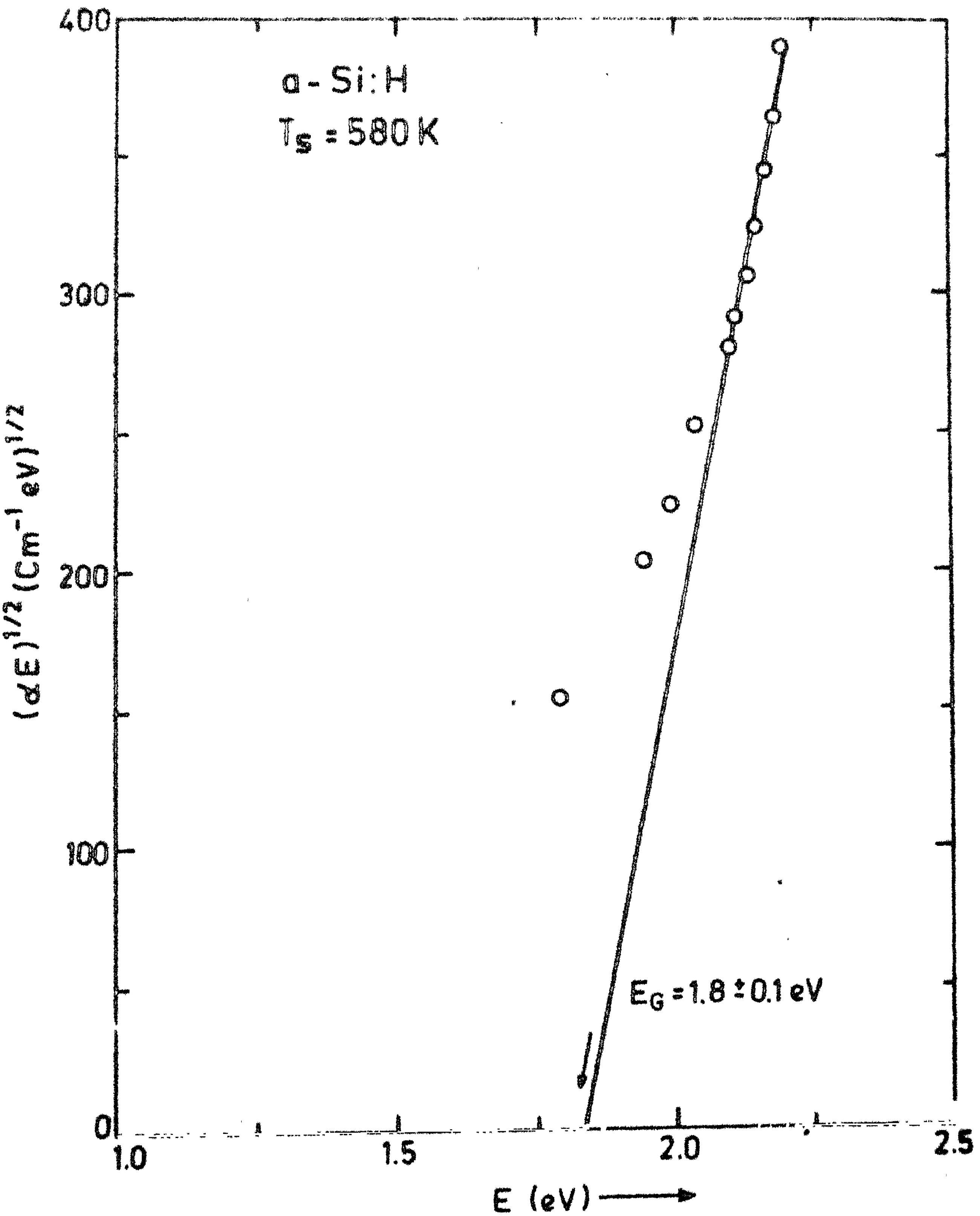

Fig.2.5 : Plot of $(\alpha E)^{1/2}$ vs photon energy (E) for a typical a-Si:H sample deposited at T_s = 580 K

2.7.1 Experimental

Preliminary measurements of σ_{dc}(300 K) and σ_{ph}(300 K) are done in air in aluminium box shown in Fig. 2.6(a). Light is shone from a 100 watt tungsten bulb. Intensity on the sample is $\approx$ 35 mW/cm^2. For samples with $T_s \approx 300$ K, $\sigma_{ph}/\sigma_{dc} \simeq 1$, whereas for T_s 580 K this ratio is usually quite high ($\gtrsim 10^4$). For the measurements in the temperature range 100 K $\leqslant T \leqslant$ 430 K and in vacuum $\lesssim 10^{-5}$ torr, a cryostat shown in Fig. 2.6(b) is used. The sample holder is connected to the cold finger of the inside chamber containing liquid nitrogen. An eutactic alloy of $In_{0.3}Ga_{0.7}$[18] which gives an excellent thermal contact between the samples and the cold finger is used to mount the sample. Electrical connections from the sample holder are taken using teflon insulated wires to the two teflon insulated feedthroughs, at the outer chamber. Copper rod holding substrate holder has a $\approx$ 20 W heater wound around it. Sample temperature is measured by a copper constantan thermocouple mounted on a glass slide, of the same size as the substrate of the sample, loaded symmetrically w.r.t. sample on the other side of the sample holder using the In Ga eutactic. The cryostat is provided with a quartz window through which light can be shone on the sample.

2.7.2 Results

All the measurements are done on the samples heat-dried at 150°C for 2 hr[4] in a vacuum $\approx 10^{-6}$ torr. This ensures the good reproducibility of the data.

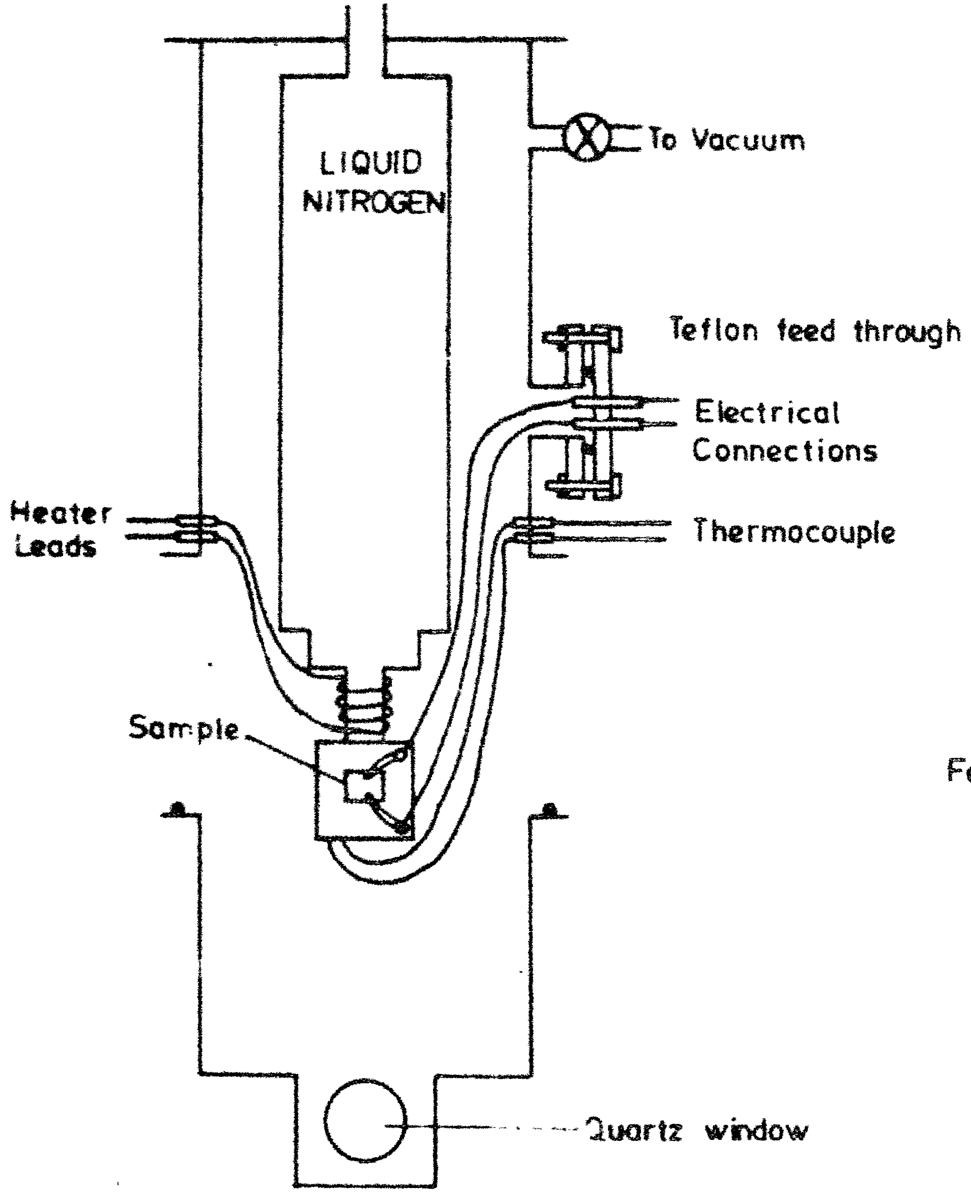

Fig.2.6(b) : Cryostat used for measurements at different temperatures in vacuum

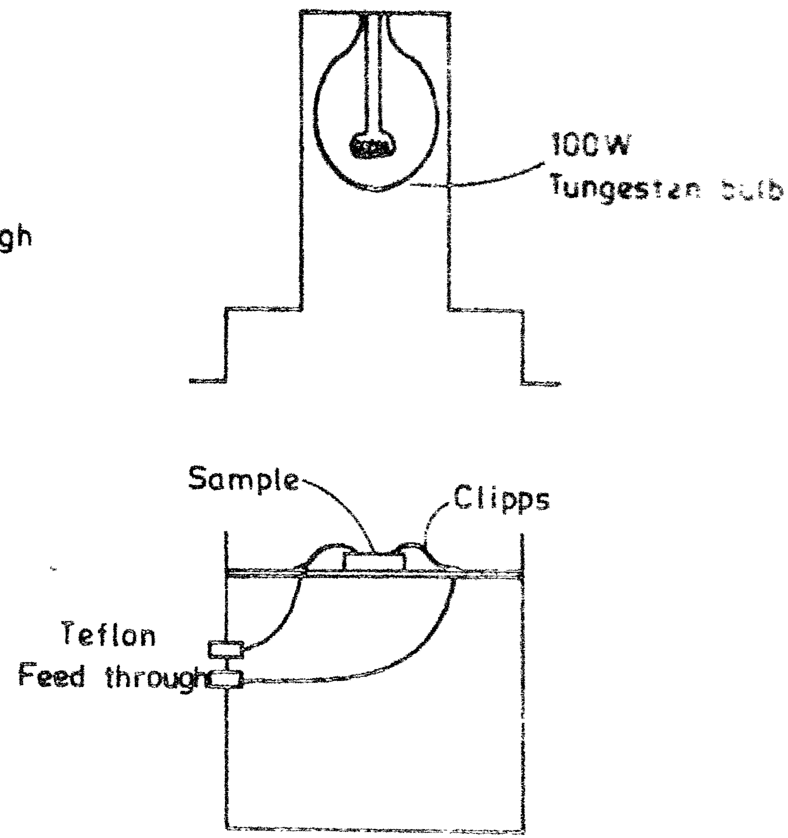

Fig.2.6(a) : Set up used for σ_{dc} and σ_{ph} measurements in air at room temperature

(a) Dark conductivity (σ_{dc})

The samples show linear and symmetric I-V characteristics upto electric fields $\gtrsim$ 500 - 1000 V/cm. Variation of σ_{dc} as a function of temperature is shown in Fig. 2.7 for the samples prepared at T_s 300 K, 450 K and 580 K. σ_{dc} vs $10^3/T$ for an evaporated Si sample[19] is also shown for comparison. Films prepared at T_s 300 K, 450 K and 580 K have activation energies of 0.70 eV, 1.00eV and 0.62 eV respectively. Table 2.3 summarizes the σ_{dc}(T) results on these and other samples. These results are in qualitative agreement with the literature[20].

Table 2.3 : Electrical parameters of a-Si:H

Sample No.	T_s	σ_{dc}(300K) ($\Omega^{-1}cm^{-1}$)	ΔE_{σ} (eV)	$_o$($^{-1}cm^{-1}$)	$_{ph}$(300 K) ($\Omega^{-1}cm^{-1}$)
30	300 K	1.0×10^{-8}	0.70	6.0×10^{3}	0
100	450 K	4.0×10^{-10}	1.0	2.7×10^{7}	5.0×10^{-6}
102	450 K	4.5×10^{-10}	1.0	3.0×10^{7}	5.0×10^{-6}
120	580 K	5.0×10^{-8}	0.62	1.3×10^{3}	1.0×10^{-4}
183	580 K	6.2×10^{-8}	0.62	1.6×10^{3}	
186	580 K	4.0×10^{-8}	0.62	1.0×10^{3}	2.0×10^{-4}
190	580 K	5.0×10^{-8}	0.62	1.3×10^{3}	4.0×10^{-4}

(b) Photoconductivity (σ_{ph}(300 K))

Samples prepared at 300 K are not found to be

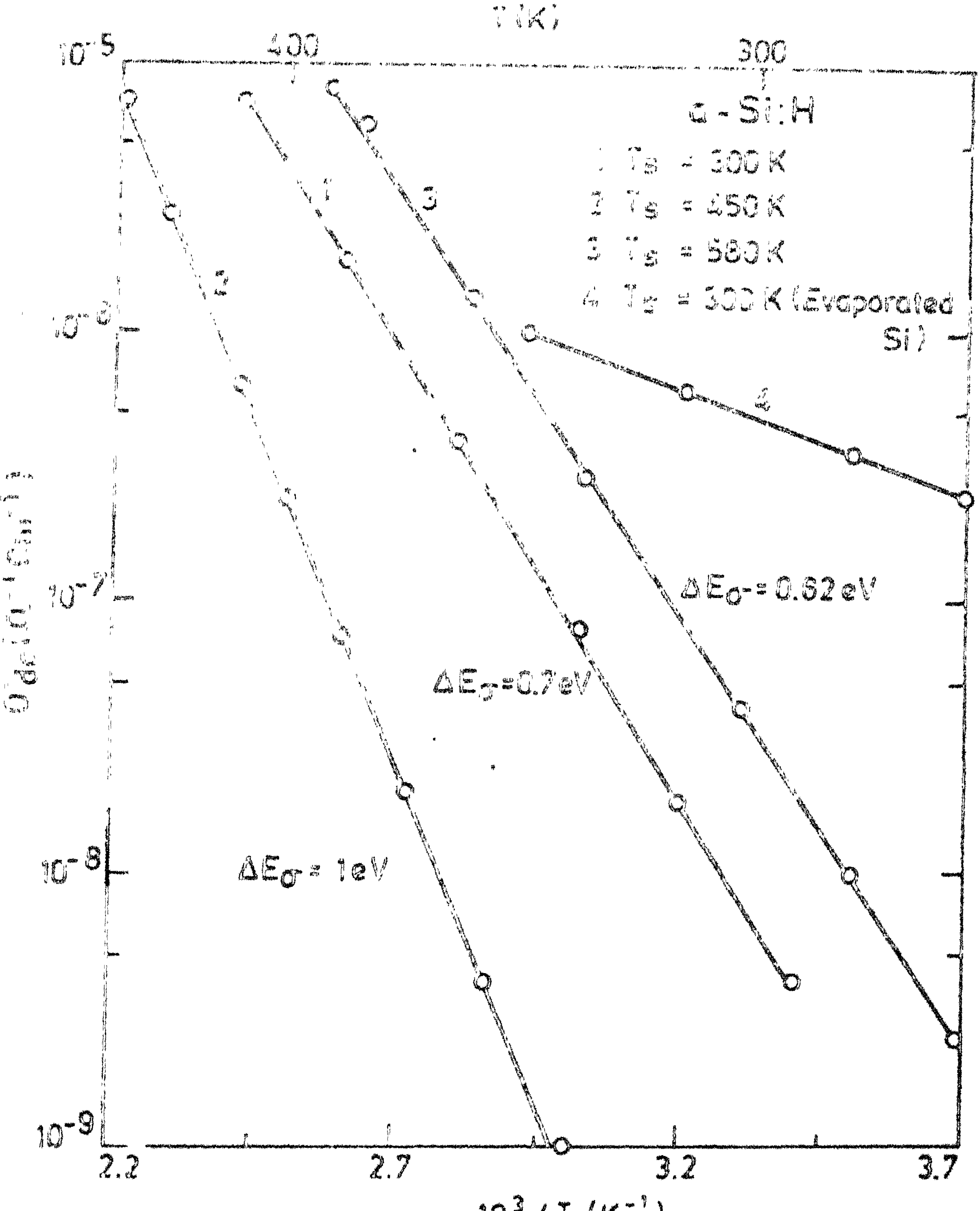

Fig.2.7: $\sigma_{dc}(T)$ of a-Si:H samples prepared at different substrate temperatures (1) T_s = 300 K, (2) 450 K, (3) 580 K. $\sigma_{dc}(T)$ of a evaporated Si sample (T_s = 300 K) is also shown for comparison

photoconducting. The photoconductivity in air (σ_{ph}(300 K)) of a few samples prepared at high T_s is listed in Table 2.3.

(c) Light induced changes

Light induced changes[16,17] are studied in samples prepared at T_s 580 K. These are found to be small in most of the samples. Changes in σ_{dc}(300 K) from heat dried, (A, annealed at 150°C, 2 hr) to light soaked state (B, after exposure in vacuum for 2 hr to white light from a 100 Watt tungsten halogen lamp $\simeq$ 100 mW/cm^2) range from a factor of 2 to 15 for various samples (see Table 2.4).

Table 2.4 : Electrical parameters of a-Si:H in states A and B

	A				B			
Sample No.	σ_{dc} (300 K) Ω^{-1}cm^{-1}	ΔE_σ (eV)	σ_o (300 K) Ω^{-1}cm^{-1}	σ_{ph} (300 K) Ω^{-1}cm^{-1}	σ_{dc} (300 K) Ω^{-1}cm^{-1}	σ_o (300 K) Ω^{-1}cm^{-1}	ΔE_σ (eV)	σ_{ph} (300 K) Ω^{-1}cm^{-1}
120	5.0×10^{-8}	0.62	1.3×10^{3}	1.0×10^{-4}	1.6×10^{-8}	1.4×10^{3}	0.65	7.0×10^{-5}
163	4.0×10^{-8}	0.62	1.0×10^{3}	1.5×10^{-4}	1.6×10^{-8}	1.1×10^{3}	0.65	8.0×10^{-5}
183	6.2×10^{-8}	0.62	1.6×10^{3}	1.0×10^{-4}	7.0×10^{-10}	1.4×10^{5}	0.85	3.7×10^{-5}
186	4.0×10^{-8}	0.62	1.0×10^{3}	2.0×10^{-4}	2.5×10^{-9}	1.0×10^{4}	0.75	1.0×10^{-4}
190	5.5×10^{-8}	0.62	1.3×10^{3}	4.0×10^{-4}	2.4×10^{-9}	2.4×10^{3}	0.68	2.0×10^{-4}

Note, that for one sample a large change in σ_{dc}(300 K) (by a factor $\simeq$100) occurs upon light soaking. Results of a typical sample are shown in Fig. 2.8. Sample in state A has σ_{dc}(300 K) $5\times10^{-8}\Omega^{-1}$cm^{-1} and E $\simeq$ 0.62 eV. After light soaking (state B)

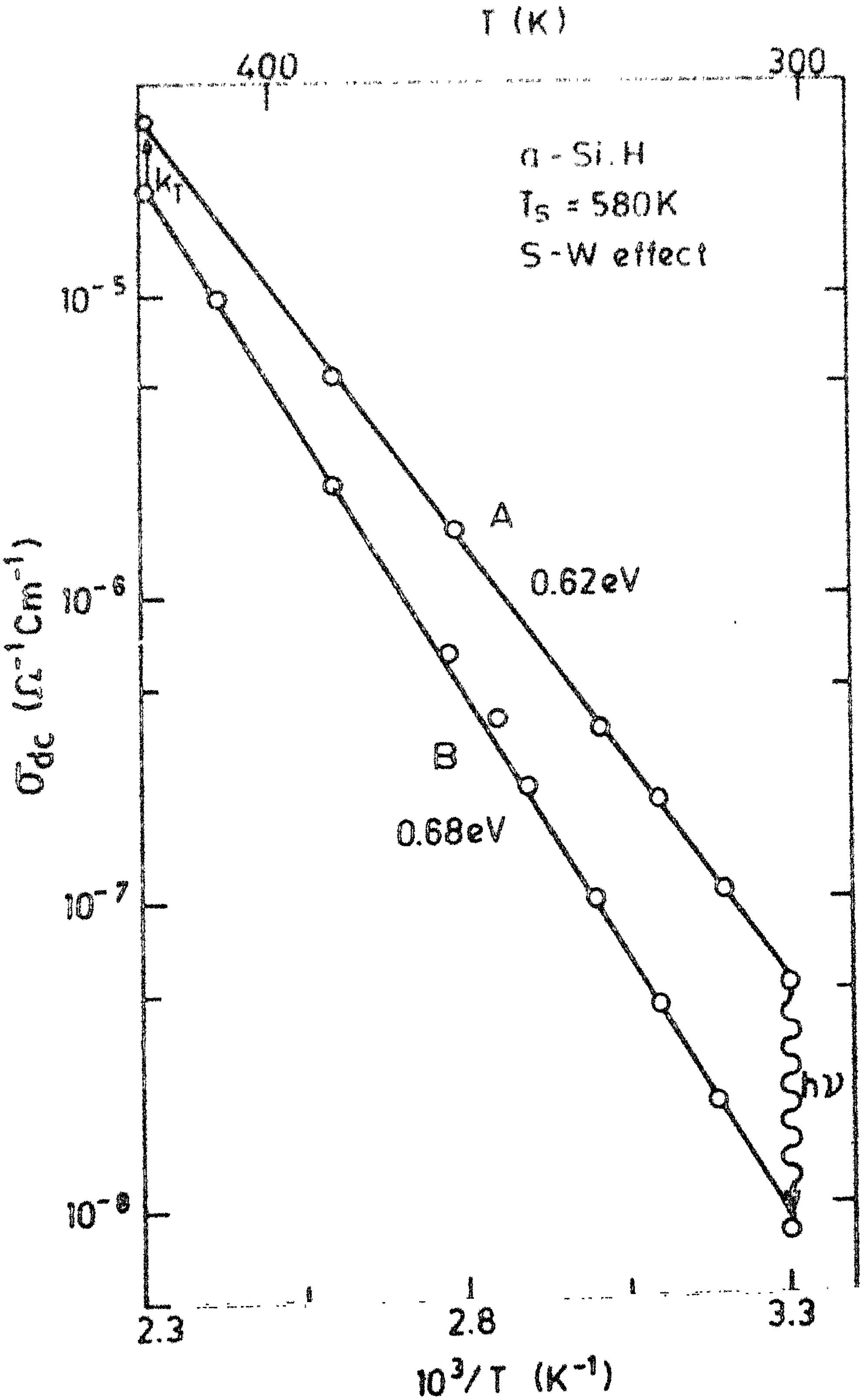

Fig.2.8 : Light induced changes (S-W effect) in σ_{dc} of a typical a-Si:H sample. A : heat-dried, B : Light-soaked

σ_{dc}(300 K) decreases, by a factor of 6, to $\approx 8.0 \times 10^{-9}\ \Omega^{-1}cm^{-1}$ and $\Delta E_{\sigma} \approx 0.68$ eV. Upon heat drying at 150°C for 2 hr, the sample returns to state A.

2.8 DISCUSSION

The results of $\sigma_{dc}(T)$ (Table 2.3) are comparable to those reported by Lecomber et al[20]. In the temperature range investigated σ_{dc} is singly activated and appears to be governed by conduction near the mobility edge following the relation[21]

$$\sigma_{dc} = \sigma_{min} \exp \left\{-(E_C - E_F)/kT\right\} \tag{3}$$

where E_C is the conduction band edge, E_F is the Fermi level and σ_{min} is minimum metallic conductivity and is given by

$$\sigma_{min} = 0.06\ q^2 \left(\frac{6}{z}\right)^2 / \hbar a \tag{5}$$

where q is electronic charge, z is coordination number, a is the interatomic distance and h is Planck constant.

Taking z=4 and a=4 A° we get $\sigma_{min} \approx 10^3\ \Omega^{-1}cm^{-1}$. This value of σ_{min} may be a little different than the actual value because the temperature dependence of the Fermi level ($E_F(T)$) has not been taken into account. $E_F(T)$ may depend on temperature due to (i) the statistical shift of the Fermi level arising from the non symmetric distribution of states above and below $E_F(T)$ and (ii) the variation of optical gap with temperature which is given by

$E_c-E_v = (E_c-E_v)_o - \gamma T$ with $\gamma = 4.4\times10^{-4}$ eV/ K^5, above 200 K. For undoped a-Si:H, the statistical shift may be neglected because $E_F(T)$ is near the middle of the mobility gap[22] . . The resulting dependence of $E_F(T)$ on temperature is governed mainly by variation of optical gap with temperature. If it is assumed that the variation of the mobility gap with temperature is the same as the temperature dependence of the optical gap , we have;

$$E_c-E_F(T) = E_c-E_F(o) - \beta T, \qquad \beta = \gamma/2 \tag{6}$$

where $E_F(o)$ is the position of Fermi level at absolute zero and $\beta = 2.2\times10^{-4}$ eV/K.

Eq. (4) along with (6), yields :

$$\sigma_{dc} = \sigma_o \exp(-\Delta E_\sigma/kT) \tag{7}$$

where $\Delta E_\sigma = E_c-E_F(o)$ and $\sigma_o = \sigma_{min} \exp \gamma/2k \approx 1.5\times10^4 \Omega^{-1}cm^{-1}$. This value of σ_o is independent of ΔE_σ and T. However, in a-Si:H, σ_o has been found to change with ΔE_σ[23]. As shown in Table 2.3 σ_o and ΔE_σ depend upon T_s. This is in agreement with the observation of Spear et al[22], who also report that σ_o and ΔE_σ vary with varying deposition conditions. However, two models which may be relevant are discussed below.

Spear et al[22] suggest that with increasing temperature, the wavefunction overlap of the neighbouring sites is increased and as a result, the mobility edge $E_c(E_v)$ shifts by an amount

$\delta_c T$ towards the center of the gap. They propose that δ_c which depends on the width of the band tails, can have a maximum value $\simeq 4.6 \times 10^{-4}$ eV/K contributing an additional factor $\exp\{\delta_c/k\} \simeq 1.5 \times 10^2$ and then the $n\,\sigma_o = \sigma_{min} \exp\{(\delta_c + \gamma/2)/k\} = 2 \times 10^6\ \Omega^{-1}\ cm^{-1}$. The scatter in σ_o and ΔE_σ in different samples is then explained on the basis of different degrees of disorder in different samples, resulting in different widths of the band tails. Thus, the samples having higher ΔE_σ and σ_o are likely to have a higher degree of disorder and wider band tail. Since samples prepared at higher T_s have smaller σ_o and ΔE_σ, this model implies that these have shorter band tails.

However, the model given by Spear et al[22] is not able to explain the strong decrease of σ_o observed with doping.[23] Doping is expected to increase the band tails width and should result in a large σ_o. This and some other observations which do not fit the Spear's model are summarized by Fritzsche[24]. An alternative explanation for the variation of σ_o with ΔE_σ has been offered by Tanielian[25]. He points out that the observed exponential decrease of σ_o with ΔE_σ in a-Si:H is governed by Meyer-Neldel rule[26] which is often obeyed in heterogeneous systems in which spatial fluctuations associated with the heterogeneities must be playing an important role. Although no quantitative analysis of this

model exists at present, this may well be the reality since a-Si:H is likely to be heterogeneous material[24].

Samples prepared at high T_s are found to be highly photoconducting. In these samples IR spectroscopy shows that hydrogen is mostly bonded as monohydride and thus, it appears that in good quality films hydrogen is bonded mostly as monohydride.

Light induced changes (S-W effect), in our samples, are smaller than usually seen by others using argon silane mixture[27]. However, it is of same order of magnitude as reported by Guha et al[28] who have used a SiH_4+H_2 mixture. Thus, the gas composition does not appear to play an important role. Other deposition conditions appear to be more important in determining the magnitude of this effect.

2.9 CHARACTERIZATION OF SCHOTTKY DIODES

2.9.1 I-V Characteristics

Typical I-V characteristics of some of the diodes, prepared in our laboratory, for voltages $-1.5V \leqslant V \leqslant 1.5$ V and temperatures 300 K $\leqslant T \leqslant$ 360 K are shown in Figs. 2.9 to 2.12. A good rectification is observed. In contrast to the results obtained by Ashok et al[29] and Han et al[30] and in agreement with Wronski et al[31] and Pietruszko et al[32] the current increases exponentially with the voltage as :

$$I(V) = I_o \left[\exp(qV/nkT) - 1\right] \qquad (8)$$

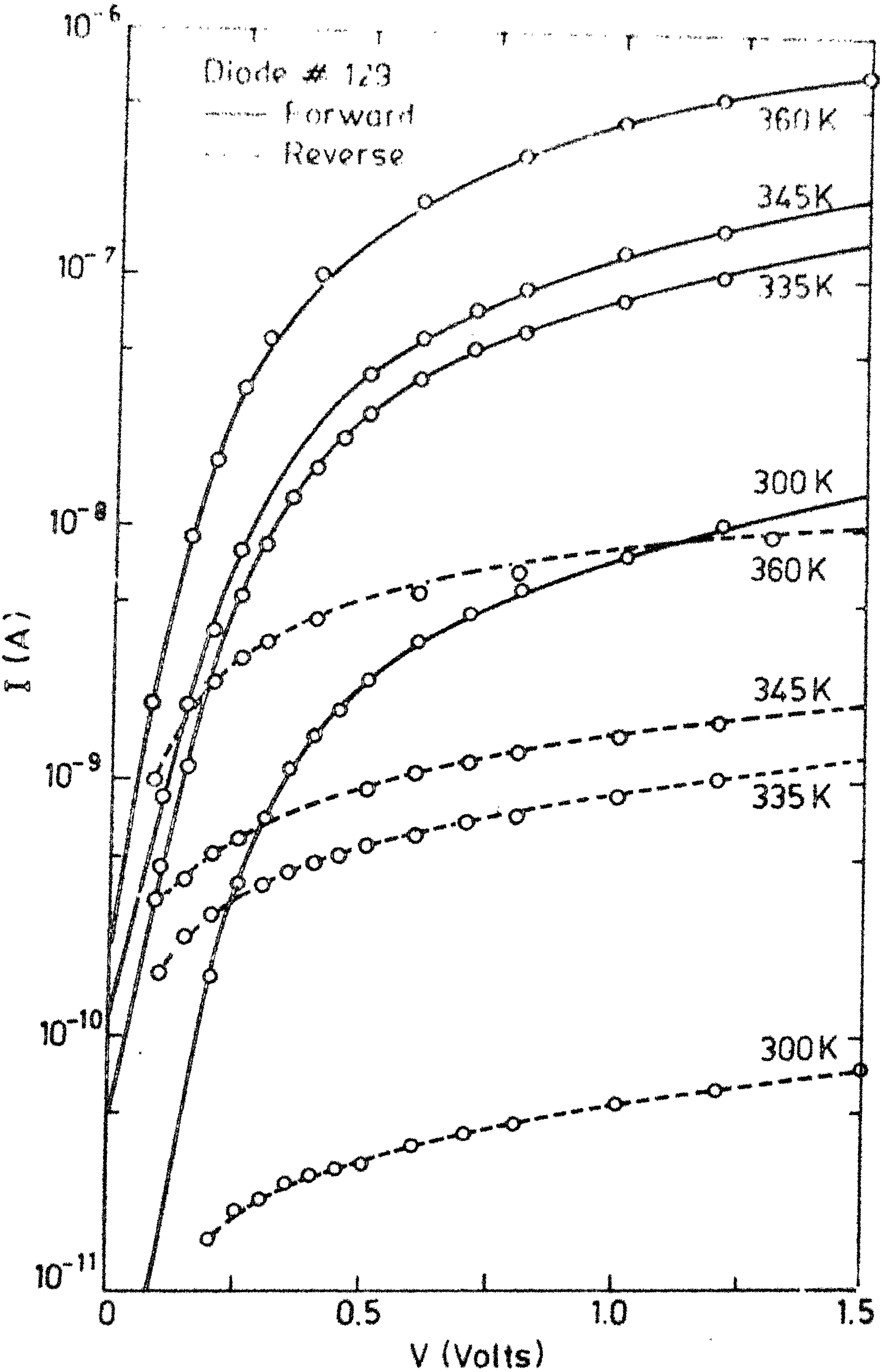

Fig.2.9 : I-V characteristics of a-Si:H/Pd Schottky diode # 129 at different temperatures, as indicated

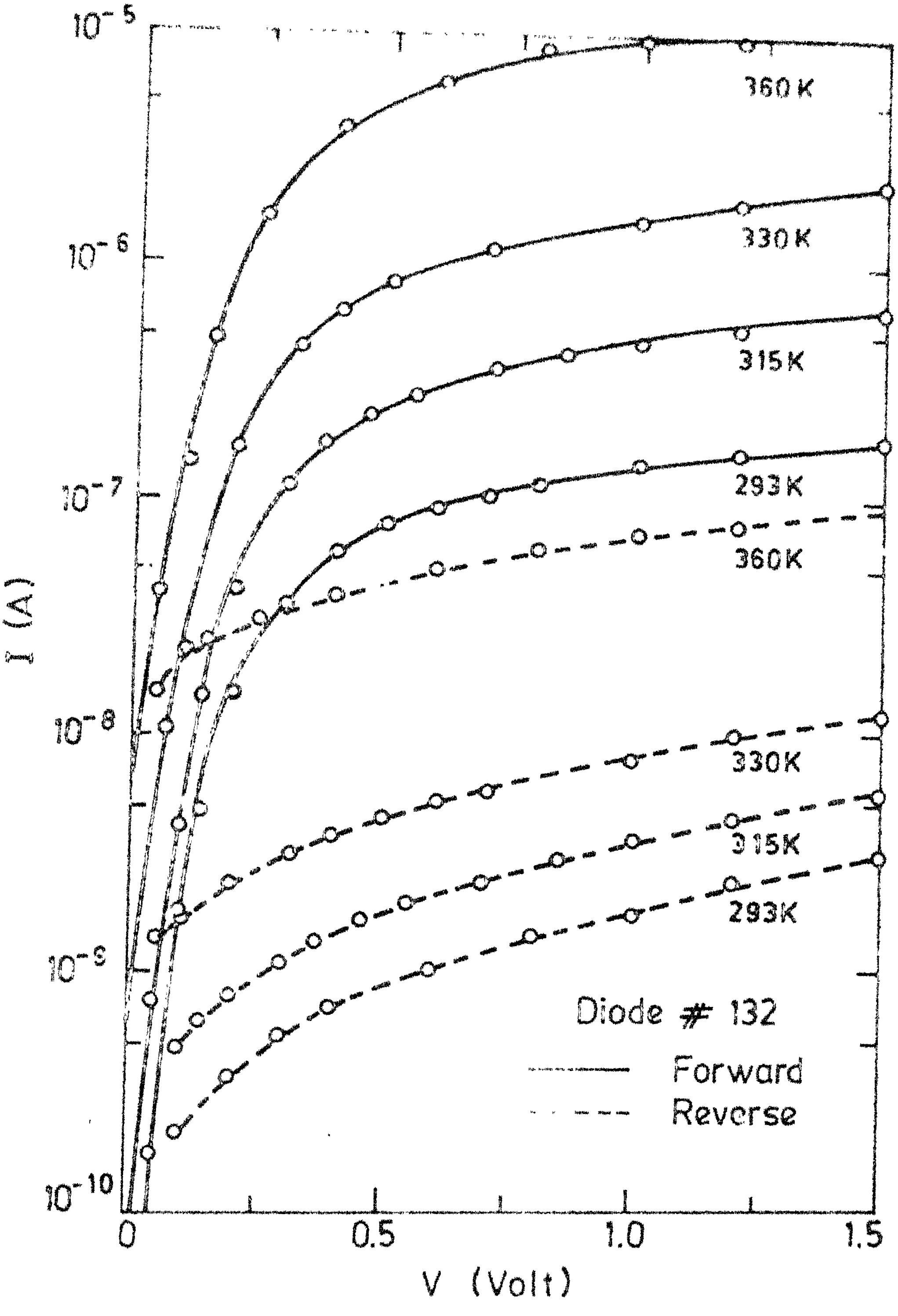

Fig.2.10 : I-V characteristics of a-Si:H/Pd Schottky diode # 132 at different temperatures

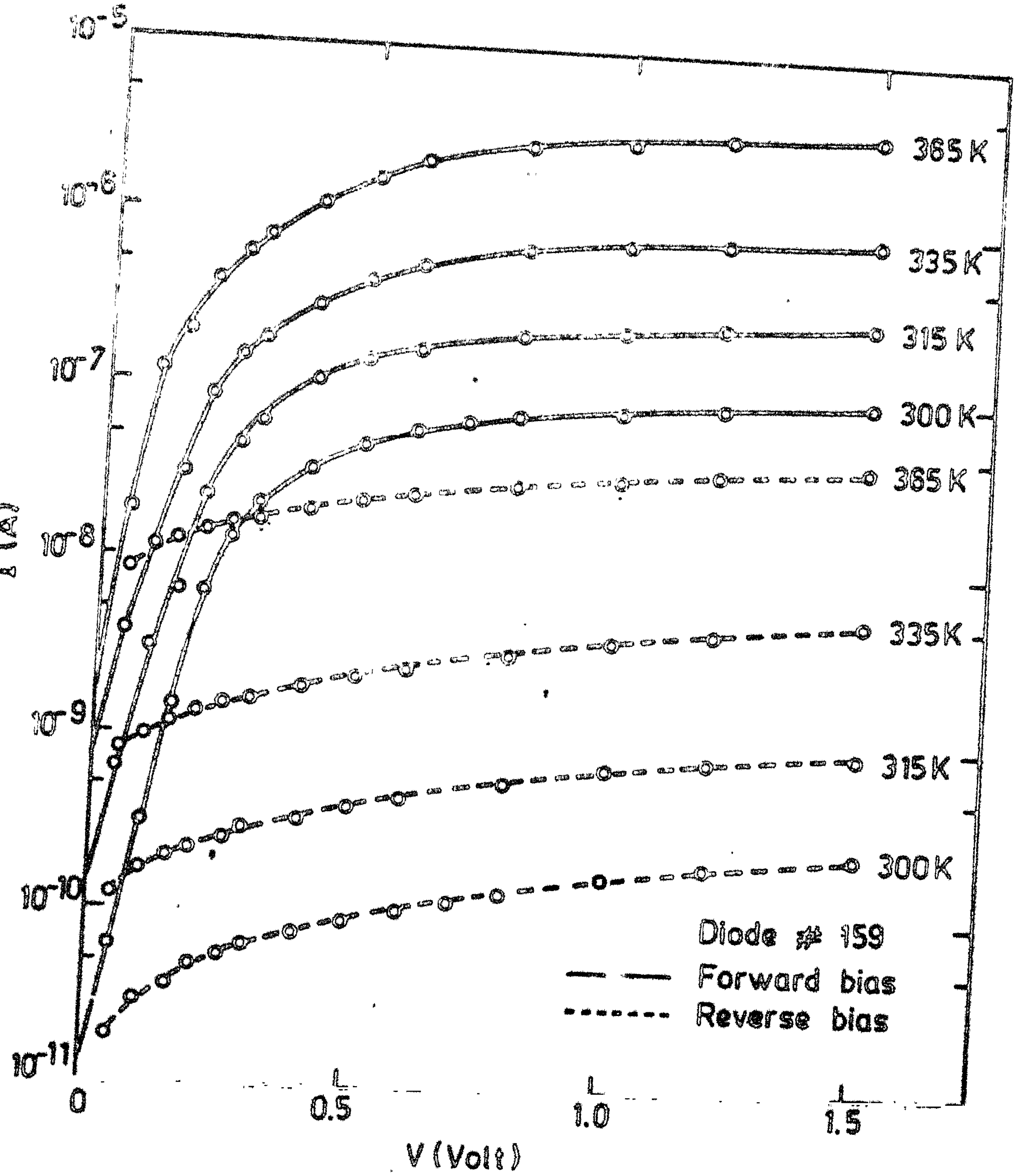

Fig.2.11 : I-V characteristics of a-Si:H/Pd Schottky diode # 159 at different temperatures, as indicated

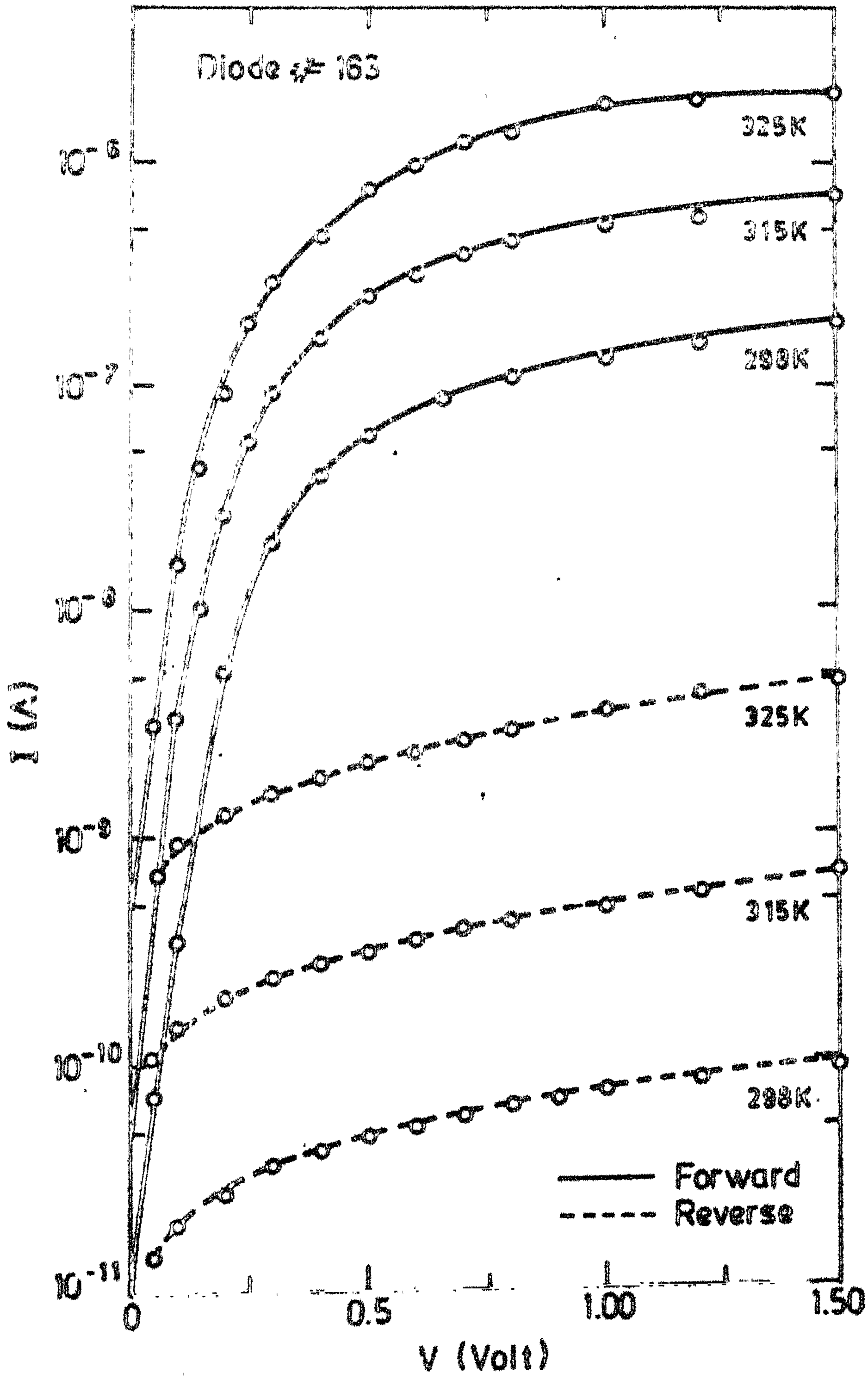

Fig.2.12 : I-V characteristics of a-Si:H/Pd Schottky diode # 163 at different temperatures, as indicated

where I_o is saturation current, n is the ideality factor. and k is Boltzmann constant.

Since the mobility of carriers in a-Si:H is low, the diffusion theory is likely to hold[31] and thus, I_o is related to the barrier height (Φ_B) by the relation :

$$I_o = I_{oo} \exp -(q \Phi_B/kT) \qquad (9)$$

The plots of ln I_o vs $10^3/T$ for various diodes are shown in Figs. 2.13 and 2.14. The values of Φ_B are estimated from the slope of straight lines in Figs. 2.13 and 2.14. Flat band voltage (V_{bi}) for different diodes is calculated from $V_{bi} = \Phi_B - \Delta E$ with $\Delta E \simeq 0.62$ eV. The constants Φ_B , V_{bi} and n for different diodes are summarized in Table 2.6 in section 2.10. These are in agreement with each other as well as with those in literature[31,32].

2.9.1 (a) Influence of light induced changes in I-V characteristics

I-V characteristics of Schottky diodes are known to be influenced by light induced changes (S-W effect)[33,34]. The effect is reported to be large when the diode is exposed to light in open circuit condition[33]. From the experiments on conductivity in coplanar configurations, in states A and B, the Staebler Wronski effect is found to be small in our samples, as already described in section

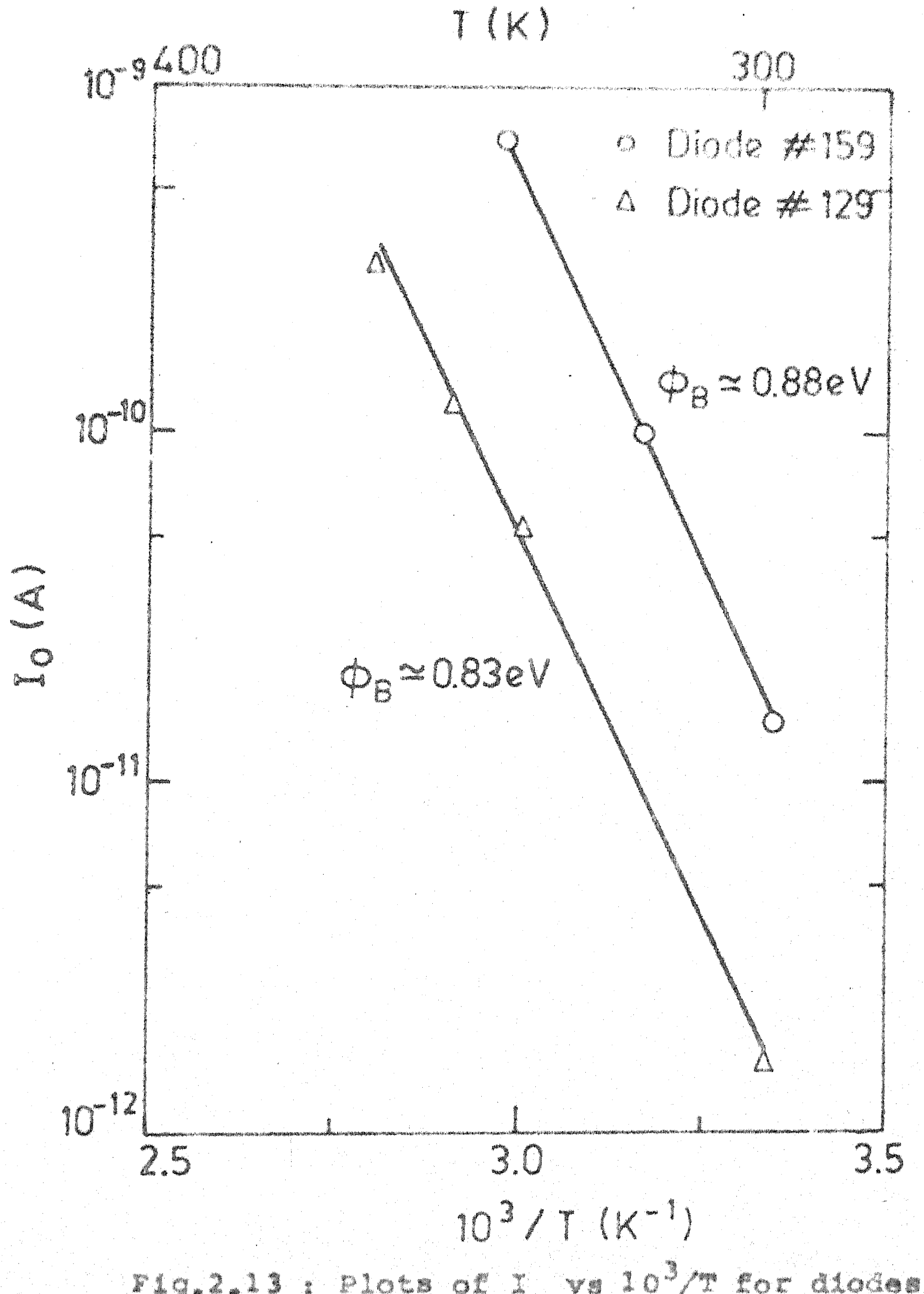

Fig.2.13 : Plots of I_o vs $10^3/T$ for diodes # 129 and 159. The slopes of the straight lines give barrier height (ϕ_B) as shown

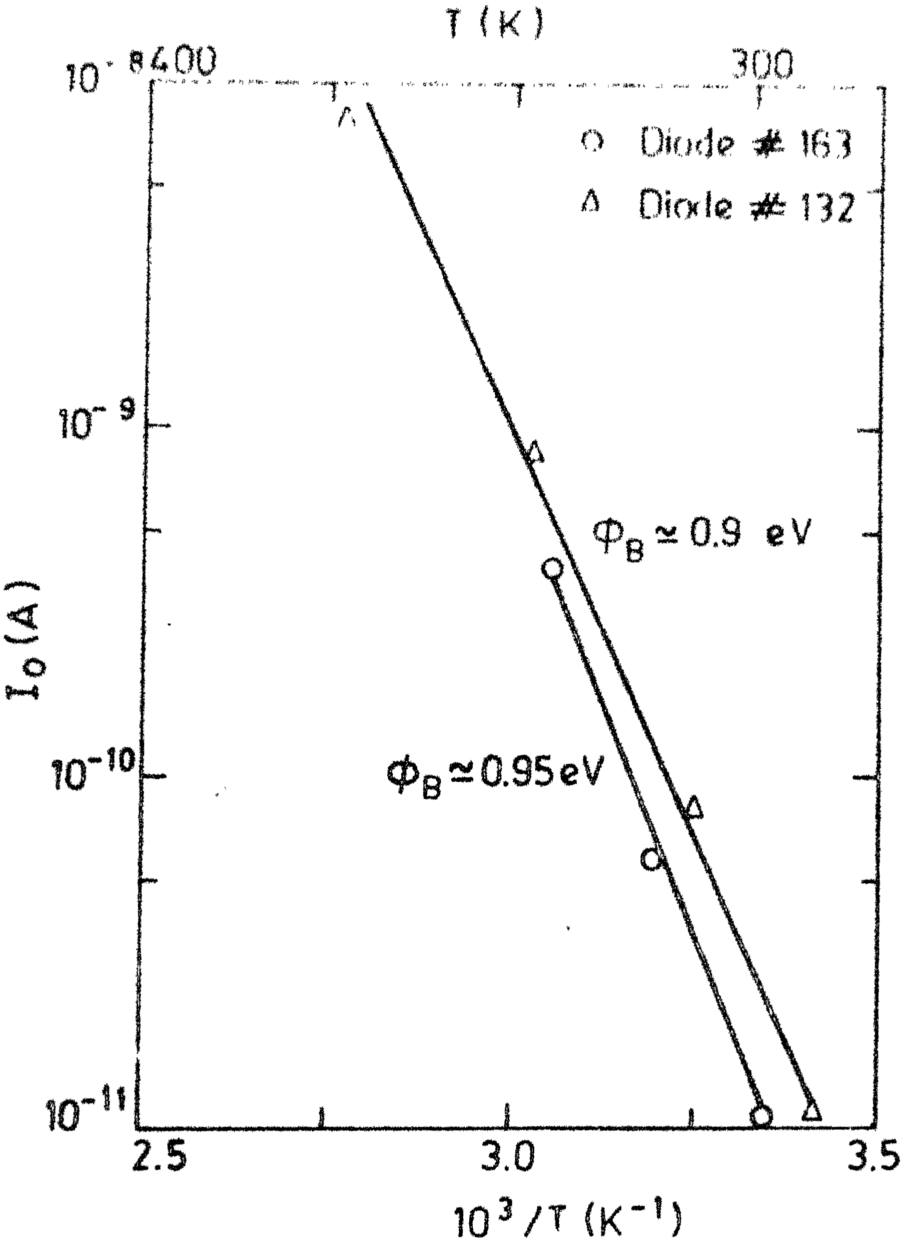

Fig.2.14 : Plots of I_o vs $10^3/T$ for diodes # 132 and 163. The slopes of the straight lines give barrier height (ϕ_B) as shown

2.7.2(c). The I-V characteristics of Schottky diodes also show a small change upon light soaking.

Figure 2.15 shows the results. The heat dried state is reached by annealing the sample at 150°C for 2 hr in vacuum. Light soaked state is after shining AM1 light on the diode (by keeping it in sun light) in open circuit condition for 8 hr. The current in forward as well as reverse bias, after light soaking, is decreased. However this decrease is much smaller than that reported by Jousse et al[33]. They have suggested that light soaking changes the shape of barrier region due to a shift in the position of Fermi level and the series resistance of the device increases. Clearly these effects are small in our case.

2.9.1 (b) <u>Changes in I-V characteristics of Schottky diodes due to sensitivity of Pd on hydrogen gas</u>

I-V characteristics of a-Si:H/Pd Schottky diode change when the Palladium is exposed to hydrogen[35]. This characteristic of Pd Schottky diode which is already known for crystalline silicon has led to successful fabrication of hydrogen detector devices[36] using polycrystalline and single crystalline silicon. In the present investigation also, the I-V characteristics of a-Si:H/Pd Schottky diode are found to be sensitive to hydrogen ambient.

Results of I-V characteristics with and without the presence of hydrogen ambient are shown in Fig. 2.16. A

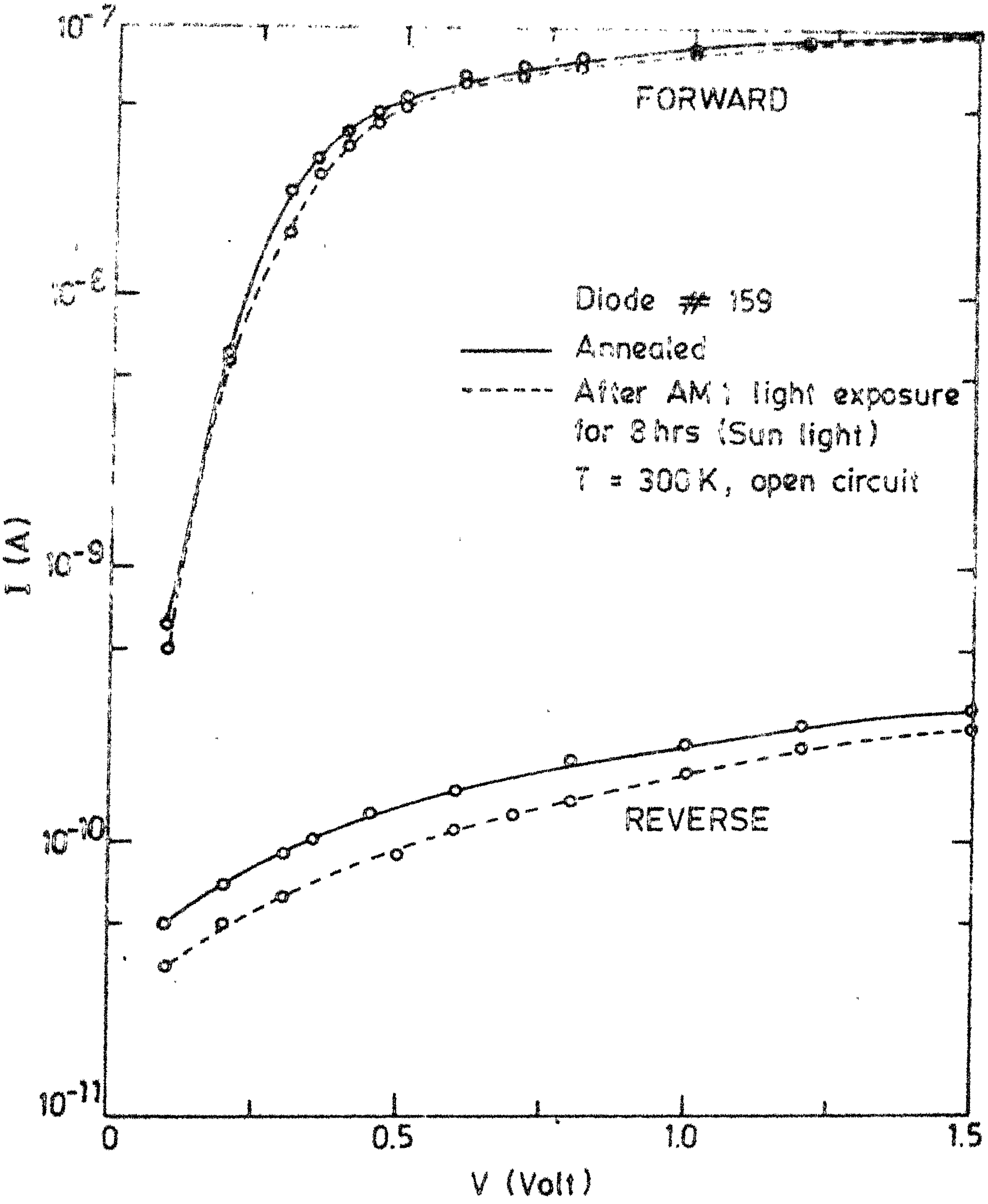

Fig.2.13 : Light induced changes (S-W effect) in a-Si:H/Pd Schottky diode

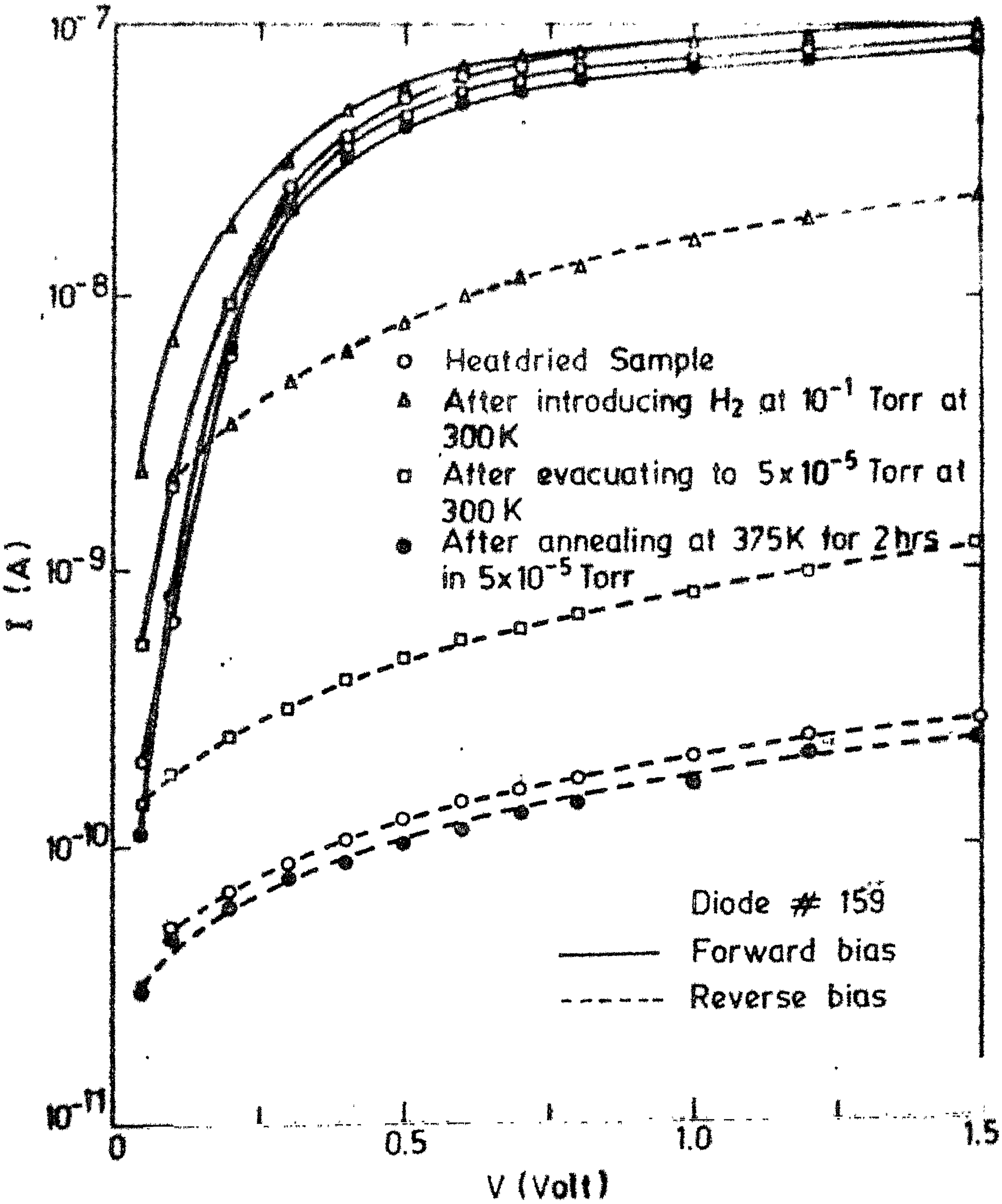

Fig. 3.16 : I-V characteristics of a-Si:H/Pd Schottky diode with and without hydrogen ambient. Notice the strong effect of hydrogen on the reverse bias characteristics

freshly heat dried diode has forward and reverse current at 1.0 V to be $\sim 9\times10^{-8}$ and $\sim 2\times10^{-10}$ A, respectively, and rectification ratio $\gtrsim 200$. After introducing hydrogen gas at 10^{-1} torr, the forward current shows a very small increase and at 1.0 V is almost unchanged. But the reverse current shows a large increase by about 2 orders of magnitude. At 1.0 V it increases to $\sim 1.6\times10^{-8}$ A, thus reducing the rectification ratio to 6. When the system is evacuated subsequently, to 10^{-5} torr, the reverse current at 1.0 V reduces to 8×10^{-10} A. The I-V characteristics are close to the heat dried state after the sample is annealed at 100°C for 2 hr in 10^{-5} torr. Heat drying completely restores the I-V characteristics.

The changes in I-V characteristics of the diode in presence of hydrogen gas can be understood in terms of the changes in the work function of Pd upon absorbing hydrogen. Hydrogen reduces the work function of Pd and as a result the barrier height Φ_B decreases[35]. This results in an increase of current in reverse bias, and reduction in rectification ratio. The reduction in the barrier height is measured by Fortunato et al[35] by photoemission experiment also. In our case the increase in reverse bias current corresponds to a decrease in Φ_B by ≈ 0.25 eV. As the system is evacuated, subsequent to the introduction of hydrogen, the gas is desorbed and Pd starts returning to its normal phase. Annealing at 100°C for about 2 hr helps Pd to return to its original

state and heat drying results in the normal I-V characteristics, before exposure to hydrogen.

This explanation may not hold if Pd forms a silicide[37] at the interface. The barrier height is expected to be higher (1.05 eV obtained by Tsai et al[37]) than in the present case ($\simeq$ 0.95 eV) if a silicide formation takes place. So we feel that either there is very little silicide formation in the present case or that it still permits the lowering of the barrier upon exposure to hydrogen.

2.10 CONCLUSIONS

Various parameters of a-Si:H, prepared at T_s 580 K are listed in Table 2.5. It is observed that these samples are amorphous in nature and contain hydrogen mostly as monohydride. Samples show σ_{dc} 5 - $6 x 10^{-8}$ $\Omega^{-1} cm^{-1}$ with $\Delta E_{\sigma} \simeq 0.60$ eV and $\sigma_o \simeq 10^3$ $\Omega^{-1} cm^{-1}$. The optical gap is found to be 1.7 - 1.9 eV. σ_{ph}(300 K) is $\simeq$ 1 - $5x10^{-4}$ $\Omega^{-1} cm^{-1}$ and is quite high. Light induced changes in our samples are small. All these parameters are comparable with those reported by various laboratories on good quality a-Si:H.

Table 2.5 : Properties of a-Si:H ($T_s \approx 580$ K)

Sl.No.	Parameters	Range
1.	σ_{dc}	$\approx 5 - 6\times10^{-8}\ \Omega^{-1}cm^{-1}$
2.	ΔE_{σ}, σ_0	≈ 0.60 eV, $10^{3}\ \Omega^{-1}cm^{-1}$
3.	σ_{ph}(300 K)	$\approx 1 - 5\times10^{-4}\ \Omega^{-1}cm^{-1}$
4.	Optical gap (E_G(300 K))	$\approx$ 1.7 - 1.9 eV
5.	Hydrogen bonding	$\approx$ Si-H, 2000 cm^{-1}
6.	Light induced changes	$\approx$ small

Parameters obtained on Schottky barriers are shown in Table 2.6 and are comparable with those reported by others. This is an indication of a small number of localized states in our samples which is confirmed by results of other experiments as discussed in chapters 3, 4 and 5.

Table 2.6 : Parameters of a-Si:H/Pd Schottky diodes

Parameters	Range of values
Barrier height (ϕ_B)	$\approx$ 0.80eV - 0.98 eV
Ideality factor (n)	$\approx$ 1.20- 1.33
Flat band voltage (V_{bi})	$\approx$ 0.20 eV - 0.35 eV
Rectification ratio (at 1.0 V)	$\approx 10^2 - 10^3$

REFERENCES

1. R.C. Chittick, J.H. Alexander and H.F. Sterling, J. Electrochem. Soc. 116 (1969) 77

2. Amorphous Semiconductors, Topics in Appl. Phys. Ser. ed. M.H. Brodsky (Springer, N.Y 1979) See Carlson and Wronski Chapter 10, p-287.

3. P.J. Zanzucchi, C.R. Wronski and D.E. Carlson, J. Appl. Phys. 48 (1977) 5227

4. S. Guha, Bull. Mater. Sci. 2 (1980) 317

5. H. Fritzsche, Bull. Mater. Sci. 2 (1980) 295; William Paul and D.A. Anderson, Solar-Energy Mater. 5 (1981) 229

6. J.C. Knights, J. Non Cryst. Solids 35, 36 (1980) 159

7. A.L. Armirotto, Solid State Techno. (1980) 43

8. Hand book of Thin Film Technology ed. L.I. Maisel and R. Glang (Mc Graw Hill, Inc., N.Y., 1970) see, R. Glang, R.A. Holmwood and J.A. Kurtz, Chapter 2 p-2-112

9. P. Kocian, J. Non Cryst. Solids 35, 36 (1980) 195

10. Amorphous and Liquid Semiconductors, ed. J. Tauc (Plenum Press N.Y. 1974 See B.G. Bagley Chapter 1 p-2

11. G. Lucovsky, R.J. Nemanich and J.C. Knights, Phys. Rev. B19 (1979) 2064

12. J.C. Knights, Jap. J. Appl. Phys. 18 (1977) 101

13. C.D. Cody, C.R. Wronski, B. Abeles, R.B. Stephans and R. Brooks, Solar Cells 2 (1980) 227

14. See, J. Tauc in Chapter 4, p 172 in ref. 10

15. C.C. Tsai and H. Fritzsche, Sol. Energy Mater. 1 (1979) 29

16. D.L. Staebler and C.R. Wronski, Appl. Phys. Lett. 31 (1977) 292

17. D.L. Staebler and C.R. Wronski, J. Appl. Phys. 51 (1980) 3262

18. K.L. Narasimhan (Private communication)

19. R.R. Arya (M.Tech. Thesis, A.C.M.S. I.I.T. Kanpur 1979, unpublished).

20. P.G. LeComber, A. Madan and W.E. Spear, J. Non Cryst. Solids 11 (1972) 219

21. Electronic Processes in Non Crystalline Materials, ed. N.F. Mott and E.A. Davis (Clarendon Press, Oxford, 1979)

22. W.E. Spear, D. Allan, P.G. LeComber and A. Ghaith, J. Non Cryst. Solids 35,36 (1980) 357

23. See ref. 2 Chapter 10,P 208

24. H. Fritzsche, Solar Energy Mater. 3 (1980) 447

25. M.H. Tanielian, Phil. Mag. 45 (1982) 435

26. W. Meyer and H. Neldel, Z. Tech. Phys. 18 (1937) 588

27. M.H. Tanielian, H. Fritzsche, C.C. Tsai and E. Symbalisty, Appl. Phys. Lett. 33 (1978) 353

28. S. Guha, K.L. Narasimhan and S.M. Pietruszko, J. Appl. Phys. 52 (1981) 859

29. S. Ashok, A. Lester and S.J. Fonash, IEEE, Electron Dev. Lett. EDL-1 (1980) 200

30. M.K. Han, W.A. Anderson, P. Sung and R. Lahri, Phys. Stat. Solidi (a) 75 (1983) 283

31. C.R. Wronski, D.E. Carlson and R.E. Daniel, Appl. Lett. 29 (1976) 602

32. S.M. Pietruszko, K.L. Narasimhan and S. Guha, Bull. Mater. Sci. 3 (1981) 157

33. D. Jousse, P. Viktorovitch, L. Vieux-Rochaz and A. Chenevas - Paule, J. Non. Cryst. Solids 35,36 (1980) 767

34. S. Guha, J. Yang, W. Czubatyz, S.J. Hudgens and M. Hack, Appl. Phys. Lett. 42 (1983) 588

35. Gugliemo Fortunato, Arnaldo D Amico and Giovanni Petrocco, J. Non Cryst. Solids 59,60 (1983) 1198

36. F. Rouths, S. Ashok, J. Fonash and J.M. Rouths, IEEE Trans. on Electron Dev. ED-28 (1981) 1003 and references therein.

37. C.C. Tsai, M.J. Thompson and R.J. Nemanich, J. Phys. (Paris) 42 (1981) C4-1077

CHAPTER 3

SCLC AND CAPACITANCE MEASUREMENTS

3.1 INTRODUCTION

The distributions of density of localized states (DOS) in a-Si:H determined by different methods do not quite agree with each other (Chapter 1). Thus, there is a need to measure DOS by as many experiments as possible on a given sample to check whether the disagreement is because of various assumptions which one makes in arriving at DOS from the different experiments or whether the samples themselves are different. Such studies have been undertaken recently[1,2]. We use well characterized Schottky diodes (area $\approx 1.1 \times 10^{-2}\,cm^2$) for determination of DOS by measurements of steady state capacitance and isothermal capacitance transient spectroscopy (ICTS) and space charge limited currents (SCLC).

Section 3.2 describes the methods of measurements. SCLC are measured as a function of temperature and results are discussed in section 3.3. Section 3.4 begins with a theory of steady state capacitance. The results of steady state $C(V)$, $C(\omega)$ and $C(T)$ measurements are discussed in section 3.4.3. ICTS measurements are described in section 3.5. The DOS obtained by different methods are compared and the assumptions involved in arriving at the DOS are spelled out explicitly in each case.

3.2 EXPERIMENTAL

SCLC, C(V), C(ω) and ICTS measurements are done in the cryostat described in section 2.7.1. The results in air as well as in vacuum are same.

For capacitance measurements, a General Radio capacitance bridge (GR 1621) is used. Care is taken to ensure that the lead capacitance is eliminated from the results. The time constant of the bridge is kept at 0.1s and ac signal at 15 mV rms.

3.3 SCLC MEASUREMENTS

One of the straight forward measurements, which can be used to obtain the DOS in a material, is the method of space charge limited currents (SCLC)[3]. In this method, the I-V characteristics of the sample are measured in the high electric field region. These non ohmic characteristics are influenced by the traps in the material and can be used to calculate the DOS. The method has been applied to obtain the DOS in a-Si:H using samples with ohmic contacts[4-6] as well as Schottky diodes in high forward bias region[7]. The results are similar. In the present investigation a Schottky diode configuration is used as this enables us to compare the results of SCLC with other experiments on the same diode.

3.3.1 Results and Discussions

For voltages greater than V_{bi}, the current in forward bias for all the diodes is found to be space charge limited

and is proportional to V^m shown in Figs. 3.1 to 3.4. For all the diodes, in general, the exponent m decreases as the temperature is increased. The values of m are shown in the respective figure, for different temperatures. A power law dependence in current is expected when the traps are distributed exponentially[3], i.e.,

$$g(E) = g_o \exp \left\{ -(E_c - E)/kT_o \right\} \tag{1}$$

where T_o is a parameter characterizing the trap distribution[3]. For such a distribution of traps and a homogeneous material, the current voltage relationship is shown to be[3]

$$I = C \frac{V^{l+1}}{d^{2l+1}}, \quad l = m-1 \tag{2}$$

with C being a constant and d is spacing between electrodes.

Eq. (2) predicts a straight line for a logarithmic plot of current and voltage. But, in general, lnI vs lnV plots have not been observed to be straight lines[4-6]. However, attempts have been made to calculate the DOS by fitting a straight line in a limited region of the plot[4,5]. Although, the DOS calculated in this manner are comparable to that obtained by other measurements[4,5], the procedure is questionable. This is because the temperature dependence of exponent l given by

$$l = T_o/T \tag{3}$$

is not obeyed as the plots of l vs 1/T do not yield straight

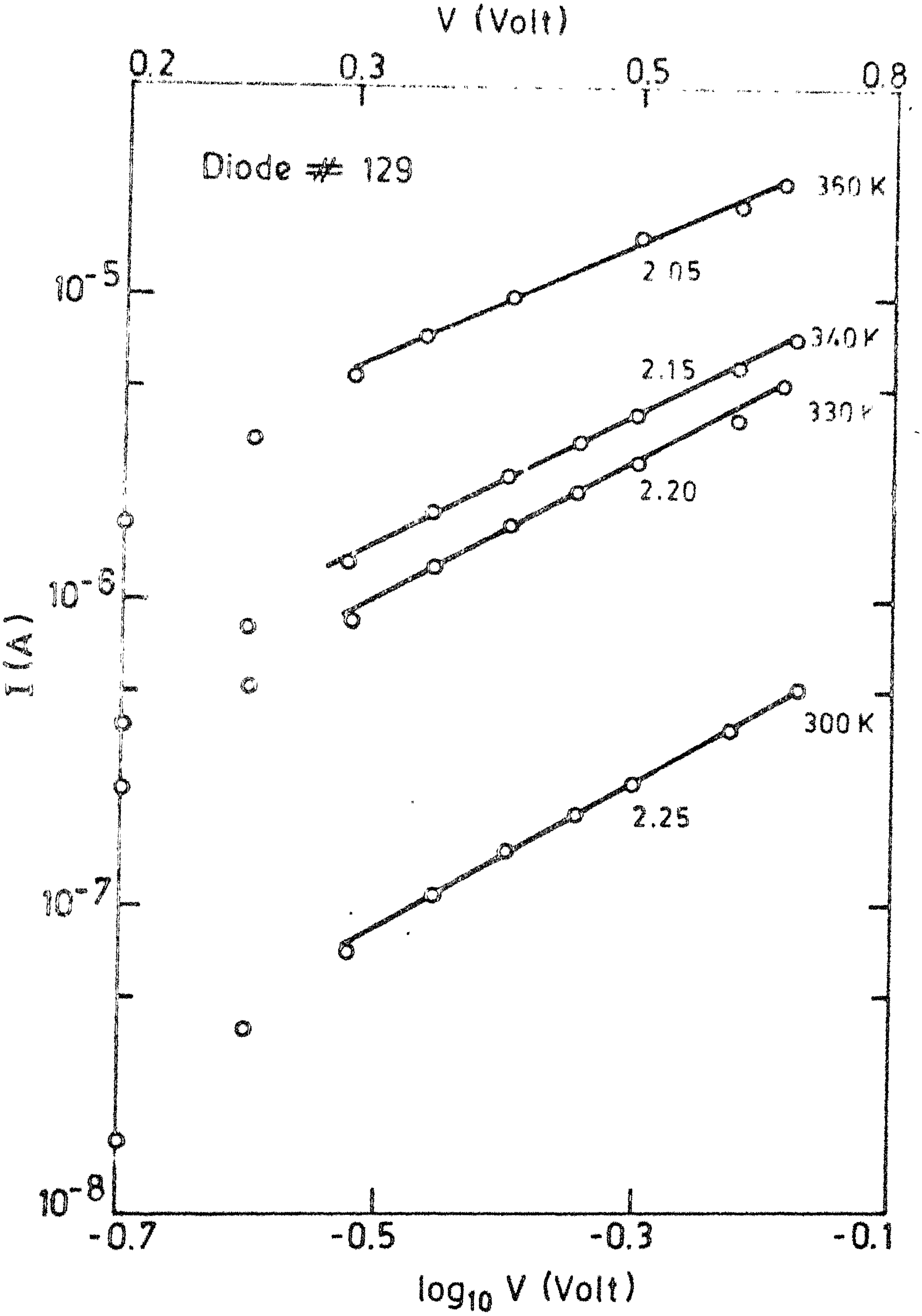

Fig. 3.1 : Logarithmic plots of I-V characteristics of a-Si:H/Pd Schottky diode # 129 at different temperatures, as indicated

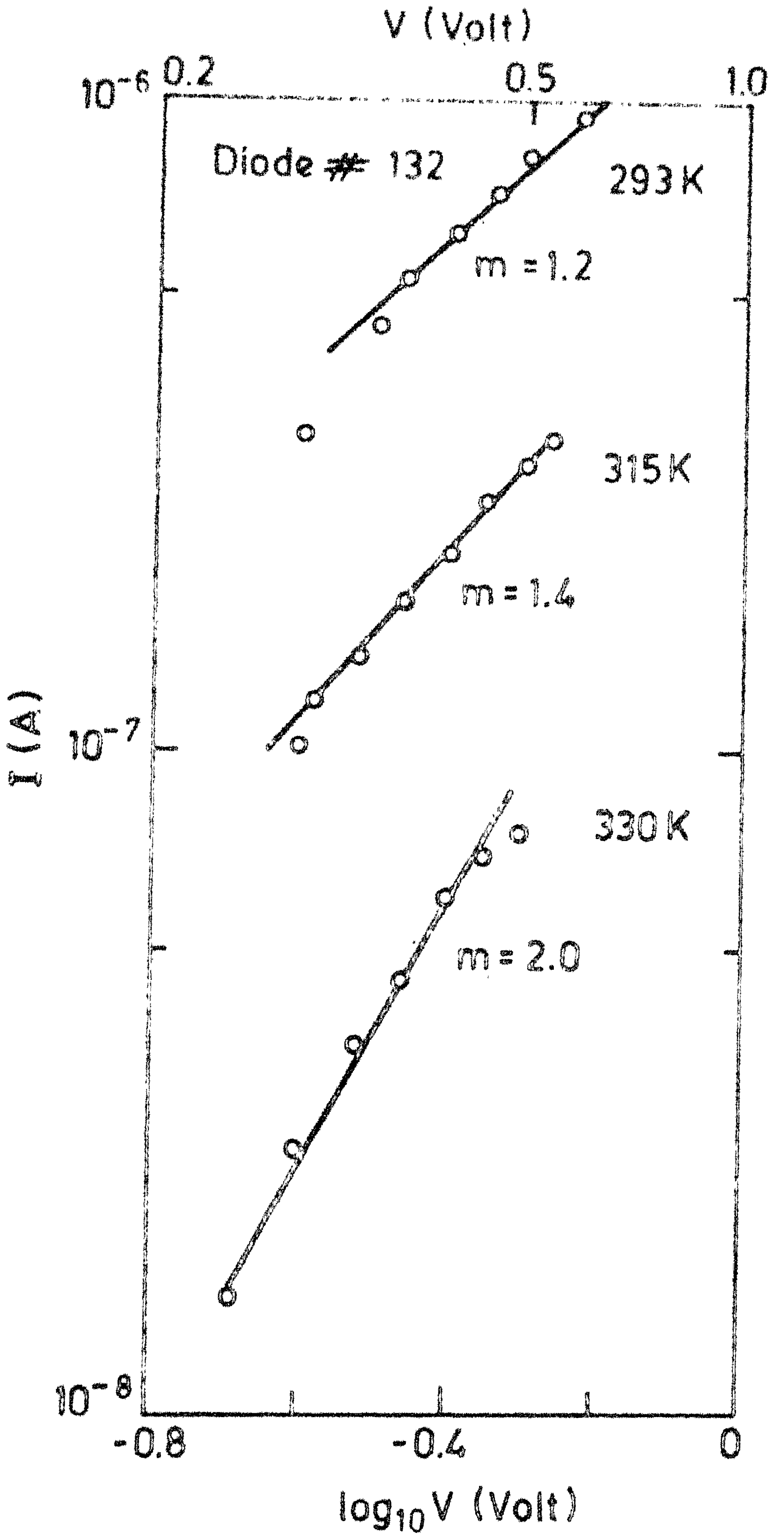

Fig.3.2 : Logarithmic plots of I-V characteristics of a-Si:H/Pd Schottky diode # 132 at different temperatures, as indicated

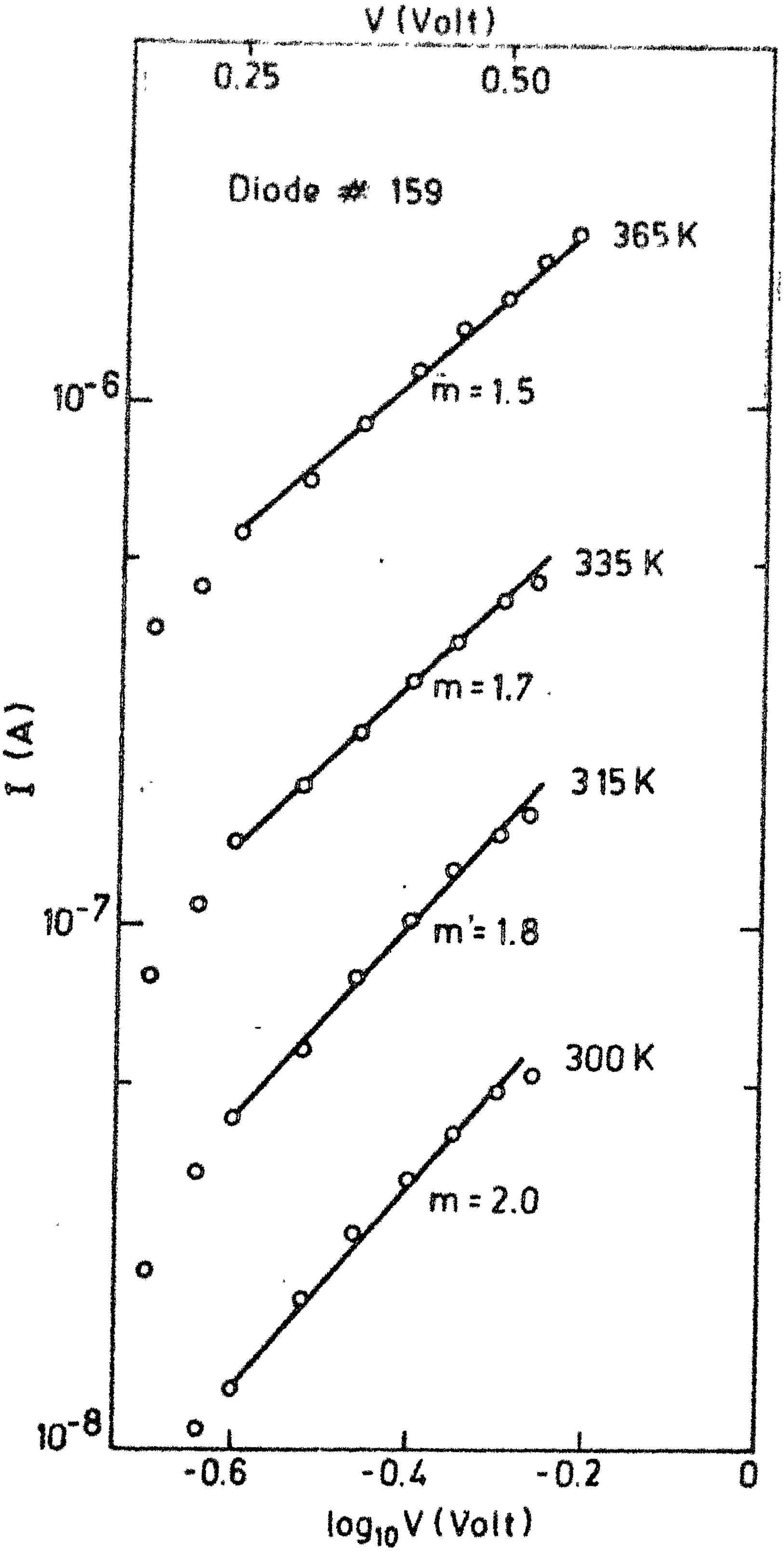

Fig. 3.3 : Logarithmic plots of I-V characteristics of a-Si:H/Pd Schottky diode # 159 at different temperatures, as indicated

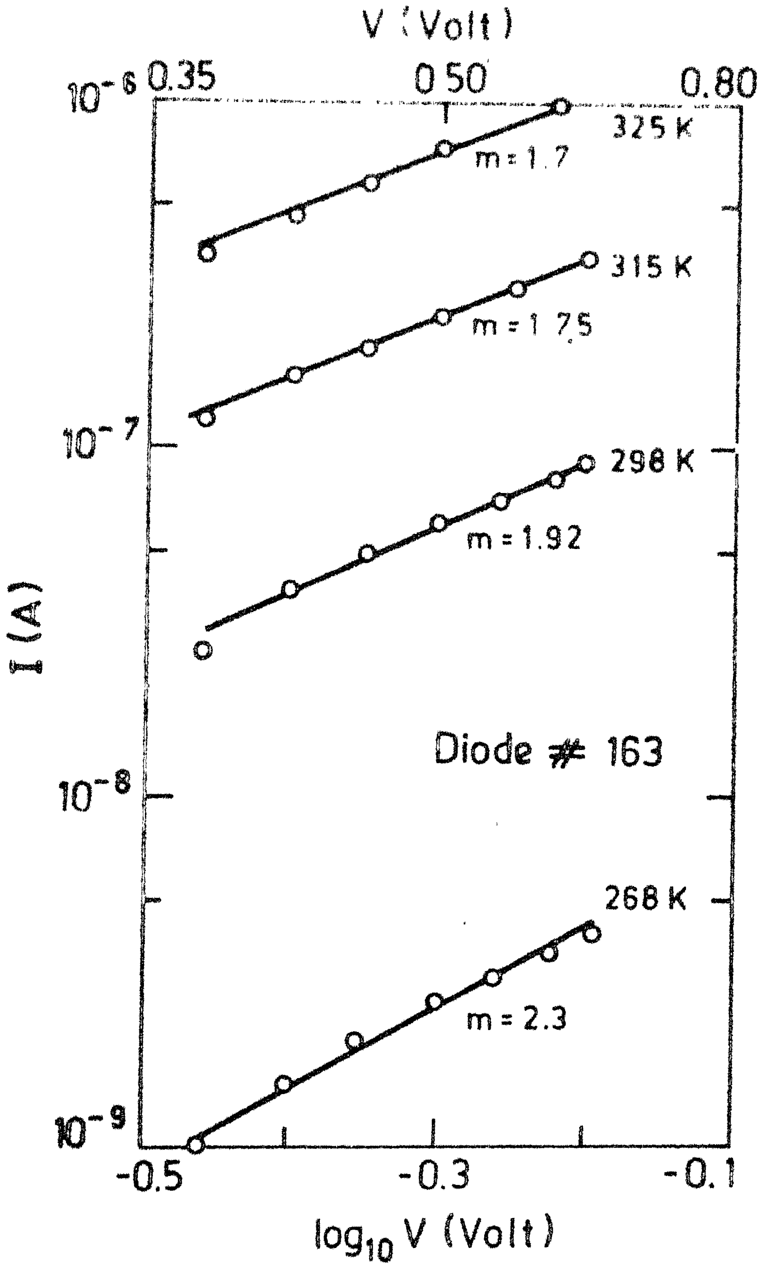

Fig. 3.4 : Logarithmic plots of I-V characteristics of a-Si:H/Pd Schottky diode # 163 at different temperatures, as indicated

lines passing through origin. The data from various laboratories is plotted in Fig. 3.5 to illustrate this point. The only exception appears to be the data of Ashok et al[7]. But, even in this case, the error bars are too large to say, with confidence, that Eq. (3) is obeyed[8].

If a constant distribution, $g(E) = g_o$ is assumed, the current is related to voltage as follows[3]

$$I(V) \quad = \quad kV \exp(2 \epsilon V/q \; g_o kTd^2 \qquad (4)$$

where K is a constant and ϵ is the dielectric permittivity of a-Si:H.

If we plot our data as ln(I/V) vs V for various fixed temperatures, we find that these are not straight lines in contrary to Eq. (4). Although Bhattacharya et al[6] find ln(I/V) vs V plots to be straight lines at various temperatures, the temperature dependence of the slope (S), which is given by

$$S \quad = \quad 2 \epsilon /qg_o kTd^2 \qquad (5)$$

is not obeyed.

Thus, it appears that neither a constant nor an exponential distribution of states can explain the SCLC data. Further, Bhattacharya and Narasimhan[9] have shown, that for several other distributions (including a gaussian and a sum of exponentials) also, $I \propto V^{l+1}$ with $l \propto 1/T$ thus

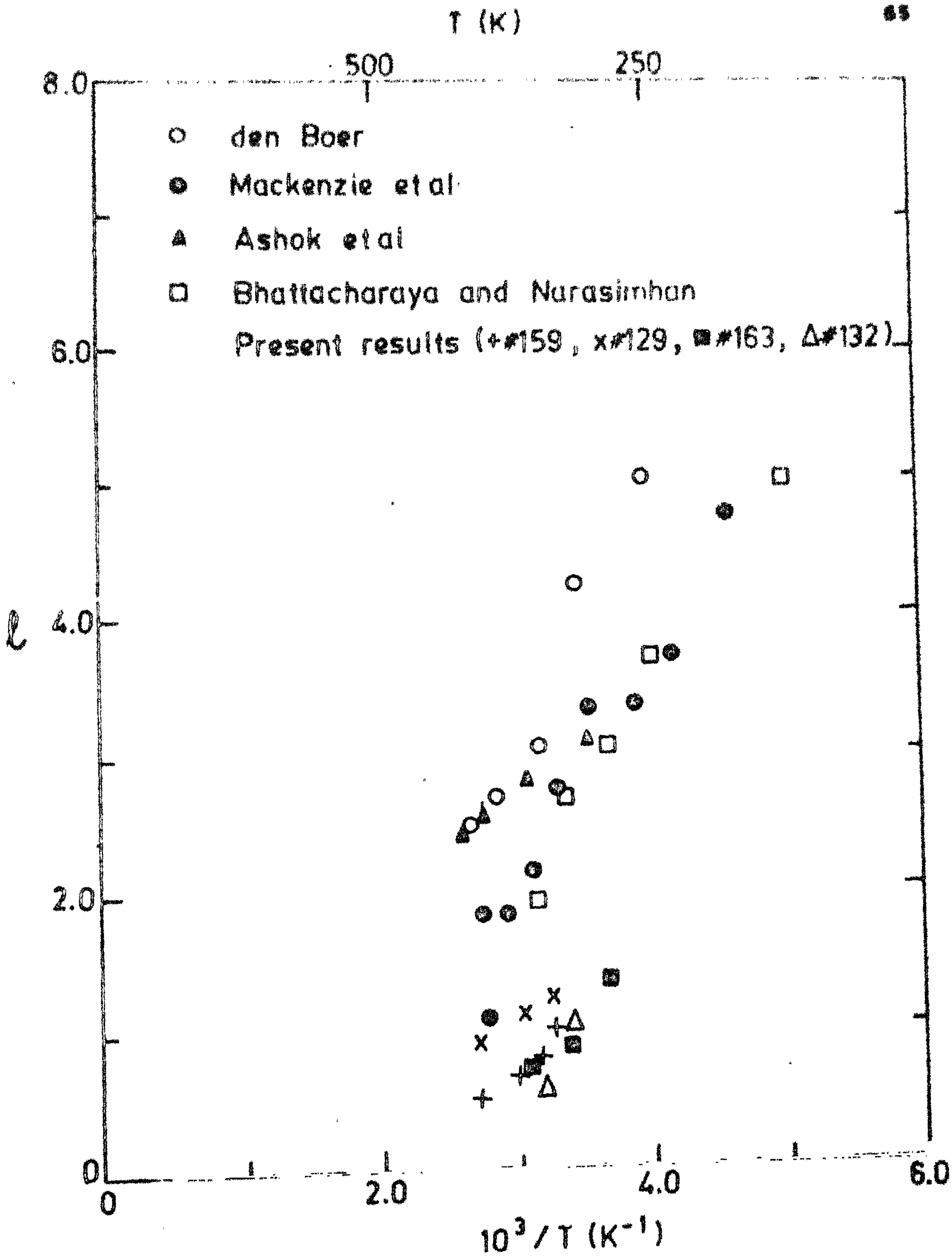

Fig.1.5 : Plots of l vs 10^3/T from different laboratories; (i)○ denBoer[3] (ii) ● Mackenzie et al[4] (iii) □ Bhattacharya and Narasimhan[9] (iv)▲ Ashok et al[7]. Note that the data from individual groups can not be fitted to a straight line passing through origin

making it impossible to distinguish between them by such arguments. As such, none of these distributions can be justified for calculating the DOS, since 1 does not have the proper temperature dependence.

In this context, the method suggested by denBoer[5] appears to be more appropriate for calculating the DOS. In this method, although the spatial variation in the DOS is neglected, no particular distribution in energy is assumed a priori. When the voltage across the sample is changed from V_1 to V_2 ($V_2 - V_1 = \Delta V$), the quasi Fermi level (E_{fn}) moves by an amount ΔE_{fn}, given by

$$\Delta E_{fn} = kT \ln(I_2 V_1 / I_1 V_2) \qquad (6)$$

Also assuming that all the injected charge goes to the traps, we can write Q_t (injected charge per unit area for a change in voltage ΔV),

$$Q_t = \frac{\chi \epsilon \Delta V}{d} = dq \int_{E_{fn}}^{E_{fn} + \Delta E_{fn}} g(E)\, dE = dq\, g(E)\, \Delta E_{fn} \qquad (7)$$

where χ is a constant assumed to be 2.0 to account for the non uniformity of the space charge[3]. The last step follows, if ΔV is chosen to be sufficiently small, so that g(E) can be taken to be constant between E_{fn} and $E_{fn} + \Delta E_{fn}$. Eqn (7) gives the DOS for small step as

$$g(E) = \frac{\chi . \epsilon \Delta V}{qd^2 \Delta E_{fn}} \qquad (8)$$

The DOS for various diodes deduced from SCLC measurements are shown in Table 3.1. In some samples Fermi level could not be shifted significantly to obtain DOS for energies other than E_F. However, for diode 129 the DOS could be determined from 0.6 eV to 0.56 eV below E_c and are plotted in Fig. 3.6 for different temperatures. This plot is comparable to that obtained by Mackenzie et al.[4] It can be said on the basis of these results that the DOS obtained for different temperatures are within reasonable agreement and also the DOS increases as one moves towards E_c.

3.4 STEADY STATE CAPACITANCE MEASUREMENTS

3.4.1 Static Capacitance of a-Si:H Schottky Diodes :

Capacitance measurements on Schottky diodes have proved useful in determining density of donors and acceptors in crystalline semiconductors[10,11]. In a-Si:H, since the space charge comes mainly from the localized states, the measurement of static capacitance on Schottky barriers can be used to obtain the DOS, as shown below.

Figure 3.7 shows the metal/a-Si:H Schottky barrier with a reverse bias V_R. The Fermi level is assumed to be flat throughout the depletion region. This assumption, although true at zero bias, may not be justified in the presence of a reverse bias. In reverse bias, a splitting of Fermi level will take place and the position of the quasi Fermi levels will be governed by the caputre and emission

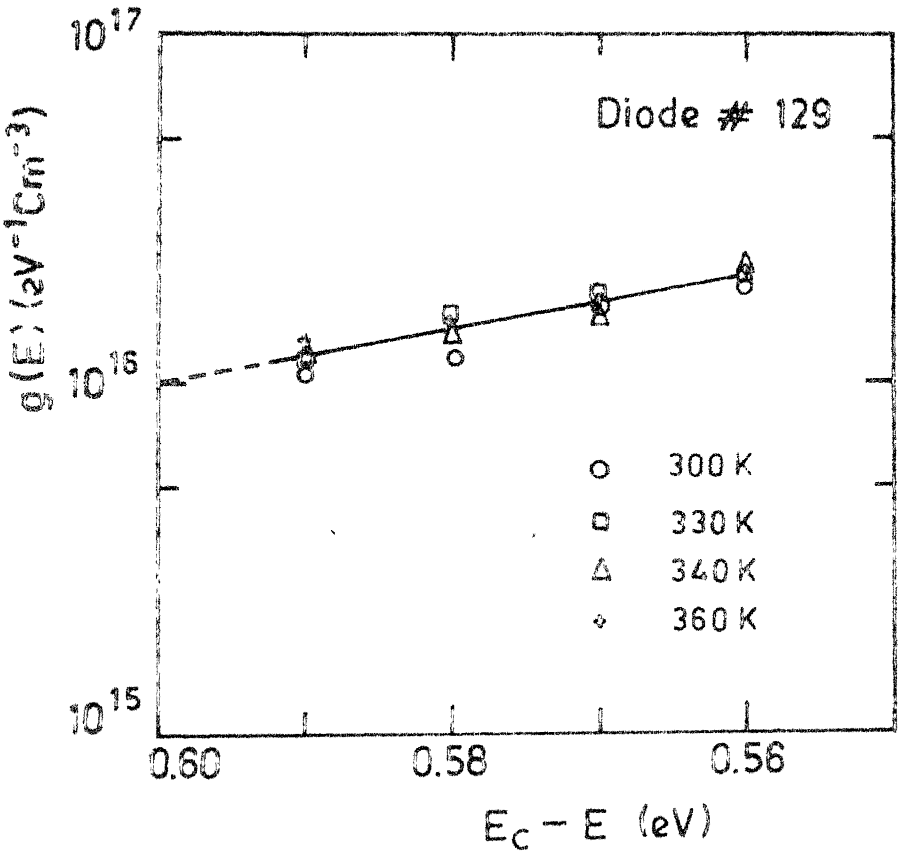

Fig.3.6 : DOS obtained at different energies using denBoer's method (# 129, ○ T = 300 K, □ T = 330 K, △ T = 340 K, ◇ T = 360 K)

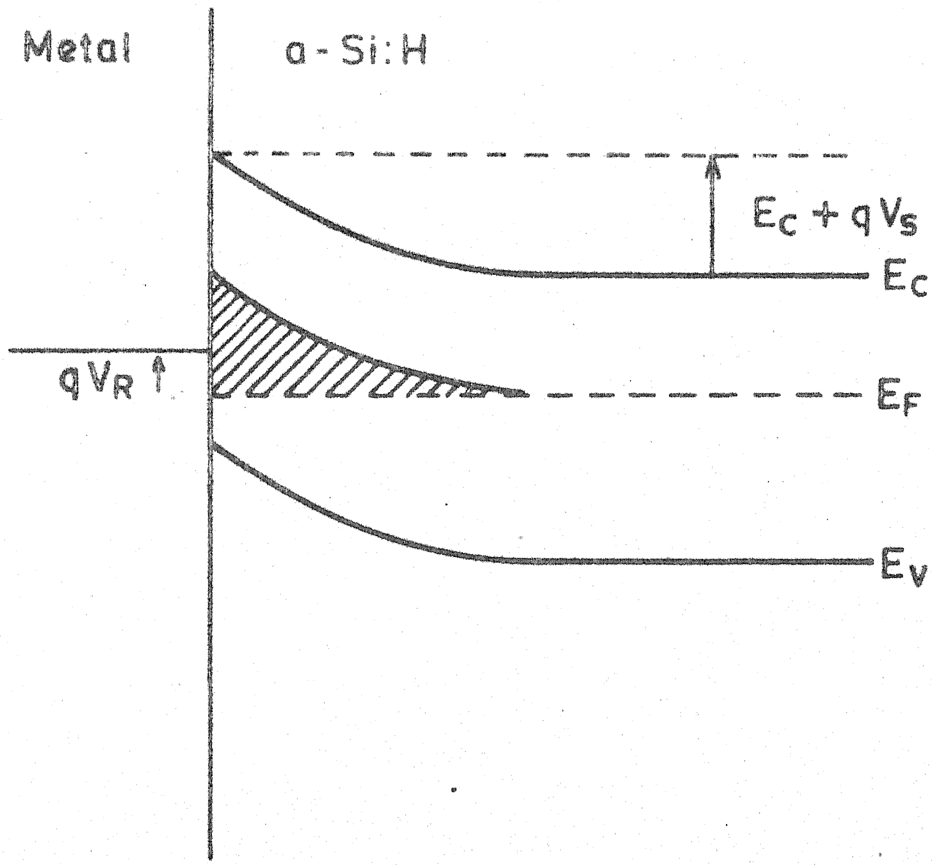

Fig.3.7 : Band diagram of a-Si:H/Pd Schottky barrier. Shaded area shows the space charge region

mechanism of the carriers in the localized states. However, we have assumed a flat Fermi level, even in presence of reverse bias, for the reasons of simplicity and because the capture cross sections are not yet known, with confidence, in this material. The electrostatic potential in the depletion region is denoted by V(x) where x is the distance from the metal/semiconductor interface. The energy of electron at the edge of conduction band (E_c) in depletion region is taken to be $E_c(x) = E_c + qV(x)$. At the interface the conduction band is at $E_c + q\,V_s$, where V_s is the sum of V_{bi} and V_R. It should be noted that V(x) is actually negative for upward band bending, whereas we have treated it as though it were positive. Accordingly, the one dimensional Poisson's equation is given as

$$\frac{\partial^2 V(x)}{\partial x^2} = \frac{\rho(x)}{\epsilon} \tag{9}$$

where $\rho(x)$ is the space charge density in the depletion region. As depicted by shaded area in Fig. 3.7, it comes mainly from those localized states whose occupancy has changed on account of having been pulled above the Fermi level. Neglecting the free carrier contribution, which is likely to be small, $\rho(x)$ is given by

$$\rho(x) = q \int_{-\infty}^{\infty} \left[f(E, E_F, T) - f(E, E_F - qV(x), T) \right] g(E, x)\, dE \qquad \ldots(10)$$

Using zero temperature statistics, f(E) becomes a step function[12], and if g(E,x) is assumed to be independent of x, Eq. (10) reduces to

$$\rho(x) = q \int_{E_F - qV(x)}^{E_F} g(E)\, dE \qquad (11)$$

Here, although approximating f(E) by a step function is not likely to cause much error, taking g(E,x) independent of x may not be justified. Besides neglecting heterogeneities, this also implies that the states at the surface have the same distribution as in the bulk.

With $\rho(x)$ given by Eq. (11), the Poisson's equation (9), when integrated with the boundary conditions,

$$V(0) = V_s, \quad V(\infty) = 0 \quad \text{and} \quad \left.\frac{\partial V}{\partial x}\right|_{x=\infty} = 0 \qquad (12)$$

yields

$$\left(\frac{\partial V}{\partial x}\right)_{V=V_x} = -\left[\frac{2q}{\epsilon}\int_0^{V_x}\int_{E_F-qV}^{E_F} g(E)\, dE\, dV\right]^{1/2} \qquad (13)$$

where $V_x = V(x)$ and the negative sign is chosen for consistency.

Eq. (13) can be integrated once again to give

$$x = \int_{V_x}^{V_s} \frac{dV'}{\left[\frac{2q}{\epsilon}\int_0^{V'}\int_{E_F-qV}^{E_F} g(E)dE\, dV\right]^{1/2}} \qquad (14)$$

The static barrier capacitance per unit area at $\omega = 0$, $C(0,V_s)$, is defined to be

$$C(0,V_s) = \frac{dQ}{dV_s} \tag{15}$$

The total charge Q in the depletion region is given by

$$Q = \int_0^{\infty} \rho(x)\, dx = \epsilon \int_0^{\infty} \frac{\partial^2 V}{\partial x^2}\, dx = -\epsilon \left(\frac{\partial V}{\partial x}\right)_{V=V_s} \tag{16}$$

where Eqs. (9) and (12) have been used.

Combining Eqs. (13), (15) and (16), we obtain the expression for the static capacitance

$$C(0,V_s) = \frac{\left(\frac{q\epsilon}{2}\right)^{1/2} \int_{E_F-qV_s}^{E_F} g(E)\, dE}{\left[\int_0^{V_s} \int_{E_F-qV}^{E_F} g(E)\, dE\, dV\right]^{1/2}} \tag{17}$$

This can be inverted, using Eq. (15), to obtain the DOS as follows

$$Q = \int_0^{V_s} C(0,V)\, dV \tag{18}$$

Using Eqs. (13), (16) and (18)

$$\int_0^{V_s} \int_{E_F-qV}^{E_F} g(E)\, dE\, dV = \frac{1}{2q\epsilon} \left[\int_0^{V_s} C(0,V) dV\right]^2 \tag{19}$$

Upon operating with $\frac{d^2}{dV_s^2}$, Eq. (19) gives the DOS in terms of static capacitance as

$$g(E-qV_s) = \frac{1}{q\varepsilon}\left[(C(0,V_s))^2 + \int_0^{V_s} C(0,V)dV \frac{dC(0,V_s)}{dV_s}\right] \quad \ldots \quad (20)$$

Thus, in principle, a knowledge of static capacitance allows one to obtain the DOS[13].

Normally, in Schottky diodes on crystalline semiconductors, upon measurements at high frequencies, a low value of the capacitance, equal to the geometrical capacitance, is obtained. As the frequency of measurement is lowered, the capacitance increases as the localized states (which are donors and acceptors) respond. The capacitance saturates at frequencies which are low enough, to allow the response from all the states. This is, then the static value of the capacitance. However, in the case of undoped a-Si:H diodes, no saturation of capacitance at low frequencies has been observed, although the measurements have been made upto frequencies as low as 10^{-3} Hz[14]. From the estimates of response time of the deepest states, one expects to reach the saturation of the capacitance below 10^{-5} Hz[15]. Measurements at such low frequencies are difficult to perform and, in the absence of the knowledge of static capacitance, the analysis described above can not be directly applied. This difficulty is further complicated by the fact that a-Si:H

is a high resistivity material and therefore, the dielectric relaxation effects start affecting the results, at forward biases $\gtrsim V_{bi}$. The latter difficulty is overcome by making measurements in the zero or reverse bias configuration. This ensures that the barrier resistance will remain higher than the bulk. The problem related with the inability to measure the static capacitance has been taken up by several authors[15,16,17]. The approach is similar for all of them and allows one to obtain the DOS near Fermi level from the low frequency capacitance data without having to reach a saturation. We describe below, briefly, the model and point out the equivalence of the results obtained by various authors, referred to above.

3.4.2 DOS From Low Frequency Capacitance

In a Schottky barrier, the separation between conduction band and the Fermi level, in depletion region, progressively increases as one moves from the bulk towards the metal/semiconductor interface. The time constants(τ) of states at the Fermi level in the depletion region are given as

$$\tau = \tau_o \exp \left\{ (E_c(x)-E_F)/kT \right\}, \quad E_c(x) = E_c + qV(x) \qquad (21)$$

where $\tau_o = 1/\nu$, ν being the attempt to escape frequency, usually chosen to be the phonon frequency ($\approx 10^{14}$ Hz). Thus the states, lying closer to the interface in the depletion region, have longer time constants, and by lowering the

frequency of measurement (ω) one probes the states at the Fermi level closer to metal/semiconductor interface. In particular, for any frequency ω there exists a x_c where the condition $\omega\tau = 1$ is satisfied and, for distances x greater than x_c, $\omega\tau \ll 1$. This means that most of the states, at the Fermi level, lying beyond $x > x_c$ are able to follow the modulation at this frequency. For distances $x < x_c$ $\omega\tau \gg 1$ and a majority of the states at the Fermi level, lying in this region, is unable to respond to the modulation. In the intermediate region, the states around x_c respond only partially to the modulation. However, the change over from responding to non-responding region is expected to be fairly rapid since τ depends exponentially on the energy difference between the Fermi level and the conduction band.

Thus, the measured capacitance $C(\omega, V_s)$ can be thought of consisting of the two capacitors in series

$$C_{<x_c} = \frac{\epsilon}{x_c} \qquad 0 \leqslant x \leqslant x_c \tag{22}$$

and

$$C_{>x_c} = C(0, V_c) \qquad x_c \leqslant x \leqslant W \tag{23}$$

where $V_c = V(x_c)$ and W is the width of depletion region.

The resultant capacitance is given by,

$$C^{-1}(\omega, V_s) = C^{-1}_{<x_c} + C^{-1}_{>x_c} = \frac{\epsilon + x_c\, C(0,V_c)}{\epsilon\, C(0,V_c)} \tag{24}$$

where x_c and $C(0, V_c)$ are given by Eqs. (14) and (17).

The value of qV_c can be deduced from Eq. (21) with the condition $\omega\tau = 1$ and is

$$q\, V_c \;=\; \left[kT \ln \frac{1}{\omega \tau_o} - \Delta E_F\right] \qquad (25)$$

$\Delta E_F = E_c - E_F$ in the bulk of the semiconductor.

Eq. (24) is a general relation obtained for the capacitance of a-Si:H Schottky diode without assuming any particular shape for the energy distribution of DOS. The expressions of the capacitance for various types of distributions can be deduced from Eq. (24) with the help of Eqs. (14), (17) and (25). Before giving any explicit expressions for some simple distributions, the limitation of the above formulation is discussed.

This analysis is valid, only in a limited range of bias, as high forward and reverse biases may lead to other effects not considered here. A forward bias approaching the flat band condition might result in injection of electrons. In addition the contribution from the states near the interface might also become significant[14]. On the other hand, at large reverse biases, an accumulation of holes near the interface may take place. These effects will modify the space charge and have not been taken into account in Eq.(11). Also the relaxation effects would become more dominant in large reverse bias, and one may have to work at lower frequencies, to get any response from the space charge region[16].

(a) Uniform distribution

For a uniform distribution of density of states ($g(E)=g_o$) the values of x_c and $C(o,V_c)$ are obtained with the help of Eqs. (14) and (17), to be

$$x_c = L_o \ln \frac{V_s}{V_c} \tag{26}$$

$$C(o,V_c) = \epsilon / L_o \tag{27}$$

and

$$L_o = (\epsilon / q^2 g_o)^{1/2} \tag{28}$$

Substitution of these values of x_c and $C(o,V_c)$, in Eq. (24) yields

$$C(\omega,V_s) = \frac{\epsilon}{L_o + L_o \ln \frac{V_s}{V_c}} \tag{29}$$

Using Eq. (29) along with Eq. (25), the following expression for the capacitance $C(\omega,V_s)$ is obtained

$$C(\omega,V_s) = \frac{\epsilon}{L_o}\left[1 + \ln \frac{q\ V_s/kT}{\ln \frac{1}{\omega\tau_o} - \frac{\Delta E_F}{kT}}\right]^{-1} \tag{30}$$

At zero bias, if ω_o is the frequency corresponding to the time constants of the states at the Fermi level located near the starting point of the depletion region, i.e., $x_c(\omega = \omega_o) = W$ and $qV_c(\omega = \omega_o\ ,\ x_c = W) = kT$, the expression

for V_c for any frequency $\omega < \omega_o$ is

$$q\,V_c = kT \ln\left(\frac{\omega_o}{\omega}\right) + 1 \qquad (31)$$

Substitution of V_c (Eq. (31) in Eq. (29) yields the relation obtained by Viktorovitch and Moddel[15]

$$C(\omega) = \frac{\epsilon}{L_o}\left[1 + \ln \frac{q\,V_{bi}/kT}{\ln(\omega_o/\omega) + 1}\right]^{-1} \qquad (32)$$

The temperature dependence of the capacitance using Eq. (30) can be written as :

$$C^2(T)\left(\frac{\partial C(T)}{\partial T}\right)^{-1} = \frac{\epsilon}{L_o}\,(T - T_o) \qquad (33)$$

where $T_o = \Delta E_F/k \ln \frac{1}{\omega \tau_o}$ and is the freeze on temperature, i.e., the temperature at which the states in depletion region start responding.

(b) g(E) varying slowly with energy

The DOS can be expanded around E_F, using Taylor's series expansion[18] as follows

$$g(E) = g(E_F) + \left.\frac{\partial g(E)}{\partial E}\right|_{E=E_F} (E_F - E) + \left.\frac{\partial^2 g(E)}{\partial E^2}\right|_{E=E_F} \frac{(E_F - E)^2}{2} + \ldots$$
$$\ldots \qquad (34)$$

If the energy dependence of g(E) is weak near $E = E_F$, the first two terms suffice. Dropping higher order terms and using Eq. (34) along with Eqs. (14), (17) and (24), the

expression for temperature dependence is :

$$C^2(T)\left(\frac{\partial C(T)}{\partial T}\right)^{-1} = \frac{\epsilon}{L_o}\left[(T-T_o) + \frac{1}{3g(E_F)}\left.\frac{\partial g(E)}{\partial E}\right|_{E=E_F}(T-T_o)^2 k \ln\frac{1}{\omega\tau_o}\right] \quad \ldots (35)$$

This expression does not depend on the applied bias and is equivalent to the relation obtained by Cohen and Lang[19].

(c) Exponential distribution

For exponential distribution of states, we have, $g(E)$ given by Eq. (1) and quantities x_c and $C(o,V_c)$, in the limit $\frac{q\,V_c}{kT_\varnothing} < 1$, are given as :

$$x_c = L_o \exp(\Delta E_F/2kT_\varnothing) \ln\frac{V_s}{V_c} \quad (36)$$

$$C(o,V_c) = \frac{\epsilon}{L_o}\exp\left\{-(\Delta E_F)2kT_O\right\}\left[1 - \frac{q\,V_c}{2kT_o}\right] \quad (37)$$

For the derivation of Eq. (36) and (37), the Eq.(1) has been used with Eqs. (14) and (17). The expressions for capacitance $C(\omega,V_s)$ can be obtained using Eqs. (24) and (25).

3.4.3 Results and Discussion of Steady State Capacitance Measurements

(a) C-V measurements

The results of C-V measurements on various diodes at

10 Hz and 300 K are shown in Figs. 3.8 and 3.9. These data are taken after waiting sufficiently at each bias to avoid transient effects described later (section 3.5).

C-V curves shown in Figs. 3.8 and 3.9 have a peak around 0.1 V for all the diodes. Such a peak has also been reported by others[14,15,20]. However, the origin of peak has still not been fully understood. Viktorovitch and Moddel[15] attribute the peak to a barrier present at the back contact. Snell et al[20] have, however, used n^+ a-Si:H at the back contact and still observe the peak. They feel that the peak appears when the barrier resistance at forward bias becomes comparable to the bulk resistance. At high forward biases, a further increase in the capacitance might be indicative of the charge injection or the contribution from the surface states as discussed in the previous section. The contribution from the surface states seems to be present in C-T measurements, as described in section 3.4.3(c).

For determination of the DOS from C-V measurements, the experimental values of the capacitance are fitted to the theoretically calculated ones using exponential and constant distributions of DOS. The parameters used to obtain the best fit are shown for different diodes in their respective figure. As is evident from Figs. 3.8 and 3.9, the observed C-V response can be fitted qualitatively using exponential as well as constant distribution. This is in agreement with Cohen and Lang[19] who observe that the

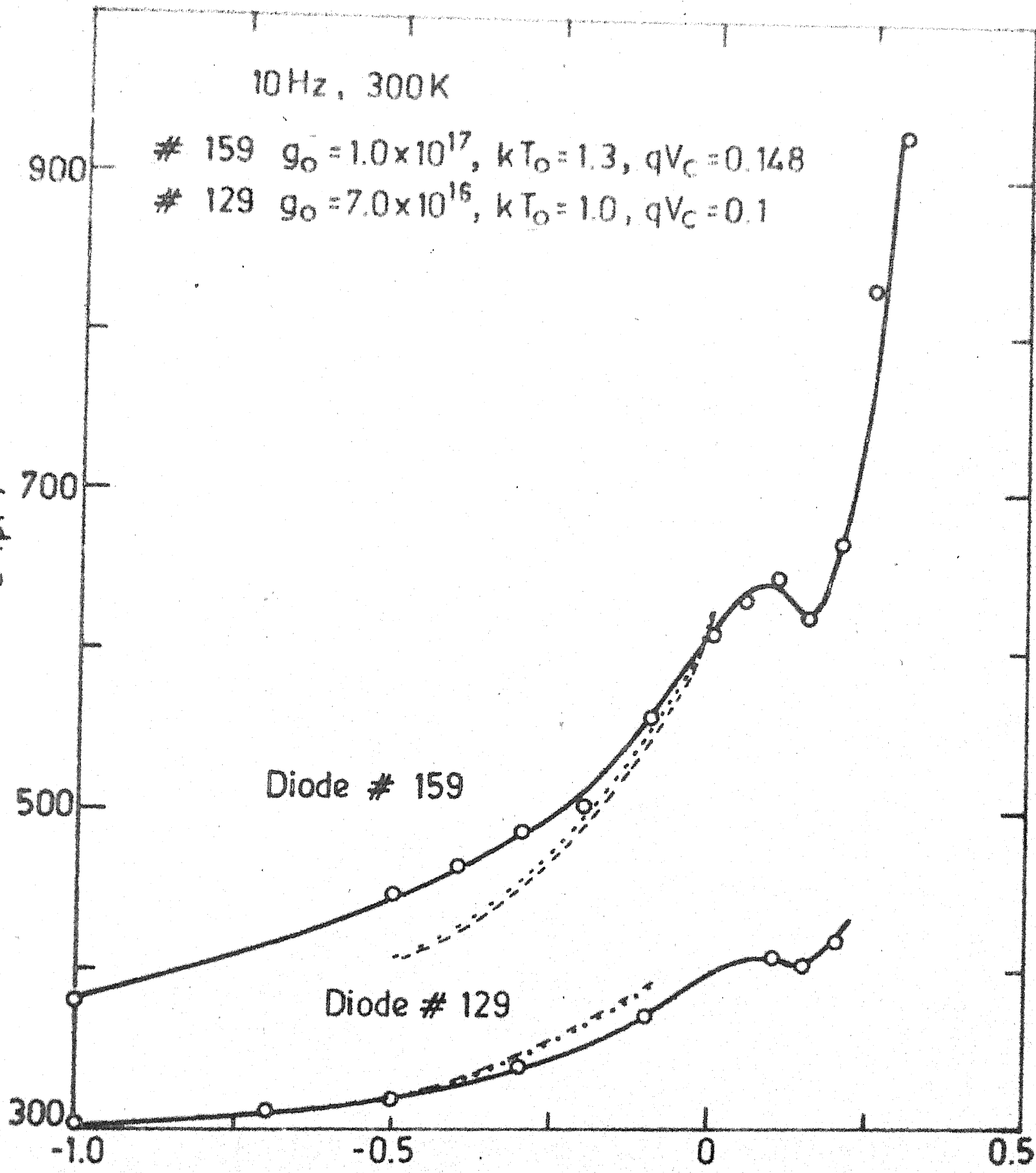

Fig.3.8 : Capacitance-voltage characteristics of a-Si:H/Pd Schottky diodes at 300 K and 10 Hz of # 129 and 159. Dashed and dotted lines are fits of experimental data to exponential and constant distributions of DOS (Parameters used for fitting the data are also listed).

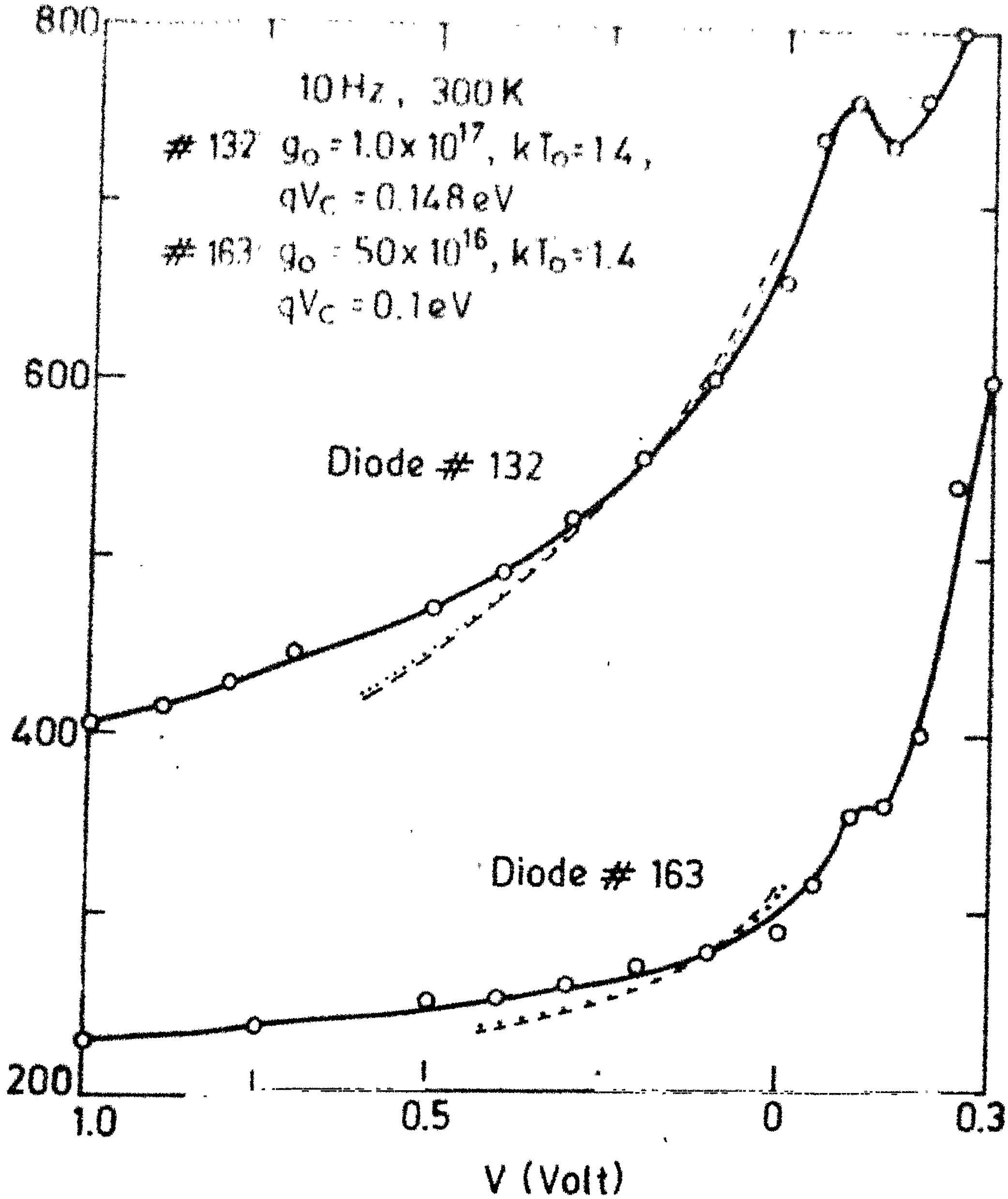

Fig.3.9 : Capacitance-voltage characteristics of a-Si:H/Pd Schottky diodes (# 132 and 163) at 300 K and 10 Hz. Dashed and dotted lines are fits of experimental data to exponential and constant distributions of DOS (Parameters used for fitting the data are also listed)

theoretically calculated C-V response of the diodes, for various distributions is essentially same. The DOS at Fermi level deduced from these results are listed in Table 3.1.

(b) C-ω measurements

The frequency dependence of all the diodes studied is investigated at 300 K and for the zero applied bias. The frequencies of the modulating signal are varied in the range $10 \leqslant \omega \leqslant 10^4$ Hz and the magnitude of the signal is = 15 mV (rms). The results of C-ω measurements on the diodes are shown in Figs. 3.10 to 3.13. With decreasing frequencies, the capacitance increases and does not saturate upto the lowest frequency of measurement (10 Hz in this case). Capacitance, in the high frequency region, decreases and levels off at the geometrical capacitance of the sample. The results on other diodes show similar trend and are in agreement with others[14,15].

To obtain the DOS from the low frequency capacitance data, the experimental values of capacitance upto the frequency ~ 50 Hz are fitted to Eq.32. The best fits between the experiment and theory for all diodes are shown in the insets of respective figure. The parameters L_o and ω_o which give the best fit are listed in the insets and also in Table 3.1. Using L_o from these data, and Eq. (28), the DOS near Fermi level is obtained. The DOS near E_F obtained

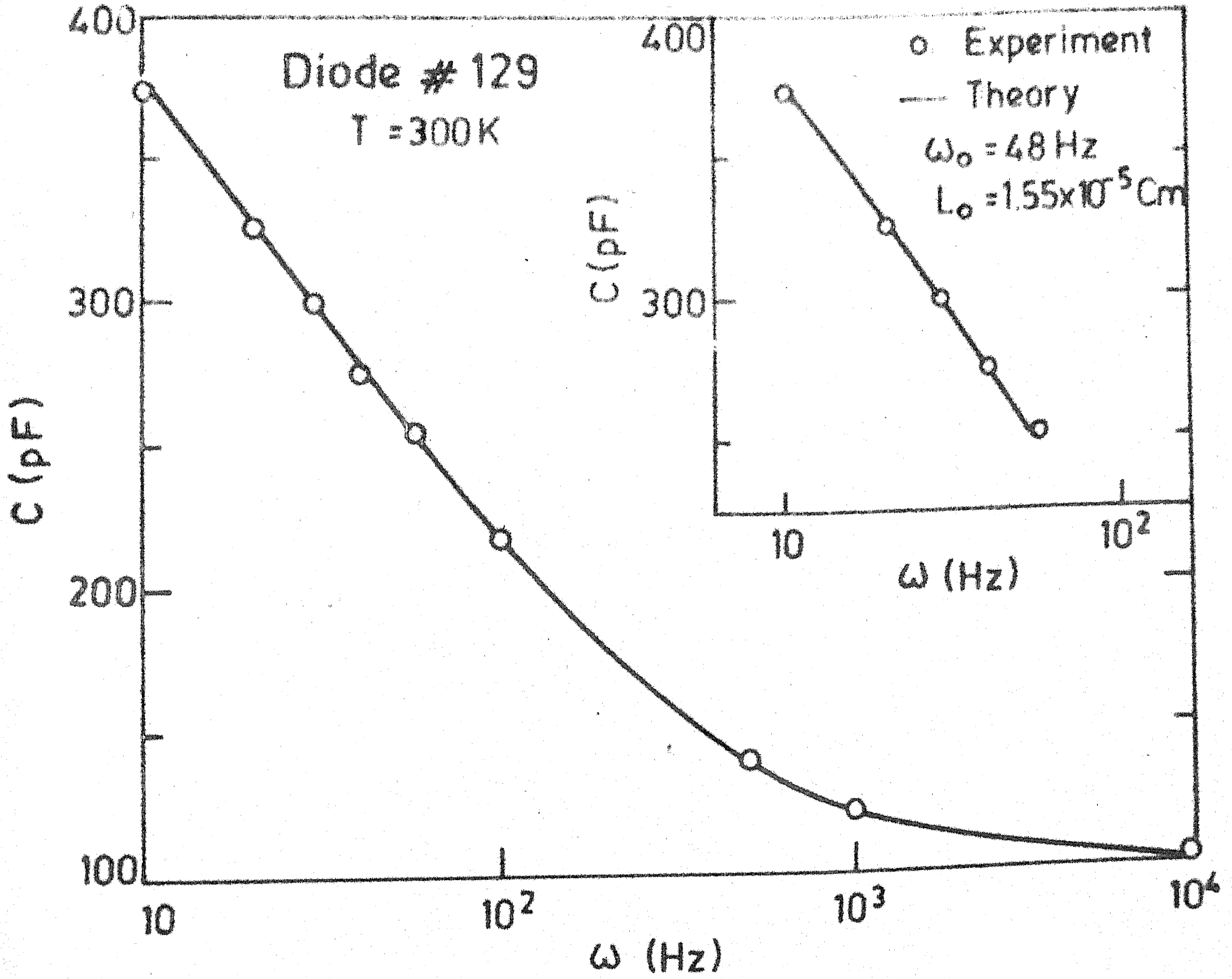

Fig.3.10 : Frequency dependence of zerobias capacitance of a-Si:H/Pd Schottky diode # 129 at 300 K. The inset shows the comparison between experiment and theory for low frequencies

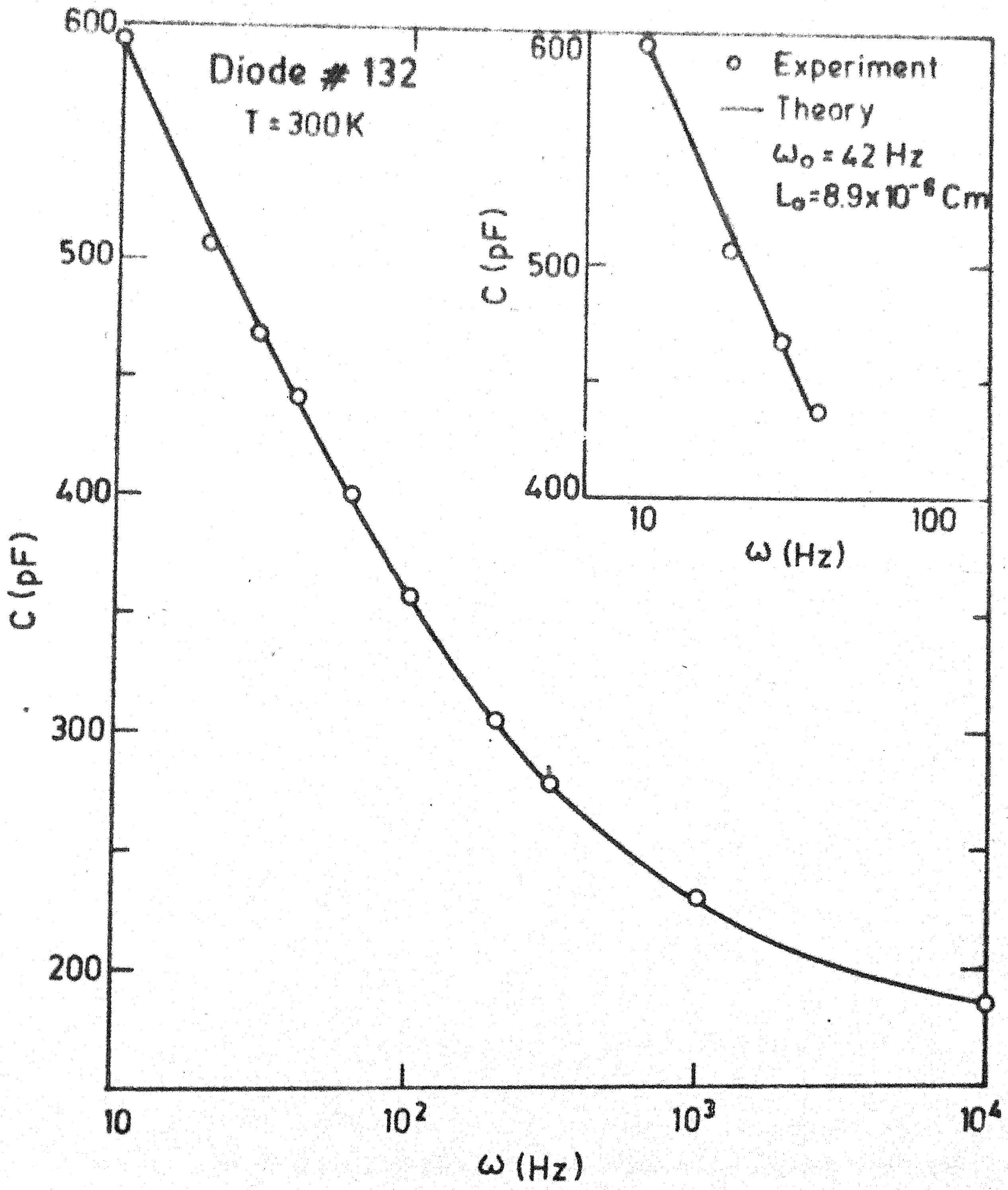

Fig.3.11 : Frequency dependence of zero bias capacitance of a-Si:H/Pd Schottky diode # 132 at 300 K. The inset shows the comparison between experiment and theory for low frequencies

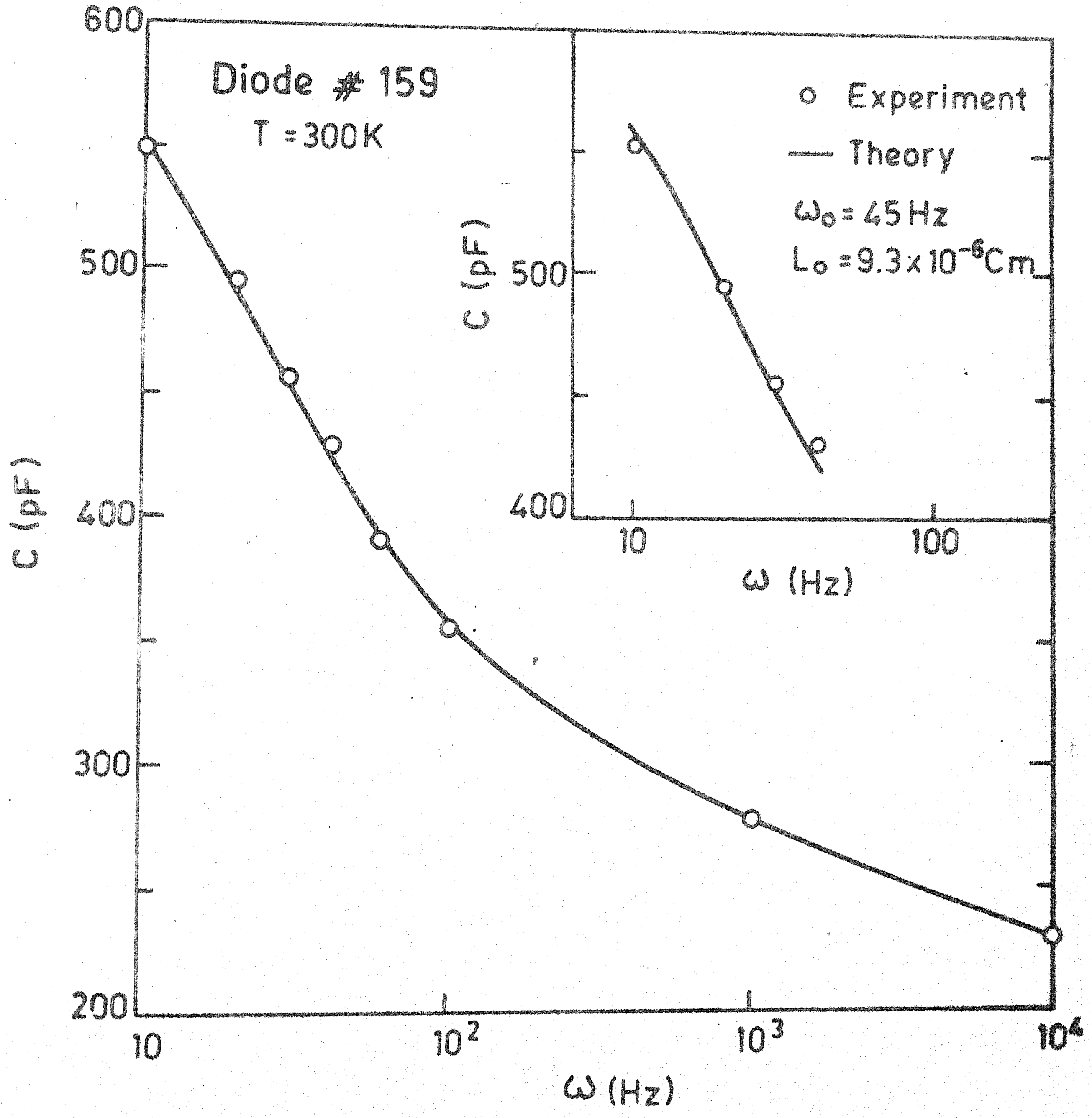

Fig. 3.12 : Frequency dependence of zero bias capacitance of a-Si:H/Pd Schottky diode # 159 at 300 K. The inset shows the comparison between experiment and theory for low frequencies

from C-ω measurements on various diodes are listed in Table 3.1 and compare well with the results obtained by other methods. This procedure adopted for obtaining DOS is similar to that of Viktorovitch and Moddel[15].

The precision in the determination of L_o is very good as it depends weakly on the choice of ω_o and V_{bi}[15]. For instance, for # 159 if V_{bi} which is 0.25 eV is taken to be 0.30 eV, the L_o will have to be changed by 8% to be still able to fit the results keeping ω_o same. Thus it can be safely asserted that L_o falls for # 159 betwen 8.5 and 9.5 x10^{-6} cm. However the precision in the determination of ω_o is not as good and it has to be changed by about 100% to fit the data, keeping L_o same, when V_{bi} is chosen to be 0.30eV.

(c) C-T measurements

From Eq. (21) it is clear that the response time of the states decreases exponentially with rising temperature. Thus, as the temperature increases, more states at the Fermi level in the depletion region start responding and the region closer to the interface is probed. Thus lowering the frequency and increasing temperature have equivalent effect on the response of a-Si:H barrier. The temperature dependence at a bias V_s and frequency ω is given by Eqs. (33) and (35).

C-T measurements, in zero bias configuration, on the diode # 159 are done at 10 Hz, 60 Hz and 100 Hz for temperatures

$300\ K \leq T \leq 420\ K$. Measurements of capacitance as a function of temperature are done in reverse bias configuration to avoid the effect of back contact. In the zero bias, the capacitance increases upto 350 K and for $T > 350$ K it shows the signs of saturation as shown in Fig. 3.14. But before the saturation is reached, it starts increasing rapidly again. A saturation of capacitance is expected when all the states in the depletion region are able to respond to the modulation[21]. A further increase in the capacitance is probably because of contribution from surface states[14].

The results of C-T measurements at 10 Hz for reverse bias V_R = 1.0, 2.0 and 3.0 V are shown in Fig. 3.15(a). The same trend of increase in capacitance with temperature is observed, in agreement with Lang et al[17].

The DOS at Fermi level is calculated by using Eq. (33). The plots of $C^2(T)\left(\frac{\partial C(T)}{\partial T}\right)^{-1}$ vs T are found to be straight lines, with a slope which is independent of the bias, in the temperature range $300\ K \leq T \leq 350\ K$ shown in Fig. 3.15(b). This is in qualitative agreement with Lang et al[17]. However, we find the DOS at Fermi level $\sim 8\times10^{16}\ eV^{-1}\ cm^{-3}$ whereas Lang et al obtain the DOS at Fermi level $\sim 10^{15}\ eV^{-1} cm^{-3}$.

3.5 ISOTHERMAL CAPACITANCE TRANSIENT SPECTROSCOPY

The isothermal capacitance transient spectroscopy (ICTS) using a voltage or a light pulse has been developed

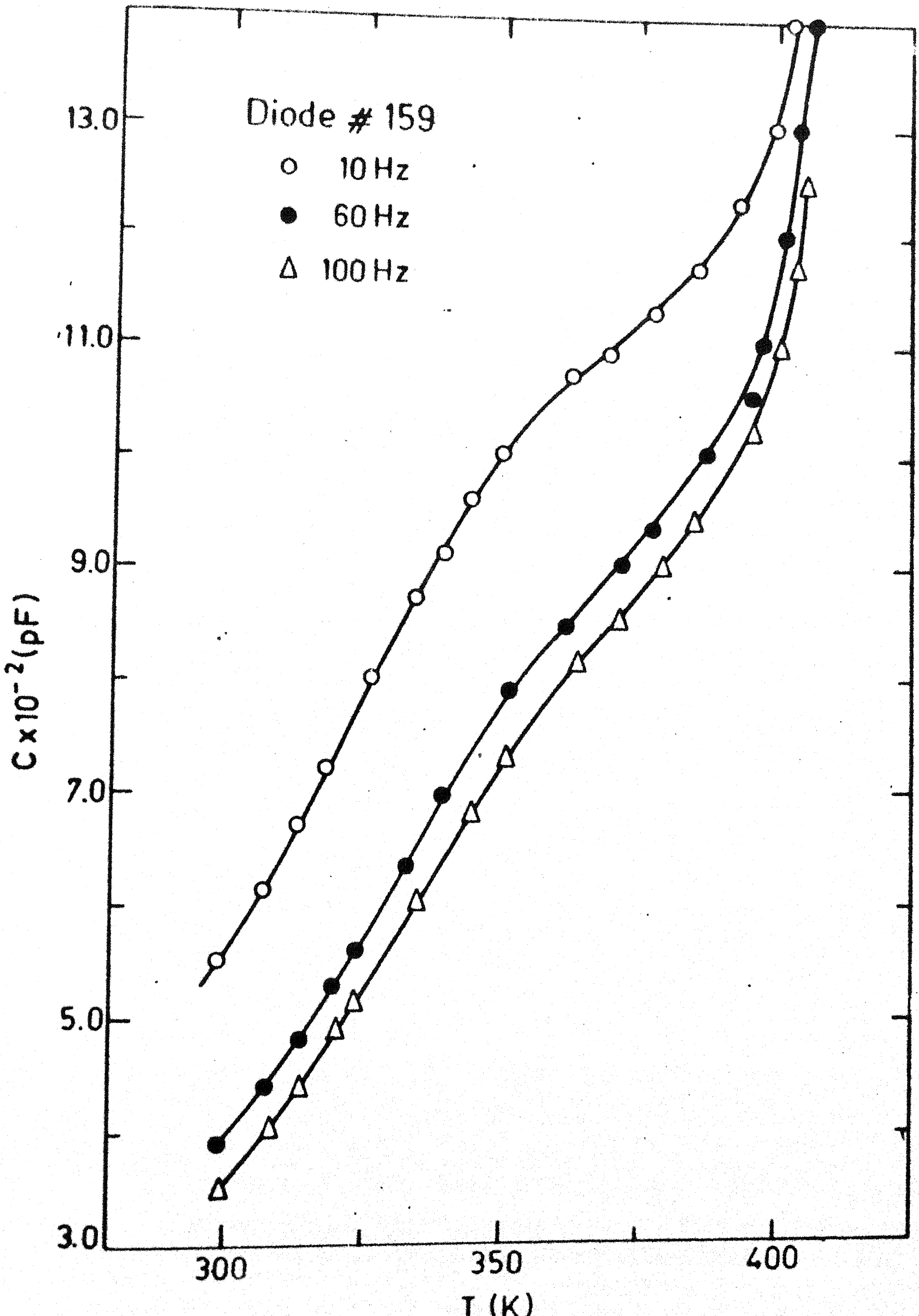

Fig.3.14 : Temperature dependence of zero bias capacitance of a-Si:H/Pd Schottky diode # 159 for ○ 10 Hz, ● 60 Hz and

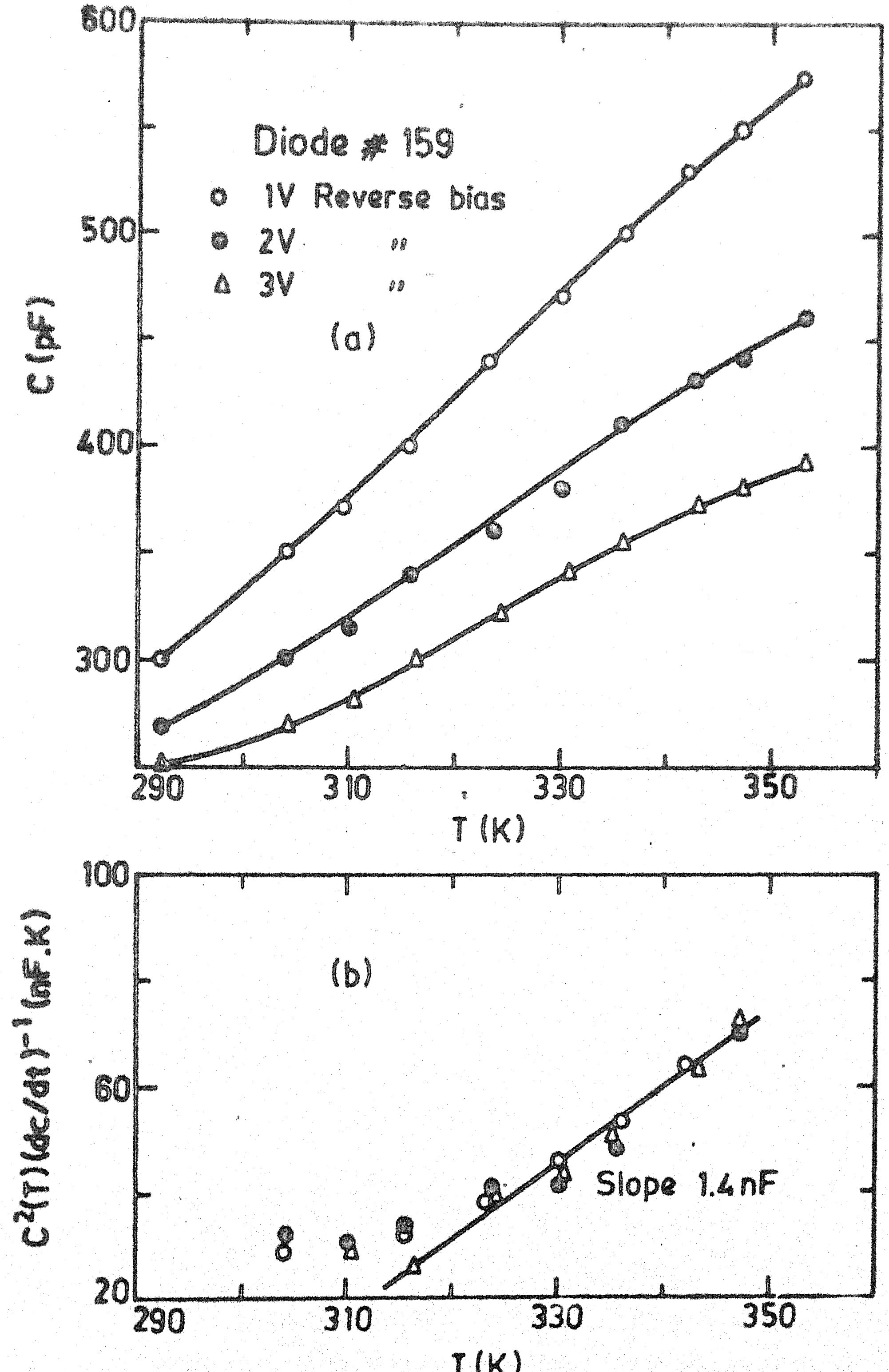

Fig. 3.15(a): Temperature dependence of 10 Hz capacitance of a-Si:H/Pd Schottky diode # 159 at V_R = 1.0 V, 2.0 V and 3.0 V

Fig. 3.15(b): Plot of $C^2(T)(\partial C(T)/\partial T)^{-1}$ vs T for V_R = 1.0 V, 2.0 V and 3.0 V

and used by Okushi et al[22,23] for finding DOS in a-Si:H. In voltage pulse filling, a reverse bias is applied across the diode to perturb the occupancy of states. However, it produces the transient corresponding to the majority carrier traps only. In n-type material, for instance, this corresponds to electron emission from the states in the upper half of the gap. In order to create a metastable initial condition for the minority carrier traps (hole traps in n-type material), one can introduce mobile minority carriers by shining band gap light on the sample. Light generates electron hole pairs which are subsequently trapped, thus perturbing the gap states occupation in the lower half of the gap. The emptying of the traps with time after either perturbation, changes the junction capacitance which when measured as a function of time, at a constant temperature, produces an ICTS signal.

Since it is a transient measurement, ICTS is insensitive to the surface states, just as DLTS is[17]. However, ICTS is considered superior to DLTS because in DLTS the sample temperature is continuously raised. This thermal scanning may lead to error as various parameters of a-Si:H may vary with temperature. Since ICTS is done at a fixed temperature, this problem does not arise[23].

3.5.1 Theory of ICTS Measurements

The transient capacitance at any time is related to

the number of electrons in traps (n_t) at any time t. Consider a trap level, at an energy E, in the band gap, having total number of traps N_t per unit volume. The rate of change of electrons in traps is given by, following Simmons and Taylor[24].

$$\frac{dn_t}{dt} = (N_t - n_t)e_p - e_n n_t \tag{38}$$

where e_n and e_p are emission rates of electrons and holes respectively from this level.

Solution of Eq. (38) is given as :

$$n_t = \exp\left\{-\int_0^t (e_n+e_p)dt\right\}\left[\int_0^t \left\{e_p N_t \exp\left[\int_0^t (e_n+e_p)dt\right]\right\} dt + n_{to}\right] \quad .. \tag{39}$$

where n_{to} = number of electrons in traps at t = o.

Simplification of Eq. (39) with the assumption that the e_n and e_p are independent of time, yields

$$n_t = \left[n_{to} - \frac{e_p N_t}{e_n+e_p}\right] \exp\left\{-(e_n+e_p)t\right\} + \frac{e_p N_t}{e_n+e_p} \tag{40}$$

If we assume that almost all the traps at energy E are filled at t=o, i.e., n_{to} N_t (40) reduces to

$$n_t = \frac{e_p N_t}{e_n+e_p} \exp\left\{-(e_n+e_p)t\right\} + \frac{e_p N_t}{e_n+e_p} \tag{41}$$

Eq. (41) is derived for a single trap level in the band gap. The corresponding equation for a-Si:H can be

written assuming a continuous density of states $g(E)$, and $e_n(E)$ and $e_p(E)$ as energy dependent emission rates for electrons and holes[23].

$$n_t = \int_{E_V}^{E_C} g(E) \frac{e_n(E)}{e_n(E)+e_p(E)} \exp\{-(e_n(E)+e_p(E))t\} dE + \int_{E_V}^{E_C} \frac{e_p(E)}{e_n(E)+e_p(E)} g(E)\, dE \quad .. \quad (42)$$

Since we find C^2 vs V_R to be a straight line(Fig.3.16) upto $V_R = 1.0$ V, as observed by others also[23,25,26], we may write $C^2(t)-C^2(\infty) = Bn_t$, in analogy with crystalline semiconductors and

$$f(t) = C^2(t)-C^2(\infty) = B\int_{E_V}^{E_C} g(E) \frac{e_n(E)}{e_n(E)+e_p(E)} \exp\{-(e_n(E)+e_p(E))t\} dE + B\int_{E_V}^{E_C} \frac{e_p(E)}{e_n(E)+e_p(E)} g(E) dE \quad .. \quad (43)$$

where $C(\infty)$ is the steady state capacitance. and $B=q\ A^2/2V_s$

If we assume $e_n(E) \gg e_p(E)$, the ICTS signal is given as

$$\frac{t\,df(t)}{dt} = -B \int_{E_V}^{E_C} t\ g(E)\ e_n(E) \exp\{-e_n(E)t\} dE \quad .. \quad (44)$$

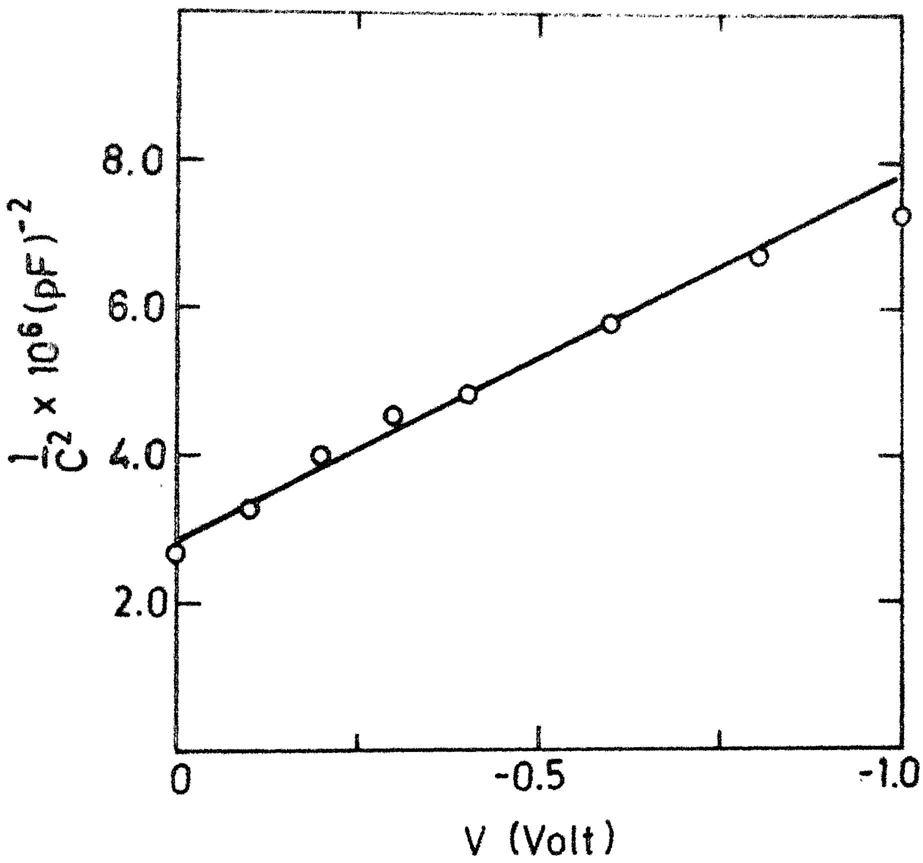

Fig.3.16 : C^{-2} vs V_R plot of a-Si:H/Pd Schottky diode # 159 (Data is taken at 300 K and 10 Hz)

The function, $e_n(E)t \exp\{-e_n(E)t\} = G(E,t)$, will have a maxima when $e_n(E)t = 1$ and it can be approximated by a delta function as[27]

$$G(E,t) = kT\,\delta(E-E_m) \tag{45}$$

and E_m is related to t_m as :

$$E_m = E_c - kT \ln(\nu(E_m)t_m) \tag{46}$$

The DOS can be obtained by combining Eqs. (44) and (45)

$$g(E) = -\frac{1}{kTB}\left|\frac{t\,df(t)}{dt}\right|_{t=t_m} \tag{47}$$

Okushi et al[23] and Balberg et al[26] have taken the constant $B = \frac{q\epsilon A^2}{2V_s}$, i.e., the same as that in the case of Schottky diodes on crystalline semiconductors. This may not be true as in the crystalline semiconductors this value of B represents the proportionality with the static capacitance. Since the value of capacitance used for a-Si:H is dependent upon frequency, one should take into account the correction for not using the static value.

Thus, we see that the analysis presented above is a considerably simplified solution of a complex problem. Actually, for the calculation of DOS, the Poisson's equation should be solved for a time varying space charge in the space domain. This needs a lot of computational efforts[1,17,19]. However, Beichler et al[2] have estimated the error caused by the use of Eq. (47) instead of the correct expression for

a-Si:H. By solving Poisson's equation in the energy domain, as has been done in the present study, they show that Eq.(47) will give DOS which may be smaller than the actual DOS by at most a factor of 5.

3.5.2 Results and Discussion of ICTS Measurements

(a) Voltage-transient

For studying the voltage transient a reverse bias of 1.0 V is applied across the diode, at 295 K. The modulating signal is of frequency 40 Hz and amplitude 15 mV (rms). The capacitance first decreases due to an abrupt increase in depletion width and then increases slowly as the electrons in the metastable states, deep in the depletion region are emitted. Capacitance attains a saturation after about 100 s. The results of voltage transient on diode # 159 are shown in Fig. 3.17(a). The inset of Fig. 3.17(a) shows the plot of f(t) vs time. The transient signal corresponds to emission of electrons from the traps in the upper half of the gap.[17]

The DOS at different energies using Eqs. (46) and (47), is calculated and found to lie between 2×10^{16} $eV^{-1}cm^{-3}$ and 3×10^{16} $eV^{-1}cm^{-3}$ for energies $0.75\ eV \leqslant E \leqslant 0.85\ eV$ below E_c. ν is assumed to be 10^{14} s^{-1} which is same as taken for fitting the C-V data and is close to the value taken by Lang et al[17] to fit their DLTS results.

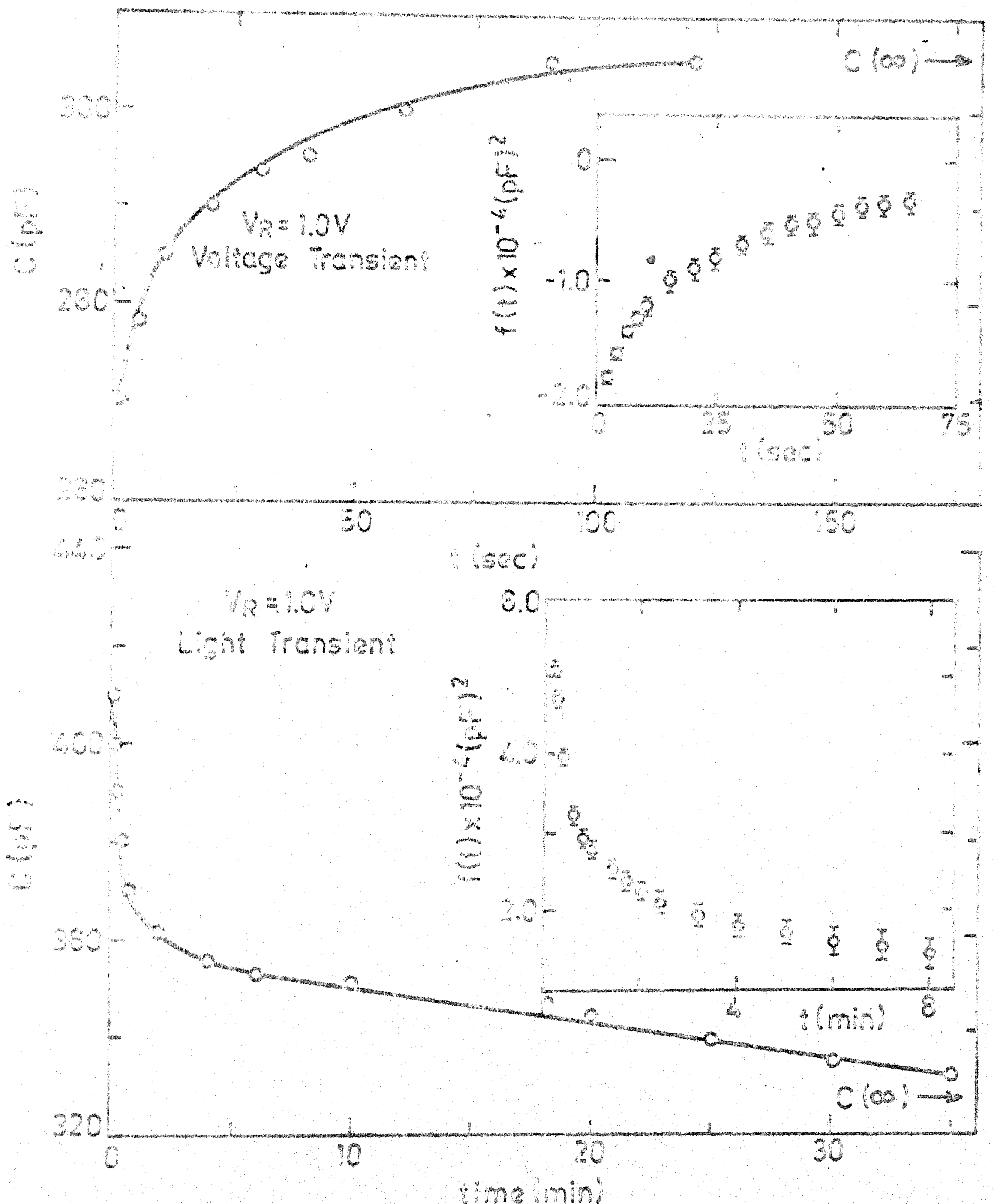

Fig.3.17(a) : 40 Hz transient capacitance signal of a-Si:H/Pd Schottky diode after perturbation of occupation of states by V_R = 1.0 V

Fig.3.17(b) : 40 Hz transient capacitance signal of a-Si:H/Pd Schottky diode after perturbation of occupation of states by light at V_R = 1.0 V.

(b) Light transient

Transient capacitance with light pulse excitation is studied by shining light on the diode # 159 from a 100 watt tungsten lamp, for 5 minutes. The diode is kept in reverse bias of 1.0 V. The time of exposure is kept long to ensure the filling of traps completely as pointed out by Lang et al[17]. As the light is shone, the capacitance increases to a high value due to a sudden decrease in depletion width. After the light is put off, the capacitance falls rapidly in the beginning and then decays slowly owing to an increase in depletion width. The transient signal measured at 40 Hz, as shown in Fig. 3.17(b), is due to the net hole minus electron emission and corresponds to hole traps in n-type intrinsic a-Si:H[17]. f(t) as a function of time is shown in the inset of Fig. 3.17(b).

The decay time is quite long in case of light pulse excitation and is a direct evidence of presence of deep traps in a-Si:H. For calculation of DOS from capacitance data with light pulse excitation, the Eqs. (46) and (47) are used and yield DOS lying between 3×10^{16} $eV^{-1}cm^{-3}$ and 1×10^{17} $eV^{-1}cm^{-3}$ in the energy range 0.9 eV $\leqslant E \leqslant 1.0$ eV below E_c.

3.6 SUMMARY AND CONCLUSION

Table 3.1 shows clearly that the parameters, (e.g., ϕ_B, n, V_{bi}) of various diodes agree with each other. This

Table 3.1 : DOS in a-Si:H obtained by different measurements

Diode No.	ϕ_B	V_{bi}	n	SCLC	C-V	C-ω	C-T	Voltage pulse	Light pulse
159	0.85	0.23	1.20	$N(E_F) \simeq 3\times10^{16}$	$N(E_F) \simeq 5\times10^{16}$	$L_o \approx 9.3\times10^{-6}$ cm $\omega_o \approx 45$ Hz $N(E_F) \simeq 7\times10^{16}$	$N(E_F) \approx 8\times10^{16}$	$2\times10^{16} \leqslant N(E) \leqslant 3\times10^{16}$ $0.75 \leqslant E \leqslant 0.85$	$3\times10^{15} \leqslant N(E) \leqslant 10^{17}$ $0.9 \leqslant E \leqslant 1.0$
129	0.82	0.20	1.30	$10^{16} \leqslant N(E) \leqslant 2\times10^{16}$	$N(E_F) \gtrsim 3\times10^{16}$	$L_o \simeq 1.5\times10^{-5}$ cm $\omega_o \approx 48$ Hz $N(E_F) \gtrsim 3\times10^{16}$	-	-	-
132	0.88	0.26	1.35	$N(E_F) \approx 2\times10^{16}$	$N(E_F) \simeq 6\times10^{16}$	$L_o \simeq 8.1\times10^{-6}$ cm $\omega_o \approx 42$ Hz $N(E_F) \approx 9\times10^{16}$	-	-	-
163	0.95	0.33	1.20	$N(E_F) \simeq 1\times10^{16}$	$N(E_F) \simeq 3\times10^{16}$	$L_o \approx 1.2\times10^{-5}$ cm $\omega_o \approx 45$ Hz $N(E_F) \approx 3\times10^{16}$	-	-	-

N(E) is in eV^{-1} cm^{-3} and E is in eV

shows a good reproducibility of these diodes. Also the DOS obtained by SCLC, C(V), C(ω), C(T), and ICTS measurements are also in qualitative agreement with each other for each diode. Considering the different assumptions involved in arriving at the DOS from each of these experiments, this agreement seems a bit surprising. A more detailed discussion is presented in Chapter 6 of this thesis . However, we can say that these results are indicative of the validity of the approximations used to deduce the DOS from the data, at least when the DOS lies around $g(E_F) \approx 10^{16} - 10^{17}$ cm^{-3} eV^{-1}, as in the present case.

REFERENCES

1. J. Beichler, H. Mell and K. Weber, J. Non Cryst. Solids 59,60 (1983) 257

2. W. Paul (Private communication)

3. Current Injection in Solids, M.A. Lampert and P. Mark, Academic Press, Inc., New York, 1970.

4. K.D.Mackenzie, P.G. LeComber and W.E. Spear, Phil. Mag. 46 (1982) 377

5. W. denBoer, J. Phys. (Paris) 42 (1981) C4-451

6. E. Bhattacharya, S. Guha, K.V. Krishna and D.R. Bapat, J. Appl. Phys. 53 (1982) 6285

7. S. Ashok and S.J. Fonash, IEEE, Electron Dev. Lett., EDL-1 (1980) 200

8. S. Ashok (Private communication)

9. E. Bhattacharya and K.L. Narasimhan (To appear in Phil. Mag.)

10. Metal-Semiconductor Contacts, E.H. Rhoderick, Clarendon Press, Oxford, 1978

11. A.M. Goodman, J. Appl. Phys. 34 (1963) 329

12. H. Fritzsche (To appear in 'Electronic and Transport Properties of Hydrogenated Amorphous Silicon, ed. J.I. Pankove, Academic Press, New York, 1984).

13. P. Viktorovitch and D. Jousse, J. Non Cryst. Solids 35,36 (1980) 569

14. J. Beichler, W. Fuhs, H. Mell and H.M. Welsch, J. Non Cryst. Solids 35,36 (1980) 537

15. P. Viktorovitch and G. Moddel, J. Appl. Phys. E1 (1980) 4847

16. R.A. Abram and P.J. Doherty, Phil. Mag. 45 (1982) 167

17. D.V. Lang, J.D. Cohen and J.P. Harbison, Phys. Rev. 25 (1982) 5285

18. Methods of Theoretical Physics, P.M. Morse and H. Feshbach, McGraw-Hill Book Company Inc. New York.

19. J.D. Cohen and D.V. Lang, Phys. Rev. B25 (1982) 5321

20. A.J. Snell, K.D.Mackenzie., P.G. Le omber and W.E. Spear, J. Non Cryst. Solids 35,36 (1980) 593

21. S. Deleonibus and D. Jousse, J. Phys. (Paris) 42 (1981) C4-487

22. H. Okushi and Y. Tokumaru, Jap. J. Appl. Phys. 19 (1980) L335

23. H. Okushi, Y. Tokumaru, S. Yamasaki, H. Oheda, and K. Tanaka, J. Phys. (Paris) 42 (1981) C4-613

24. J.G. Simmons and G.W. Taylor, Phys. Rev. B5 (1972) 1619

25. A.R. Moore (Private communications)

26. I. Balberg, E. Gal and B. Pratt, J. Non Cryst. Solids 59,60 (1983) 277

27. J.G. Simmons and M.C. Tam, Phys. Rev. 7 (1973) 3706

CHAPTER 4

THERMALLY STIMULATED CURRENTS IN a-Si:H

4.1 INTRODUCTION

The thermally stimulated currents (TSC) technique has proved very useful in obtaining information about the traps and their parameters in crystalline semiconductors.[1-13] In this method, the traps in semiconductors are filled by excitation (by light or a high electric field) at a low temperature and then the excitation is put off. If the temperature is low enough the carriers remain trapped even in the absence of excitation. The temperature of the semiconductor is then raised at a constant rate and as a result the carriers are freed. The liberated carriers contribute to an excess conductivity, measured as an excess current in the presence of an electric field. This excess current when measured as a function of temperature during heating, is known as the TSC curve. A single trap level in the semiconductor shows a peak in TSC curve at a temperature which depends upon the energy of trap level, capture cross sections of the traps and the heating rate. By making suitable assumptions about trapping kinetics, the position of trap level and its capture cross sections can be determined by varying the heating rate.[6,7,8] If there is a discrete distibution of traps in the material, the TSC may show several peaks or a structure corresponding to the distribution of the trap

depths. These peaks can be separated by using a technique called step heating[6,9] which consists of measuring the TSC while the sample is heated to successively higher temperatures in steps. After each step the sample is cooled back to the lowest temperature. The carriers from deeper traps are liberated progressively and the logarithmic plot of the TSC as a function of 1/T is expected to yield a straight line for each step. It's slope is directly related to trap depth[6]. Other methods of analysing the TSC data use the peak position[6] and their detailed shape[5]. However, with the exception of the heating rate and the initial rise analyses, most of these are dependent on the recombination mechanism of the carriers.

TSC measurements in the case of disordered solids, have been done mainly on chalcogenide glasses and have not yielded much information.[14,15] This is mainly because the carriers in the chalcogenide glasses have usually small drift range (Schubweg) and that their drift mobility is small[16,17] a-Si:H which is relatively free from these difficulties, has recently been studied by this technique[18-22]. In the present investigation also, the TSC measurements have been done on a-Si:H and the experimental set up used for the measurements of the TSC in a-Si:H is described in section 4.2. Section 4.3 contains the analysis of the TSC measurements for a single trap level as well as for a continuous distribution of traps.

In section 4.4 we give the results of the TSC measurements on heat dried and light soaked states in a-Si:H.

In the interpretation of these results in section 4.5, it is suggested that the observed structure in TSC does not necessarily imply a structure in the DOS distribution of a-Si:H.

4.2 EXPERIMENTAL

Well characterized samples of undoped a-Si:H in coplanar configuration (section 2.7) are used for TSC measurements. The sample is mounted using In Ga eutactic (section 2.7) on the cold finger of a closed cycle helium refrigerator (CTI Cryogenics) shown in Fig. 4.1. The sample temperature which can be varied between 8.5 K and 300 K is measured and controlled using a temperature controller (Model, DTC 500 A, Lake Shore). Teflon feed throughs are used to reduce the leakage current. The sample is cooled in dark to 30 K. At this temperature a red light ($\lambda \sim 670$ nm, ~ 30 mW/cm^2) from an oriel monochromator is shone on the sample for ≈ 30 s. Shorter exposures yielded the same TSC, showing that the light induced changes (S-W effect) have negligible effect on TSC for this exposure. After waiting for $\approx$ 10 min to allow the transients to subside, the sample is heated at a constant rate β and the TSC recorded with an electric field $\approx$ 50 V/cm across the sample. The circuit

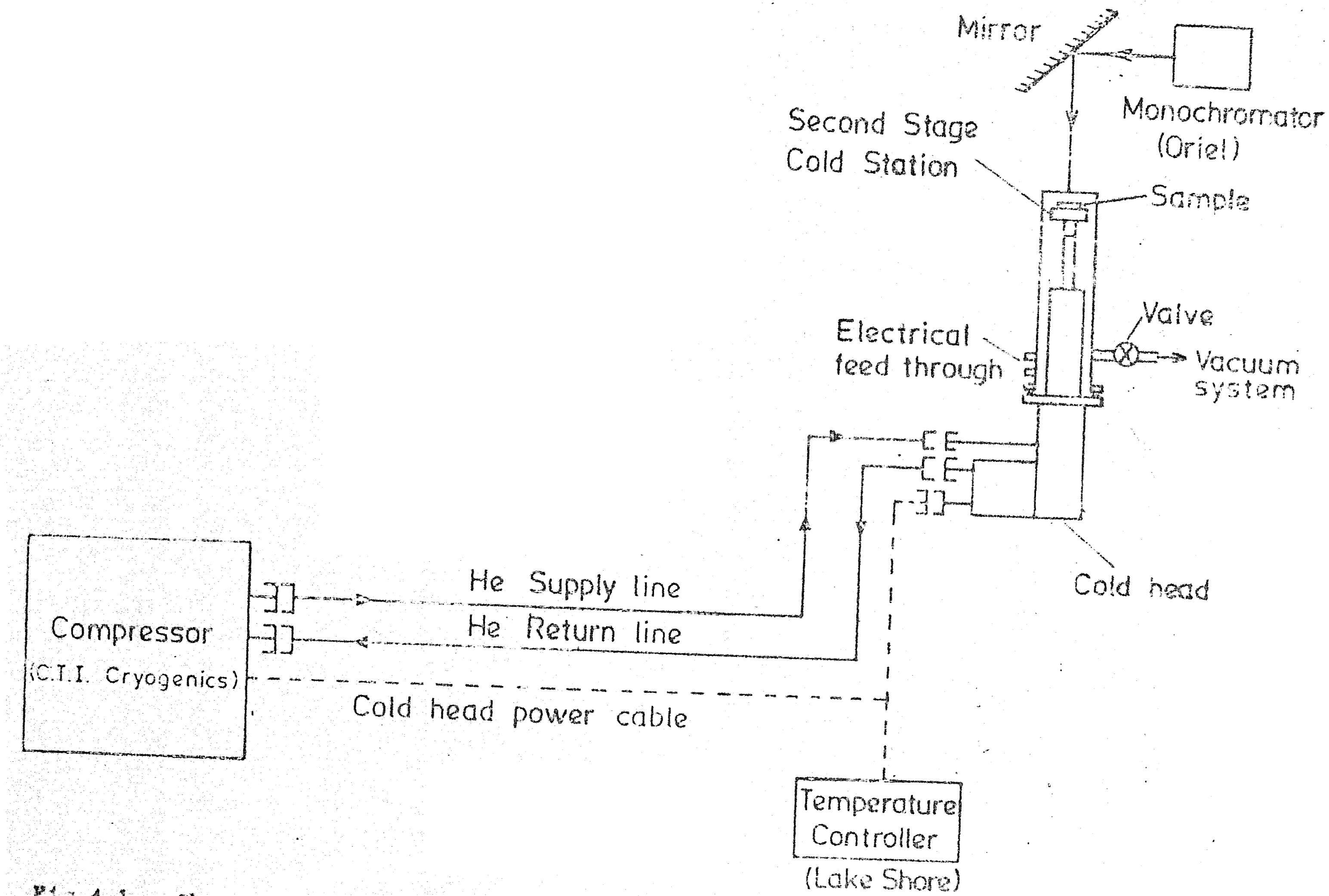

Fig.4.1 : Closed cycle He refrigerator and cold head used for measurements in $8.5\ K \leq T \leq 300\ K$ range

used for measuring TSC is given in Fig. 4.2(a) and is one of the configurations proposed by Braunlich.[1]

TSC and dark currents become comparable near 300 K and thus to separate the TSC peak in this region two almost identical samples (prepared in the same run) in a bridge configuration, shown in Fig. 4.2(b), are used. Prior to each TSC set, the samples are balanced at 300 K using a 9 V battery and cooled in dark. The difference between the currents of the unexcited samples (called the error signal) is measured from 120 K to 300 K as the samples are heated at a constant rate β. For TSC, they are cooled in dark and one of them is excited with a red light at 120 K. After waiting for transients to subside, samples are heated in dark at a constant rate β. The measured current which is the difference in currents of the excited sample and the sample in dark is the required TSC.

4.3 THEORY OF TSC

4.3.1 Single Trap Analysis

The simplest case is for the material in which only one trap level is contributing maximum to TSC at a time. Although a-Si:H has traps distributed throughout the mobility gap, it appears to be justified to use the single trap analysis to calculate the trapping parameters of a-Si:H, in view of the analysis of Simmons (4.3.3). Thus, we describe analysis of a single trap (see Fig. 4.2(c) to illustrate

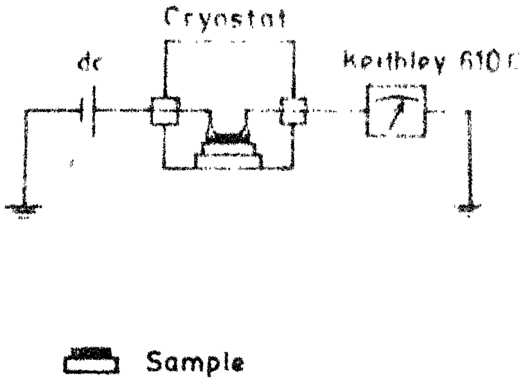

Fig.4.2(a) : Electrical circuit used for measuring TSC (The circuit is one of the configurations proposed by Braunlich[1])

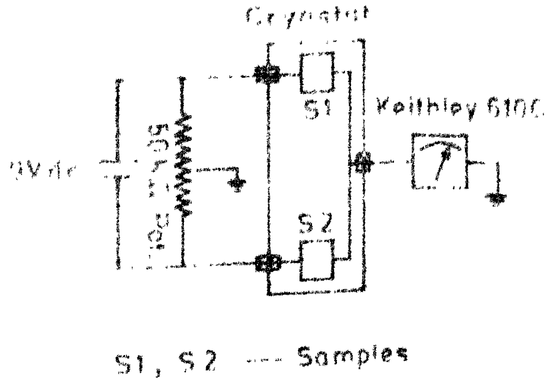

Fig.2(b) : Bridge configuration used for subtraction of TSC and dark currents near ≈ 300 K (S_1 and S_2 are almost identical samples

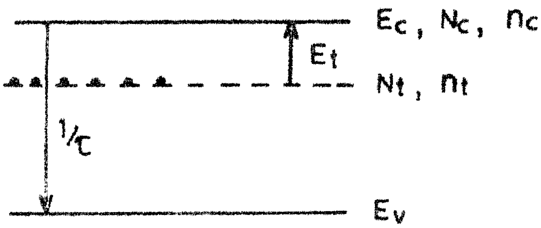

Fig.4(c) : Single trap level model used for the analysis of TSC (for details see section 4.3)

how the trap parameters can be obtained in this simple case from the TSC measurements. It is assumed that the conduction is governed only by electrons. Following is the list of various symbols used in the analysis.

q	Electronic charge
N_t	Total no. of traps at E_t per cm^3
E_t	Trap depth
N_c	Effective density of states in conduction band
n_t	Total no. of electrons in traps per cm^3
n_c	Total no. of electrons in conduction band per cm^3
S	Capture cross section of the traps
v	Thermal velocity of electrons
μ	Electronic mobility in conduction band
τ	Recombination life time
E	Electric field
T	Temperature
β	Heating rate
t	time
k	Boltzmann constant
C	Cross sectional area

The rate of change of no. of electrons in traps is governed by the capture and emission of electrons in traps and is given as[8]:

$$\frac{dn_t}{dt} = -n_t S v \, N_c \exp\left\{-E_t/kT\right\} + n_c (N_t - n_t) \, Sv \qquad (1)$$

The number of electrons in conduction band is controlled by the following equation

$$\frac{dn_c}{dt} = -\frac{n_c}{\tau} - \frac{dn_t}{dt} \tag{2}$$

Eqs. (2) and (3) can be solved[8] to obtain the n_c for two special cases (i) slow retrapping and (ii) fast retrapping.

(i) Slow retrapping

Slow retrapping means that the recapture of electrons is less as compared to recombination, i.e., $(N_t-n_t)Sv \ll 1/\tau$.[8] With this condition Eq. (1) reduces to :

$$\frac{dn_t}{dt} = -n_t\, N_c\, Sv \exp\{-E_t/kT\} \tag{3}$$

Integration of Eq. (3) with the following boundary conditions

$$n_t\Big|_{T=T_o} = n_{to} \quad \text{and} \quad n_t\Big|_{T=T} = n_t \tag{4}$$

yields

$$n_t = n_{to} \exp\left\{ -\frac{1}{\beta} \int_{T_o}^{T} \nu \exp\{-E_t/kT\}\, dT \right\} \tag{5}$$

where $\nu = N_c Sv$ is the attempt to escape frequency and $T = T_o + \beta t$.

Since the recombination life time τ is assumed to be short $\frac{n_c}{\tau} \gg \frac{dn_c}{dt}$, and as a result, from Eq. (2)

$$n_c = -\tau \frac{dn_t}{dt} \tag{6}$$

Combining Eqs. (5) and (6) yields an expression for n_c as :

$$n_c = \tau n_{to} \nu \quad \exp\left\{ -\frac{E_t}{kT} - \frac{\nu}{\beta} \int_{T_o}^{T} \exp\left\{-E_t/kT\right\} dT \right\} \tag{7}$$

Eq. (7) can be used to obtain the TSC, I(T), following

$$I(T) = n_c q \mu E C = q n_{to} \nu \tau E \mu C \exp\left\{ -\frac{E_t}{kT} - \frac{\nu}{\beta} \right.$$

$$\left. \int_{T_o}^{T} \exp\left\{-E_t/kT\right\} dT \right\} \tag{8}$$

Using Eq. (8), the condition for the maxima (peak) in TSC can be obtained with $\frac{dI(T)}{dT} = o$ and is,

$$\exp(E_t/kT) = \frac{\nu k T_m^2}{\beta E_t} \tag{9}$$

Eq. (9) predicts an increase in T_m with increasing β. Also near $T = T_m$, the contribution from the integral on the RHS of Eq. (8) is small and one has

$$I_m = I_o \exp\left\{ -\frac{E_t}{kT_m} - 1 \right\} \tag{10}$$

with $\qquad I_o = q \mu \nu \tau n_{to} E C$

Eq. (9) and (10) can be used to calculate ν and n_{to} if the $\mu\tau$ product of the material is known.

(ii) Fast retrapping

Fast retrapping implies that the electrons are retrapped before they are able to recombine, i.e., $(N_t - n_t)Sv \gg 1/\tau$[8]. Because of fast retrapping, an effective equilibrium is established between the electrons in traps and those in the conduction band, i.e.,

$$\frac{n_c}{n_t} = \frac{N_c}{N_t} \exp\left\{-\frac{E_t}{kT}\right\} \qquad (11)$$

Let n be the sum of electrons in the traps and the conduction band

$$n = n_c + n_t \qquad (12)$$

From Eq. (11), it is clear that when $N_t \gg N_c \exp\left\{-\frac{E_t}{kT}\right\}$ $n_c \ll n_t$ and thus Eq. (2) becomes

$$\frac{dn_t}{dt} = -\frac{n_t}{\tau}\frac{N_c}{N_t} \exp\left\{-\frac{E_t}{kT}\right\} \qquad (13)$$

Eq. (13) when integrated with boundary conditions of Eq. (4), gives

$$n_t = n_{to} \exp\left\{-\frac{N_c}{\beta\tau N_t}\int_{T_o}^{T} \exp\left\{-\frac{E_t}{kT}\right\} dT\right\} \qquad (14)$$

TSC, I(T) obtained by combining Eq. (11) and (14)

is given by

$$I(T) = \frac{q\mu n_{to} N_c EC}{N_t} \exp\left\{ -\frac{E_t}{kT} - \frac{N_c}{\beta N_t \tau} \int_{T_o}^{T} \exp\left\{ -\frac{E_t}{kT} \right\} dT \right\} \quad (15)$$

The condition for TSC maximum is

$$\exp\left\{ \frac{E_t}{kT_m} \right\} = \frac{N_c}{N_t \beta \tau} \frac{k\, T_m^2}{E_t} \quad (16)$$

Eq. (16) implies that T_{max} shifts with β as before, I(T) at T_m is given by

$$I(T_m) = I_o \exp\left\{ -\frac{E_t}{kT_m} - 1 \right\} \quad (17)$$

where $I_o = \frac{q n_{to} N_c \mu EC}{N_t}$

Eq. (16) and (17) can be used to determine the TSC parameters.

4.3.2 Differences and Similarities of the TSC Between Fast and Slow Retrapping Cases

By comparing Eqs. (8), (9) and (10) which hold in case of slow retrapping with the corresponding ones for the fast retrapping, viz., Eqs. (15), (16) and (17) respectively, we find them to be quite similar. This allows us to write the following general equations.

$$I(T) = A \exp\left\{ -\frac{E_t}{kT} - \frac{B}{\beta} \int_{T_o}^{T} \exp\left\{ -\frac{E_t}{kT} \right\} dT \right\} \quad (18)$$

$$\exp\left\{\frac{E_t}{kT_m}\right\} = \frac{B}{\beta}\ \frac{kT_m^{\ 2}}{E_t} \tag{19}$$

and

$$I(T_m) = A \ \exp\left\{-\frac{E_t}{kT_m} - 1\right\} \tag{20}$$

where A and B are constants whose dependence on the various trapping parameters is given in Table 4.1.

In literature one normally uses Eqs. (18) and (20) to obtain the trap depth (E_t). Two experimental techniques are used.

(i) Initial rise method[9]

If T is not far from T_o, the integral in Eq. (18) may be neglected to obtain

$$J(T) = A \ \exp\left\{-\frac{E_t}{kT}\right\} \tag{21}$$

Thus by heating the sample to a temperature T which is not much greater than T_o, the slope of lnI vs 1/T is expected to yield E_t. Since A does not affect the slope, the value obtained will be independent of the trapping kinetics.

(ii) Variation of heating rate

By performing the experiment with different heat rates (β), Eqs. (19) and (20) can be used to obtain the

Table 4.1 : Values of A and B for slow as well fast retrapping cases

Parameter	Fast	Slow
A	$\frac{q\, n_{to}\, N_c \mu E\, C}{N_t}$	$q\, n_{to} \nu \tau \mu E\, C$
B	$N_c/\tau N_t$	ν

trap depth E_t as follows :

(a) If two heat rates β_1 and β_2 are used[7] Eq. (19) gives,

$$E_t = k \left(\frac{T_{1m} \, T_{2m}}{T_{1m} - T_{2m}} \right) \ln \left(\frac{\beta_1 \, T_{2m}^2}{\beta_2 \, T_{1m}^2} \right) \tag{19a}$$

(b) A plot of $\ln \left(\frac{T_m^2}{\beta} \right)$ vs $\frac{1}{T_m}$ is expected to be a straight line whose slope is related to E_t.

(c) From Eq. (21), if $\frac{E_t}{kT_m} \gg 1$, a plot of $\ln I(T_m)$ vs $\frac{1}{T_m}$ is a straight line for different heat rates with slope E_t.

It is interesting to note that in these cases also, the trap depth obtained does not depend on the trapping kinetics, since the constants A and B do not play any role in this analysis.

Whereas it may appear to be advantageous to use these methods when the trapping kinetics are not known, in order to obtain the trap parameters other than E_t, one must know which of the two cases (whether fast or slow retrapping) is applicable. In principle it should be possible to decide between the two alternatives for trapping kinetics by looking at the detailed shape of TSC and comparing with Eq. (18). Lushick[11] has shown that for fast retrapping

$$E_t = \frac{k \, T_m^2}{T' - T_m}$$

where T' is temperature at which TSC is half of its maximum

value in the decay region of TSC. In practice, such detailed comparison is usually not possible, since for $T > T_m$ other peaks usually start appearing. Garlick and Gibson[9] described two ways of distinguishing between the slow and fast retrapping.

(i) Decay of TSC

Heating is stopped during the TSC measurements at a temperature T and the decay of TSC is observed with time. It is argued[9] that the decay will be exponential for slow retrapping and hyperbolic for fast case. However, this holds only for the case of a single trap level. For an exponential distribution of traps, a hyperbolic decay will be observed even in the case of slow retrapping.

(ii) Shape of the TSC peak

It can be argued that in the case of slow retrapping, the shape of TSC is independent of n_{to} (i.e., initial excitation conditions, such as, temperature of excitation, intensity and wavelength of excitation etc.). However, it should depend on n_{to} if the strong retrapping takes place.

Thus it does not seem easy to find out which of the two extreme cases, discussed here, is important by measuring TSC and one needs information from the other experiments before one can determine the trap parameters, other than the trap depth, with any confidence.

4.3.3 TSC for a Continuous Distribution of Traps

Problem of thermally stimulated currents in materials having continuous distribution of traps has been taken up by Simmons et al[23]. They consider a distribution of traps $g(E)$ from an intrinsic level E_i to conduction band edge E_c and assume that the retrapping is negligible. The recombination is also neglected since it is assumed that the field is high enough to sweep out all the carriers before they recombine. With these assumptions the rate of change of electrons in an small strip dE, in the upper half of the gap is given by using Eq. (1),

$$\delta \frac{dn_t}{dt} = - n_t \nu \exp \left\{ - \frac{E_t}{kT} \right\} dE \qquad (22)$$

n_t can be used from Eq. (5) and then Eq. (22) becomes,

$$\delta \frac{dn_t}{dt} = - \left[\nu \exp \left\{ - \frac{E_t}{kT} \right\} \times n_{to} \exp \left\{ - \frac{1}{\beta} \int_{T_o}^{T} \exp \left\{ - \frac{E_t}{kT} \right\} dT \right\} \right] dE \qquad \ldots \quad (23)$$

where $n_{to} = f_o(E)\, g(E)$ with $f_o(E)$ being the initial occupancy function and is given by

$$f_o = \frac{v\, S_n\, n}{v S_n\, n + v\, S_p p} \qquad (24)$$

where S_n and S_p are capture cross sections for electrons and holes and n and p are the steady state free electron and hole densities. Summing over E in Eq. (23) for the

contributions from all the trap levels,

$$\frac{dn_t}{dt} = - \int_{E_i}^{E_c} \nu f_o(E)\; g(E) \exp\left\{- \frac{E_t}{kT} - \frac{1}{\beta}\int_{T_o}^{T} \nu \exp\left\{-\frac{E_t}{kT}\right\} dT\right\} dE \quad \text{... (25)}$$

The corresponding TSC according to Simmons et al is given as

$$I(T) = \frac{1}{2}\, qdC \int_{E_i}^{E_c} f_o(E)\; g(E)\; P(E,T)\; dE \qquad (26)$$

where d is spacing between the electrodes and the function p(E,T) is given by

$$P(E,T) = \nu \exp\left\{- \frac{E_t}{kT} - \frac{1}{\beta}\int_{T_o}^{T} \nu \exp\left\{-\frac{E_t}{kT}\right\} dT\right\} \qquad (27)$$

The function P(E,T) exhibits a pronounced narrow peak whose position E_{mn} depends on T and it has a half width of 2kT. This important result clearly means that during the thermal scan of the sample in TSC, it is those traps positioned within $\gtrsim$ 2kT of E_{mn} which contribute significantly to the current at a certain temperature. In view of this, it appears to be justified to apply single trap analysis to a-Si:H because each energy level in band gap with a half width $\gtrsim$ 2kT can be considered a discrete trap level. Further Simmons et al[23] have shown that TSC in samples which contain a continuous distribution of traps

is proportional to initial occupancy, i.e.,

$$I(T) = \frac{1}{2} q d C D f_o(E)\, g(E_{mn}) \tag{28}$$

where D is a constant and is only very slightly temperature dependent.

Eq. (28) implies that TSC provides a direct image of the occupied trap distribution after initial excitation, i.e., $f_o(E)g(E)$. Further the escape frequency (ν) according to the model for a system with continuous traps is given as[23]:

$$\nu = 10^Y$$

with

$$Y = \frac{(T_{2m}\log_{10}\beta_2 - T_{1m}\log_{10}\beta_1)}{T_{2m} - T_{1m}} - 1.66 \tag{29}$$

where β_1 and β_2 are two heating rates and T_{1m} and T_{2m} are corresponding temperatures of maxima.

4.4 RESULTS

Electrical parameters of samples (# 183, 186 and 190) used for TSC measurements are shown in Table 2.4 (Chapter 2) in the heat dried (A) as well as light soaked (B) states. Figs. 4.3 to 4.5 show the TSC for three samples (full curves, A and B) along with their respective dark currents (dashed curves, A and B) in the states A and B. In state A, the TSC shows a peak at low temperature (110 K,

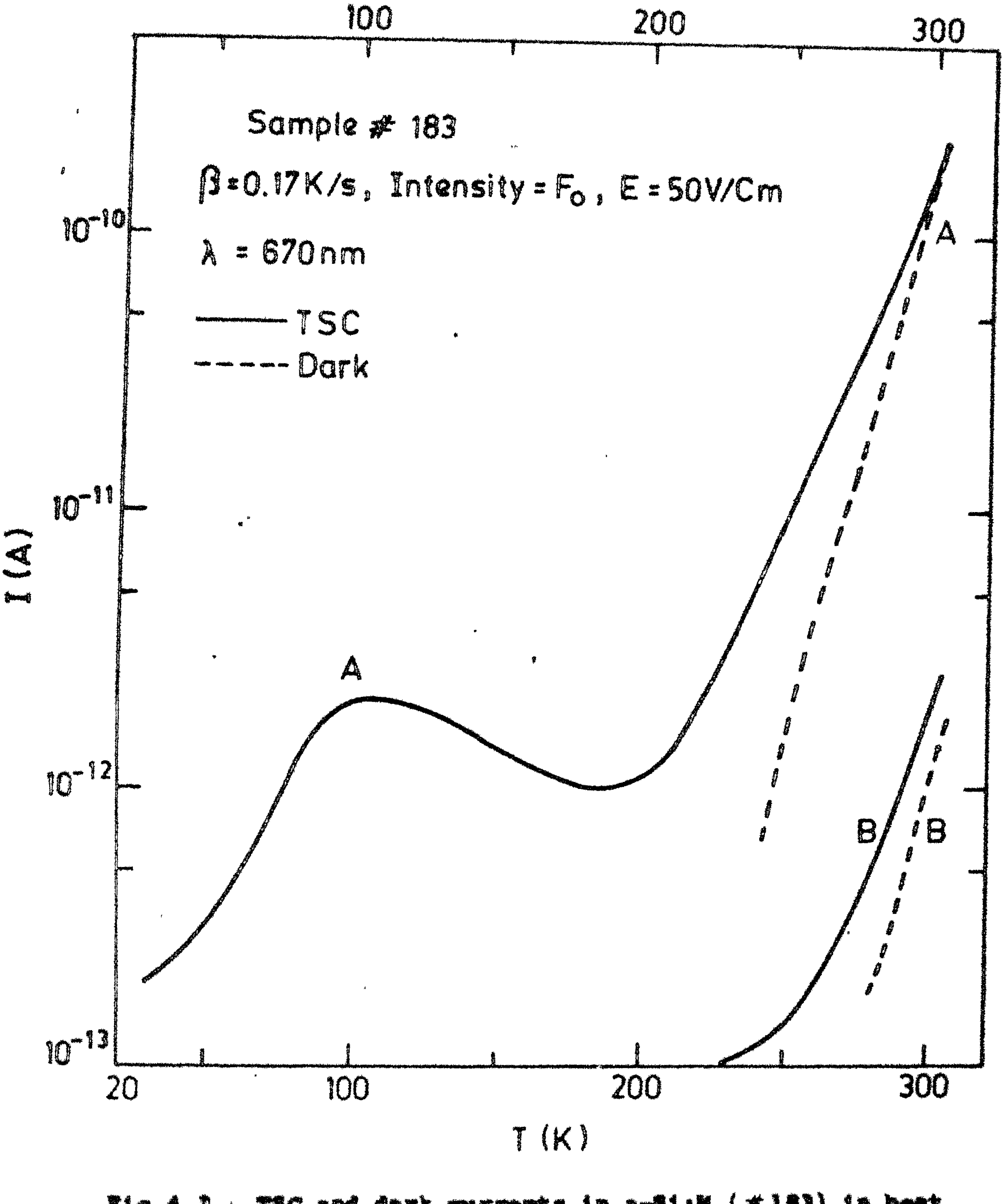

Fig.4.3 : TSC and dark currents in a-Si:H (#183) in heat dried (A, after annealing in dark at $\simeq$150°C for 2 hr) and after S-W effect (B, after shining light from a 100 watt tungsten halogen lamp for 2 hr). It may be noted that the TSC peak at $\simeq$120 K in state B reduces below the detection limit due to large S-W effect in this sample

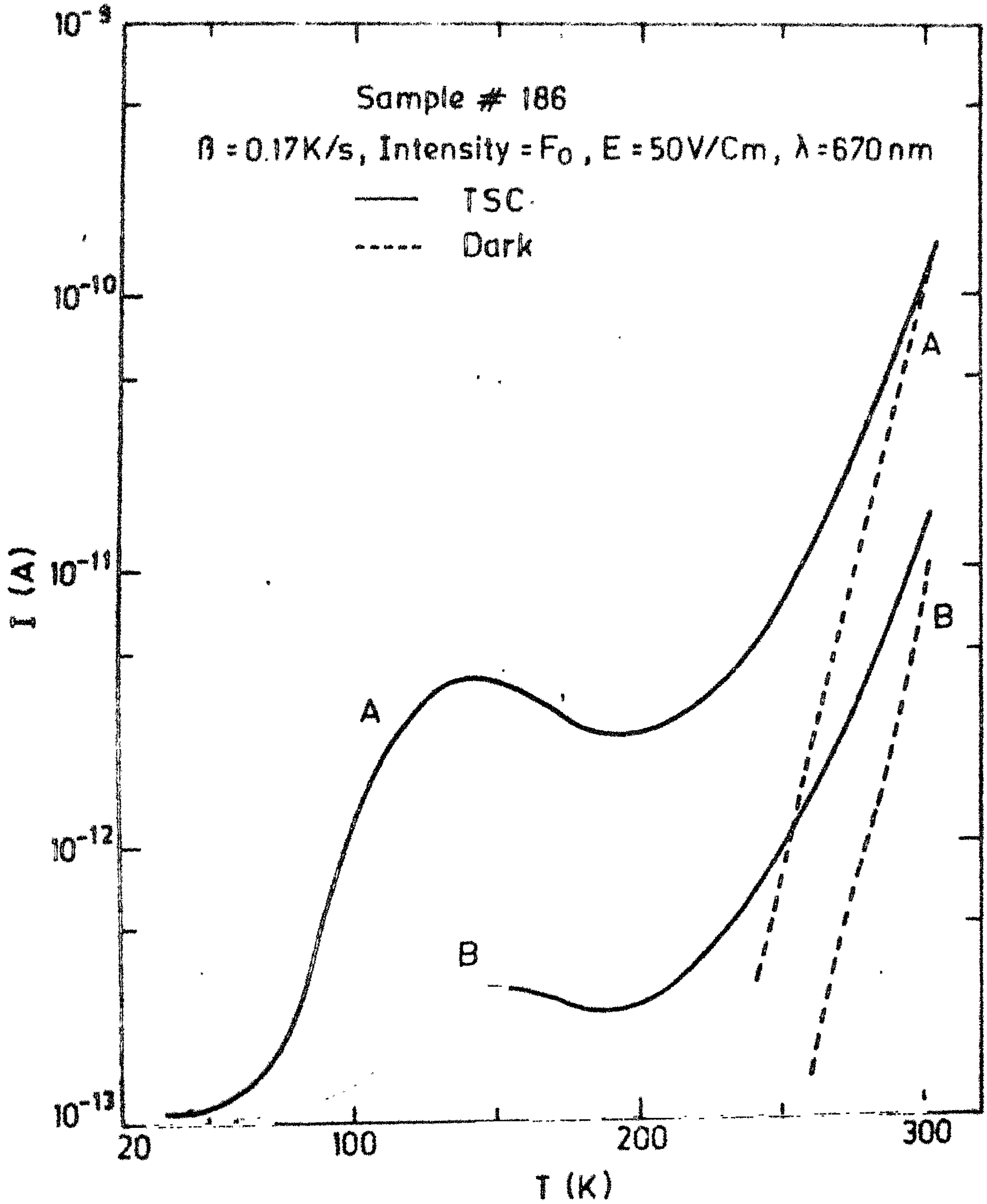

Fig.4.4 : TSC and dark currents in a-Si:H (# 186) in heat dried (A) and after S-W effect (B) states

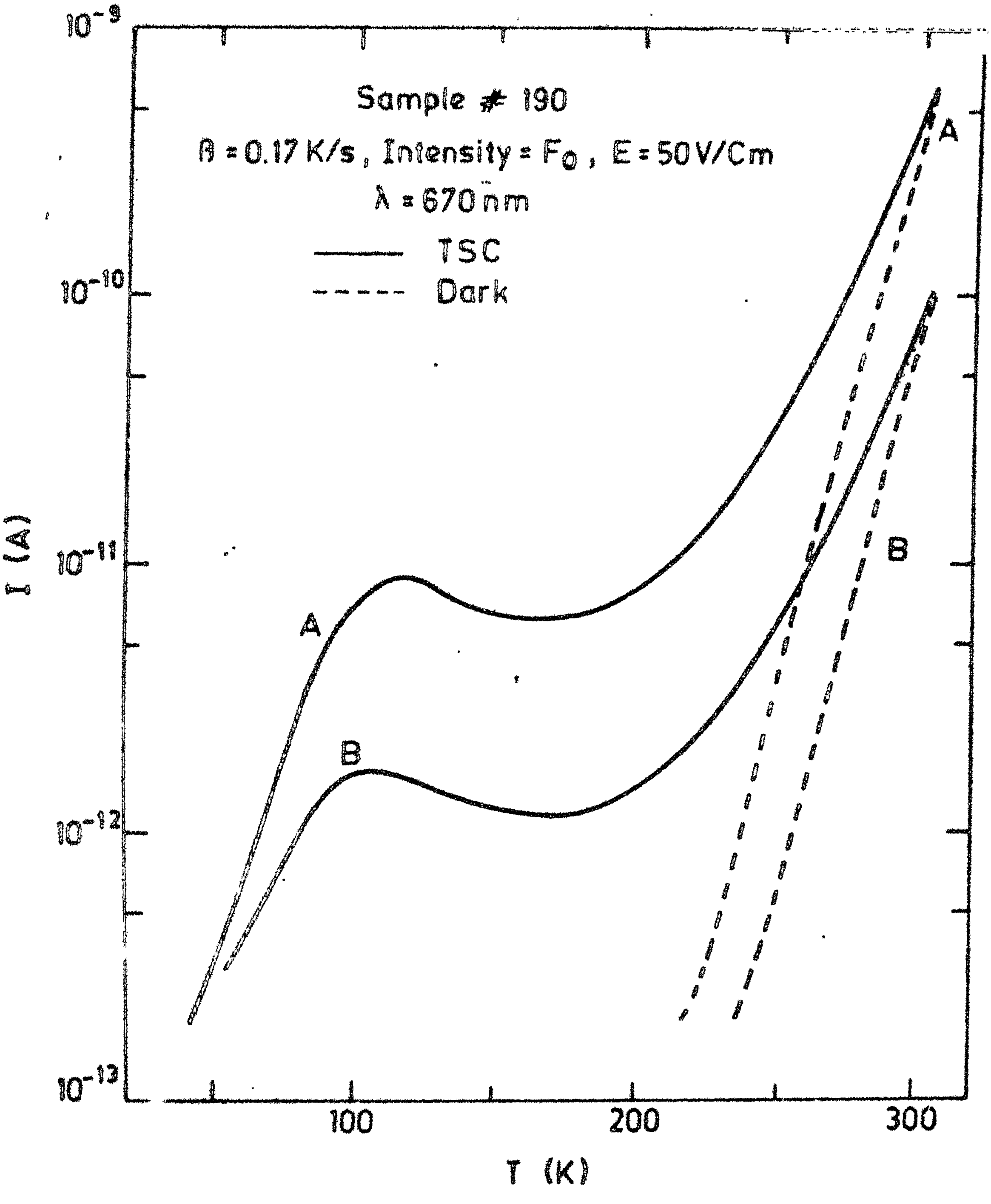

Fig.4.5 : TSC and dark currents in a-Si:H (#190) in heat dried (A) and after S-W effect (B) states

140 K and 120 K for samples # 183, 186 and 190, respectively) and then increases monotonically upto 300 K. A peak exists near 300 K also, but can not be seen in this experiment because of the large dark currents (see section 4.4.4). The TSC reduces considerably in the state B and in the sample which shows a large S-W effect, the peak is reduced below the limit of detection (see Fig. 4.3). These results are in agreement with others.[18-21] If the vacuum is poor ($\approx 10^{-1}$ torr), an additional peak at $\approx$ 200 K appears. This peak is observed even without exciting the sample with light at low temperature. It is probably caused by adsorbates in the poor vacuum, since when the vacuum of the system is better ($\approx 10^{-5}$ torr) the peak does not appear.[20]

Since the TSC results on different samples are qualitatively similar, sample 190 is chosen for further experiments.

4.4.1 Intensity Dependence of the TSC Peak ($\approx$ 120 K)

Effect of variation of relative intensities of excitation is shown in Fig. 4.6. TSC does not change appreciably upon changing the intensity from F_o to $10^{-2}F_o$ ($F_o \approx$ 30 mW/cm^2). Below $10^{-2}F_o$, however, the height of the peak reduces with intensity but the position of the peak remains unchanged.

4.4.2 Dependence of the TSC Peak ($\approx$ 120 K) on the Wavelength of Excitation

To check whether the peak near 120 K arises from the

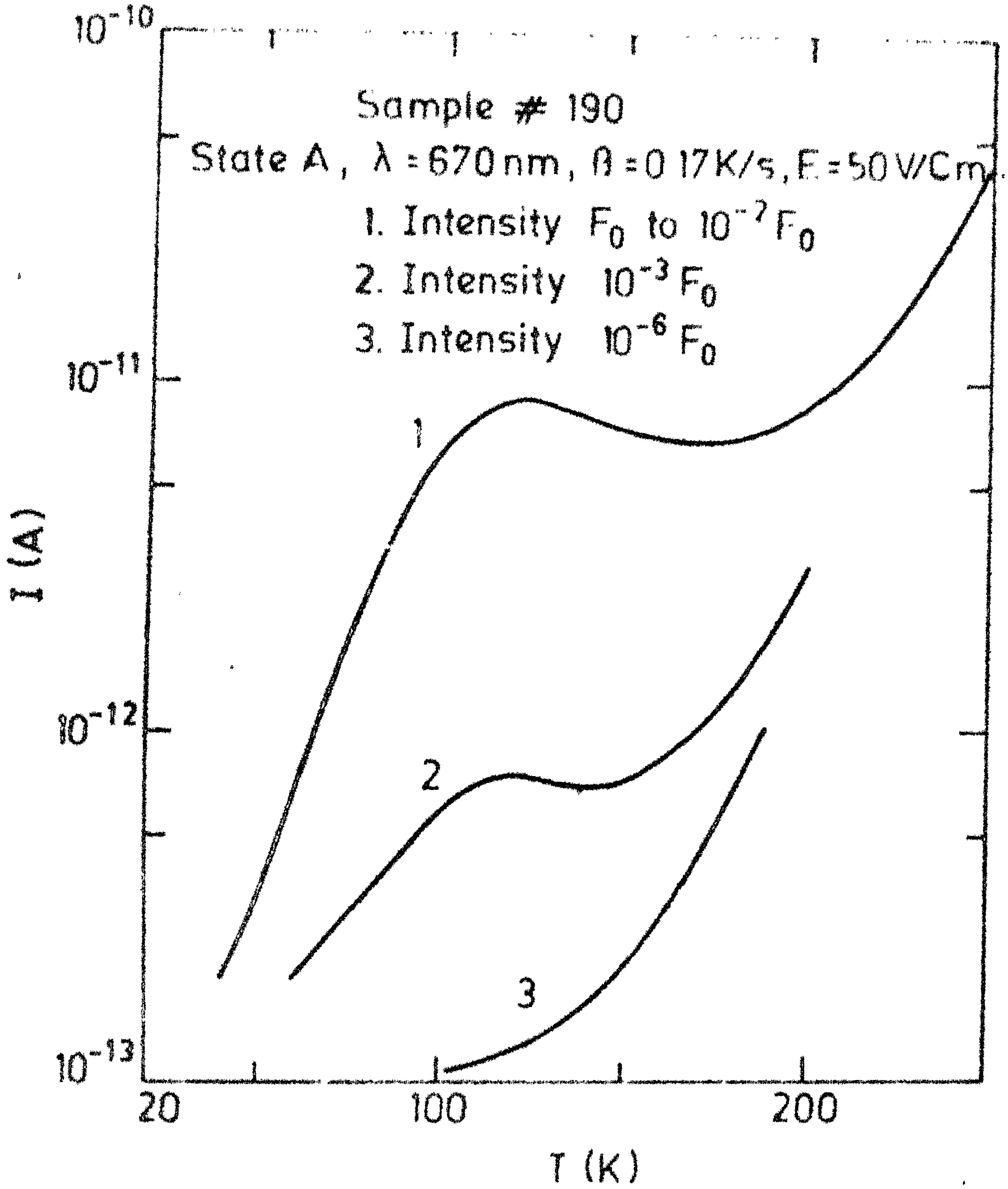

Fig.4.6 : Dependence of TSC peak near 120 K in a-Si:H (# 190), in heat dried state (A) on intensity of excitation. For intensities $10^{-2}F_0$ to F_0 (F_0 30 mW/cm^2), the sample is in saturation region of TSC

surface or the bulk, light of different wavelengths (λ) is used for excitation of the sample, in state A. The results are shown in Fig. 4.7. The intensities of various wavelengths are high enough so that the TSC lies in the saturation region (i.e., between F_o and $10^{-2}F_o$). It is observed that the height of the peak is maximum for the red light ($\lambda \approx 670$ nm) and the peak reduces to a shoulder for the violet light ($\lambda \approx 400$ nm). This is because the light of high energy is absorbed only in the few top layers of a-Si:H due to the high absorption constant. This decreases effective volume of the sample and hence a decrease in TSC. From these results it appears that the dominant contribution to the TSC is from the bulk states.

4.4.3 Electric Field (E) Dependence of TSC Peak ($\approx$ 120 K)

A saturation of TSC is observed when the collection field is about 100 V/cm as shown in Fig. 4.8 and in the plot of TSC at T_m vs E in Fig. 4.9.

4.4.4 Results in Bridge Configuration

As shown in Fig. 4.3, the TSC and the dark currents become comparable near 300 K and therefore, the TSC peak in this region is resolved by using the bridge configuration[14] described in section 4.2. Fig. 4.10 shows the results. The technique allows us to see clearly, for the first time, this peak near 300 K whose position and height depend on

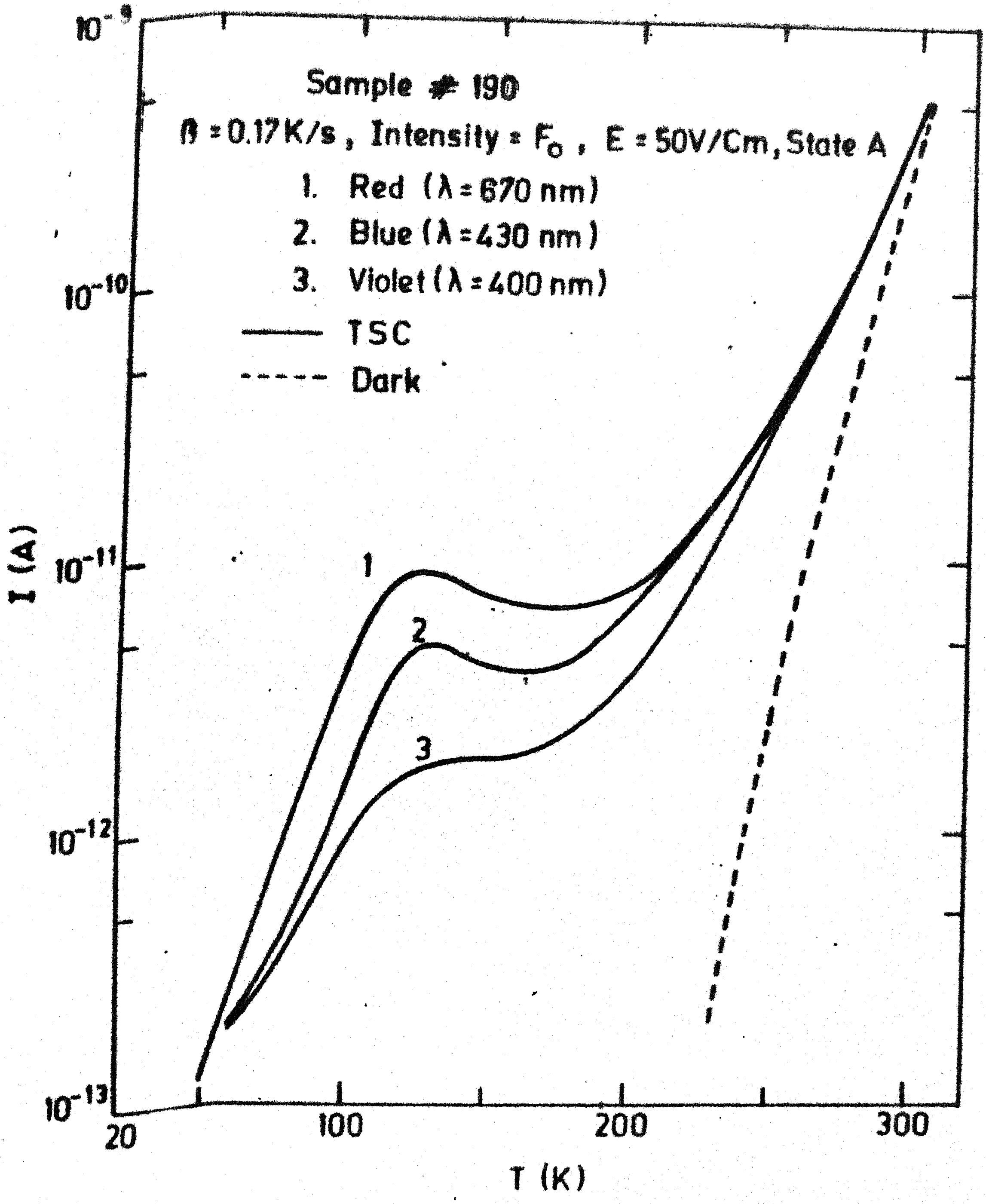

Fig.4.7 : Dependence of TSC peak near ≈ 120 K in a-Si:H (# 190) in heat dried state (A) on wavelength (λ) of excitation. The intensity of TSC peak is highest for band gap light (λ = 670 nm) and for highest energy light (λ : 400 nm) the TSC peak reduces to a shoulder

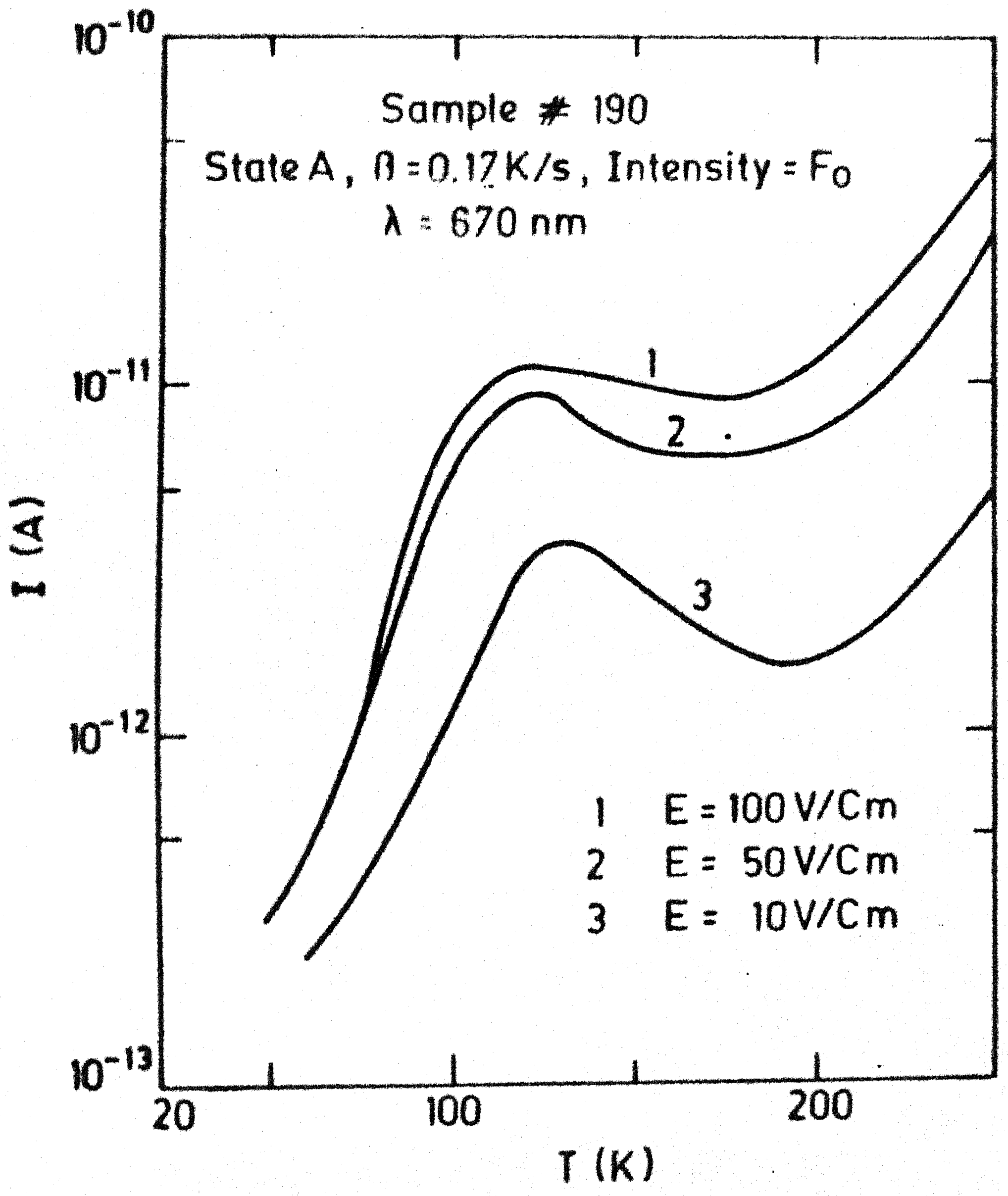

Fig.4.8 : Electric field (applied across the sample for collecting the carriers) dependence of TSC peak near ≈ 120 K in a-Si:H (# 190) in heat dried state (A). The electric field at which the TSC saturates is ≈ 100 V/cm

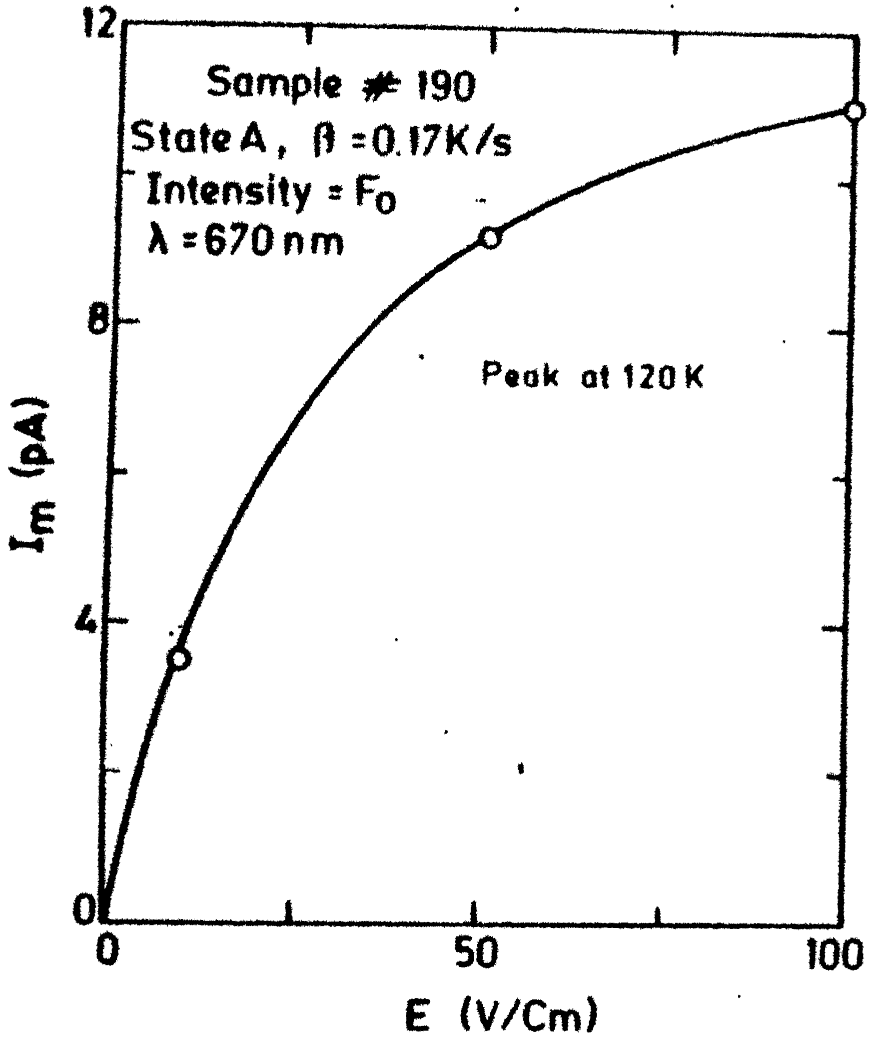

Fig. 4.9 : Plot of I(Tm) vs applied electric field for collection

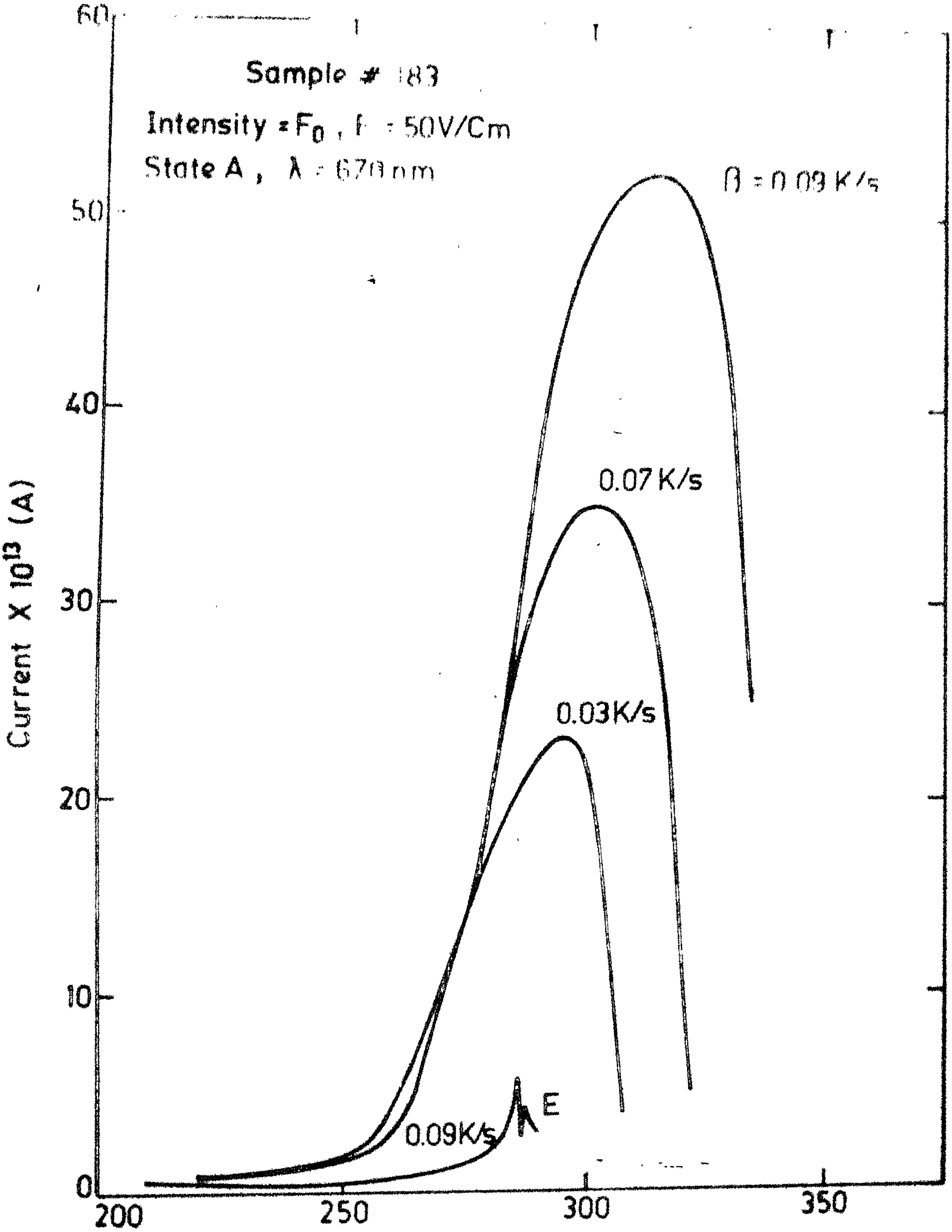

Fig.4.18 : TSC peak at ≃ 300 K observed using two (almost identical samples in a bridge configuration in heat dried state (A). Heating rate dependence of the peak is also shown. E is error signal.

the heating rate β. Curve E shows the error signal (section 4.2) of the samples in dark and is negligible in comparison to TSC.

4.5 DISCUSSION AND CONCLUSIONS

The appearance of a structure in the form of two peaks in TSC in a-Si:H seems at first sight to imply a structure in DOS in this material. However, we show in section 4.5.3 that this is not necessarily so, and an alternative explanation following Simmons et al[23] adequately explains the results.

As shown in Eqs. (8) and (15), the TSC depends upon the various TSC parameters, e.g., N_t, n_{to} and ν etc., and therefore, a change in the value of these parameters due to light soaking[24] may be responsible for reduction in TSC in state B (see also section 4.5.3).

4.5.1 Step heating

To test whether a-Si:H contains a discrete or a continuous distribution of DOS, the step heating analysis, described in section 4.1, is employed. The results are shown in Fig. 4.11 (for low T region) and 4.12 (for high T region using bridge). The plots of ln I vs $10^3/T$ are found to be straight lines with slopes ranging from 0.02 eV to 0.62 eV (i.e., the dark value of E_F). It is evident from this figure that a-Si:H contains a continuous distribution of traps throughout the mobility gap.

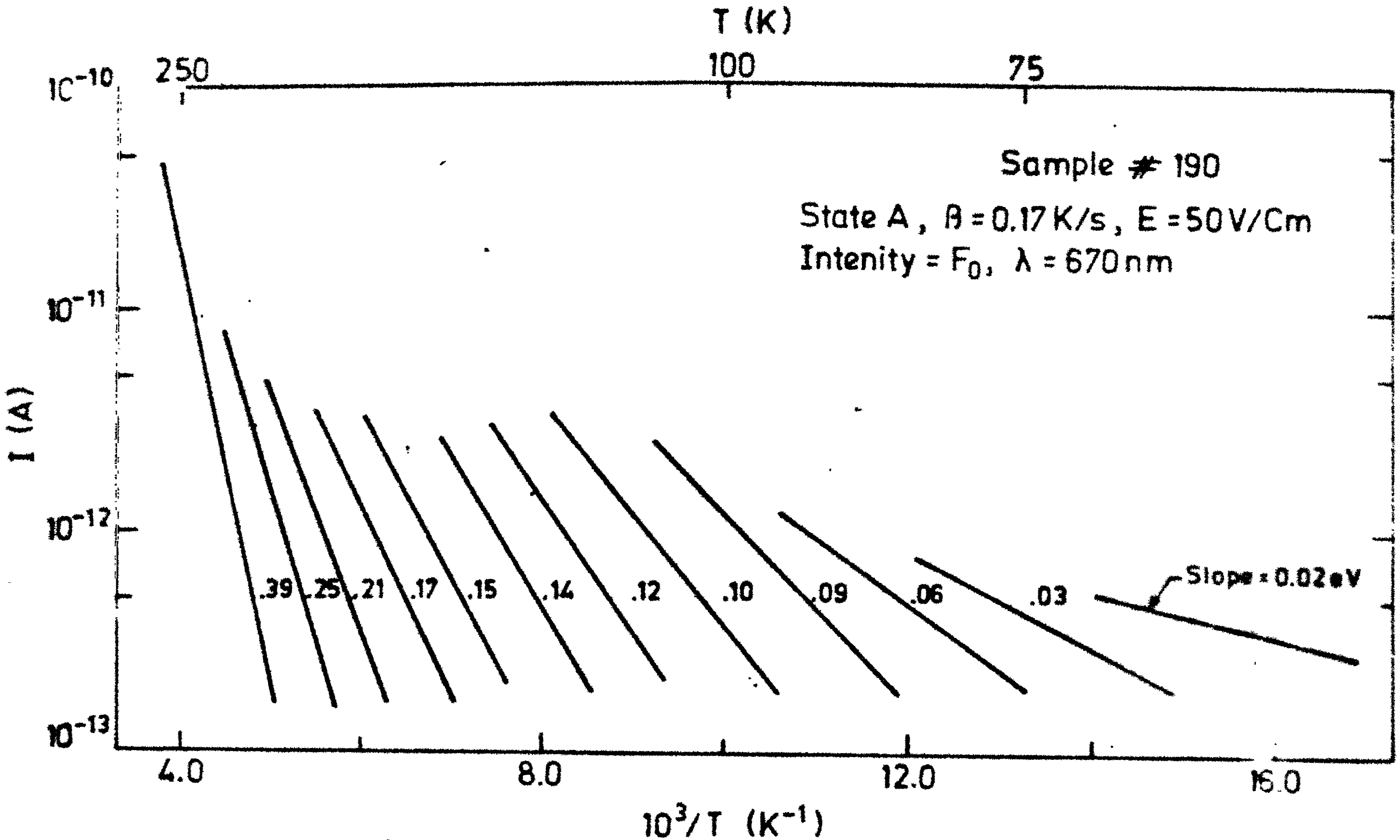

Fig.4.11 : Plots of lnI vs $10^3/T$ for various steps of step heating analysis in a-Si:H in heat dried state (A) for 50 K $\leq$ T $<$ 200 K. After each step the sample is cooled back in dark to 30 K (T_o)

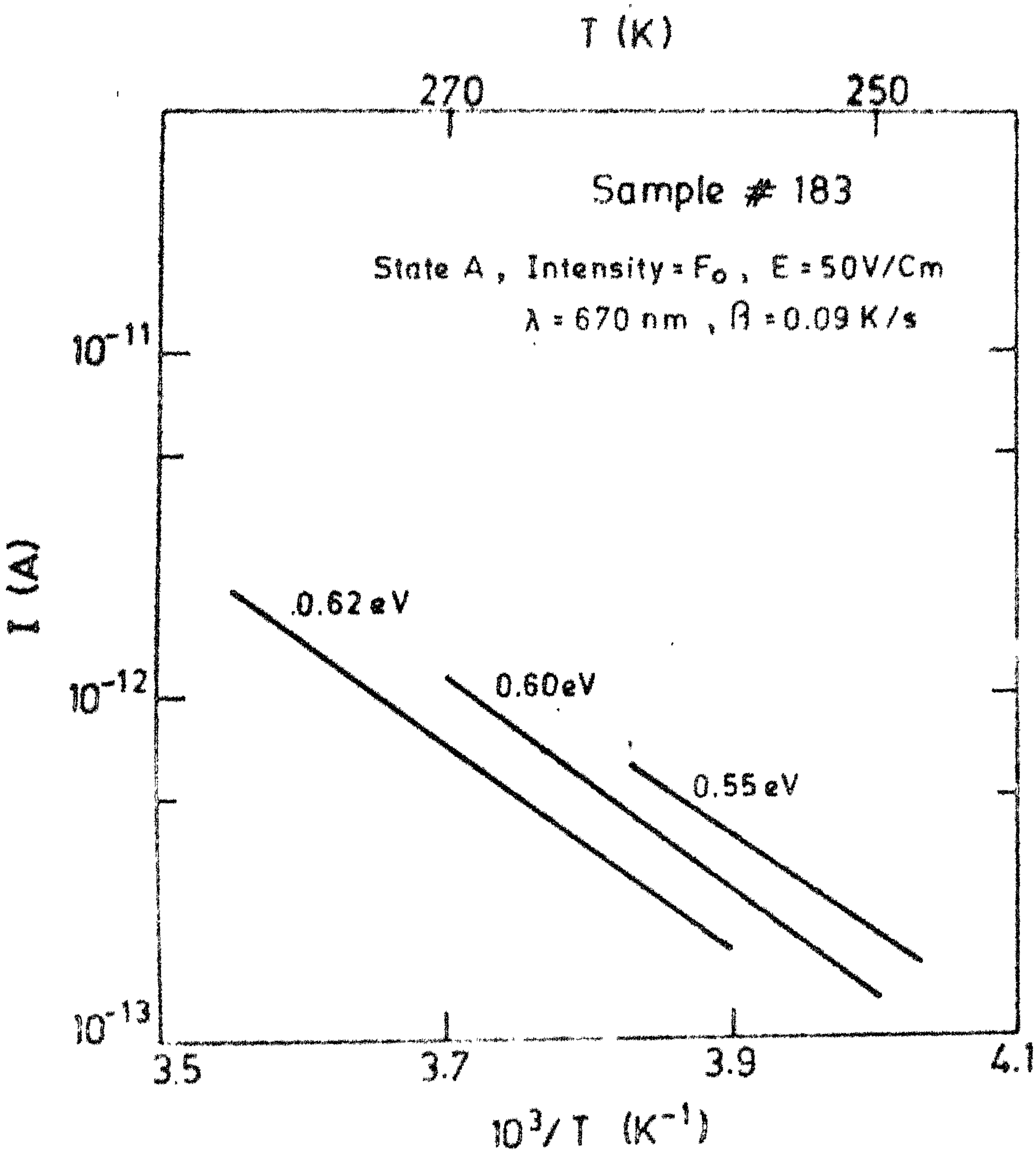

Fig.4.12 : Plots of lnI vs $10^3/T$ for various steps of step heating analysis in a-Si:H in heat dried state (A) in brige configuration (in the temperature range 250 K ≤ T ≤ 300 K). After each step the sample is cooled back in dark lto 120 K (T_o)

Test for a single (discrete) trap level corresponding to peak $\sim$ 120 K is also performed on our sample[1] by heating it at a constant rate β repeatedly to a temperature T below the peak ($T \lesssim 120$ K) and cooling back to lowest temperature T_o. The plots of ln I vs $10^3/T$ are found to be straight lines with constantly increasing slopes (see Fig. 4.13). Thus, it appears that the peak at ≈ 120 K does not arise from a single trap level.

4.5.2 Analysis of TSC Peaks

Simmons et al have given a way to analyse TSC in the materials with a continuous distribution of traps. They have pointed out that for a sample containing a continuous distribution of traps, the maximum contribution to TSC at a certain temperature comes mainly from the traps which lie within 2 kT of the energy ($E_{mn}(T)$) being probed. In view of this it appears worthwhile to first analyse the TSC results in a-Si:H with one trap level model.

(a) Calculation of trap depth (E_t)

The results of heat rate analysis (section 4.3.2) for low temperature peak are shown in Fig. 4.14 and for high temperature peak in Fig. 4.10. The plots of $\ln I(T_m)$ vs $\frac{10^3}{T_m}$ are shown in Fig. 4.15 (a) and (b) which are straight lines as expected. The slopes are 0.16 eV and 0.60 eV for low and high temperature peaks respectively. This implies that the states contributing maximum to these TSC peaks

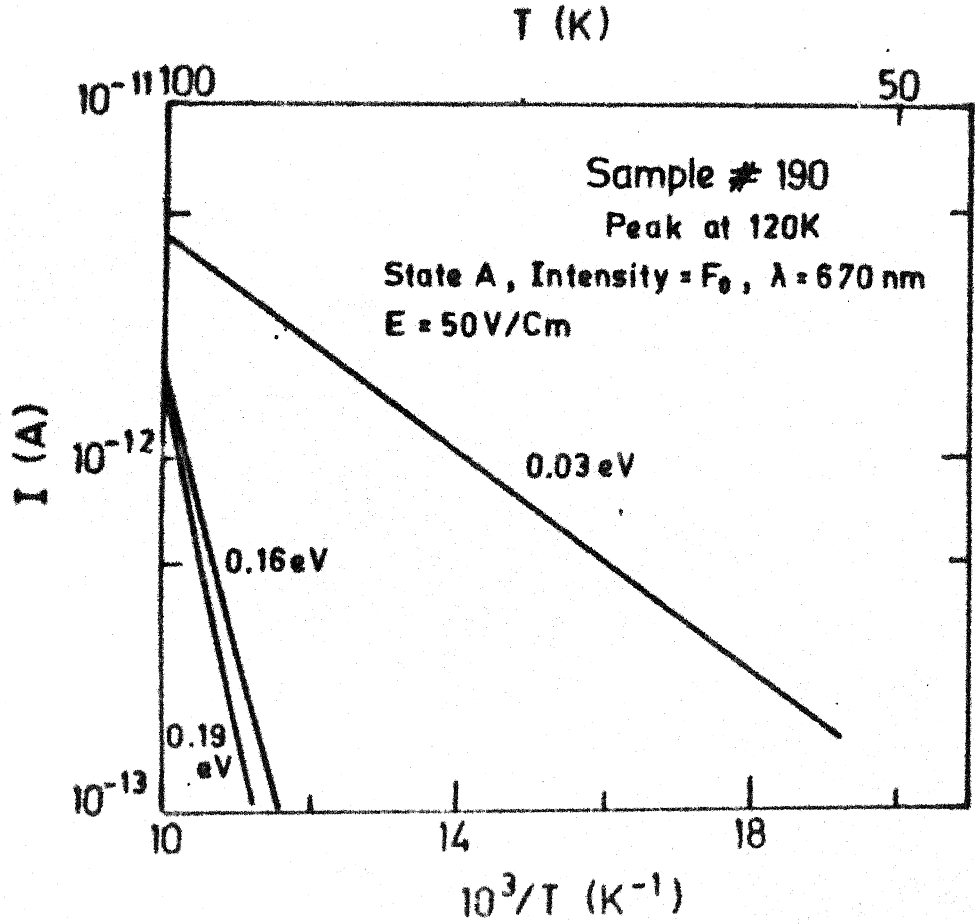

Fig.4.13 : Plots of lnI vs $10^3/T$ for various steps of test for a single trap level near TSC peak $\simeq$ 120 K in a-Si:H in heat dried state (A). This test is performed by heating the sample, after excitation at T_0, to a temperature $T < T_m$ and cooling back to T_0 repeatedly. The plots of lnI vs $10^3/T$ for various such steps are expected to be straight lines with same slope, if a single trap level is present

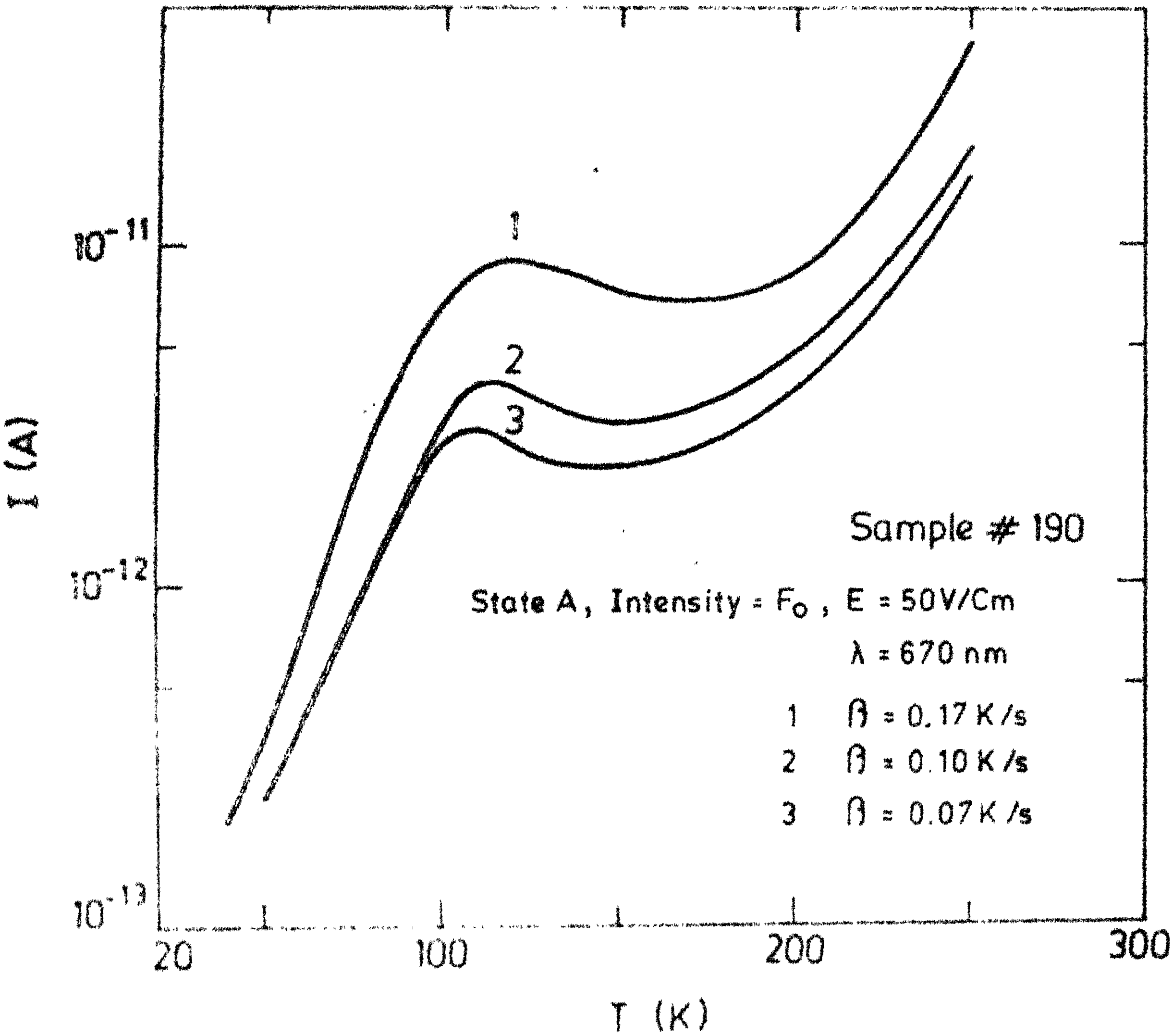

Fig.4.14 : Heating rate (β) dependence of TSC peak near 120 K in a-Si:H in heat dried state (A)

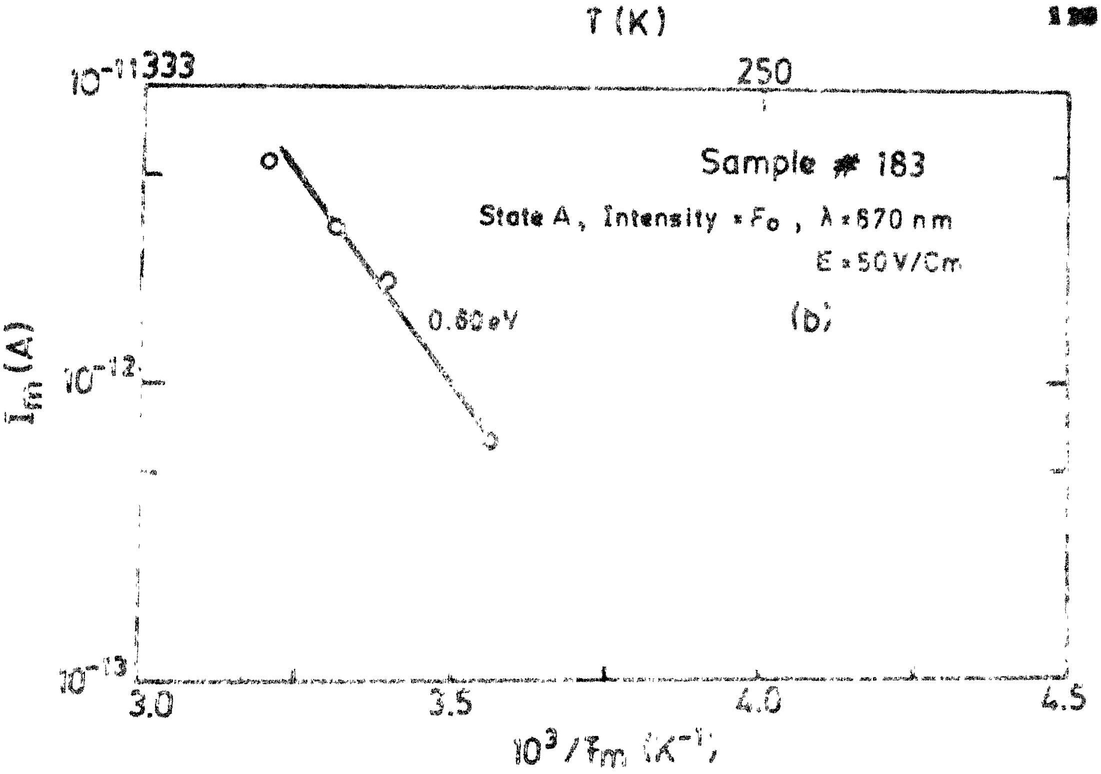

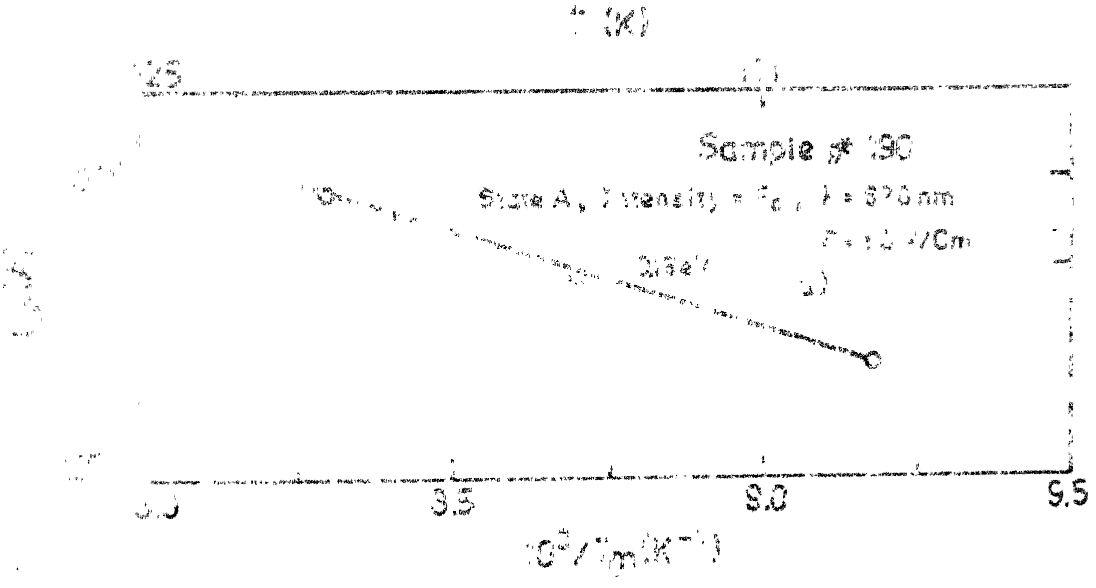

Fig.4.15(a) : Plot of lnI(T_m) vs $10^3/T_m$ for 3 different heating rates used for analysis of TSC peak at ≃ 120 K (see Fig. 3.14)

Fig.4.15(b) : Plot of lnI(T_m) vs $10^3/T_m$ for 4 different heating rates used for analysis of TSC peak at ≃ 300 K (see Fig. 4.10)

are expected to be those which are within 2 kT of 0.16 eV and 0.60 eV below E_c. Plots of $\frac{T_m^2}{\beta}$ vs $\frac{1}{T_m}$ (see Eq. 19) also yield straight lines which show the similar trap depths (0.12 eV and 0.60 eV for low and high temperature peaks respectively). It may be mentioned that these methods used for determination of trap depths are independent of the trapping kinetics.

(b) Calculation of TSC parameters

We have already shown in section 4.3.2 that

$$\exp\left\{\frac{E_t}{kT_m}\right\} = \frac{B}{\beta}\,\frac{kT_m^2}{E_t} \tag{19}$$

and

$$I(T_m) = A \exp\left\{-\frac{E_t}{kT_m} - 1\right\} \tag{20}$$

with A and B as in Table 4.1.
From the intercept at $1/T_m = o$, $A \approx 10^{-5}$ and $B \approx 10^5$ for the peak at $\approx$ 120 K and A 10^{-1} and $B \approx 10^9$ for the peak at $\approx$ 300 K. Using reasonable values[25] of $\mu \approx 1\ cm^2V^{-1}s^{-1}$ and $\tau \approx 5\times10^{-3}$ s, the various TSC parameters N_t, n_{to} and ν are calculated for the fast and slow retrapping and are listed in Table 4.2. ν_s obtained from Simmons' formula (Eq. 29) is also listed.

n_{to} can be obtained for fast as well as slow retrapping and is $\approx 10^{15}\ eV^{-1}\ cm^{-3}$ for all the cases.

Table 4.2 : TSC parameters of a-Si:H

Parameters	# 190		# 183	
	Peak $\gtrsim$ 120 K, $E_t \approx 0.16$ eV $A \gtrsim 10^{-5}$, $B \approx 10^{5}$		Peak $\gtrsim$ 300 K, $E_t \gtrsim 0.60$ eV $A \lesssim 10^{-1}$, $B \gtrsim 10^{9}$	
	Slow	Fast	Slow	Fast
n_{to}	10^{15} eV^{-1} cm^{-3}	10^{15} eV^{-1} cm^{-3}	10^{15} eV^{-1} cm^{-3}	10^{15} eV^{-1} cm^{-3}
N_t	X	10^{19} eV^{-1} cm^{-3}	X	10^{15} eV^{-1} cm^{-3}
ν	10^{5} s^{-1}	X	10^{9} s^{-1}	X
ν_s	10^{3} s^{-1}	X	10^{8} s^{-1}	X

X - Can not be calculated for that case.

However, it may be wrong by about 2-3 orders of magnitude due to uncertainties in constants A and B.

N_t can be obtained only for the fast retrapping case (Table 4.2). N_t for low temperature TSC peak (0.16 eV) is $\approx 10^{19}$ eV^{-1} cm^{-3} and is $\gtrsim 10^{15}$ eV^{-1} cm^{-3} for the TSC peak at $\gtrsim$ 300 K (0.60 eV). Although these values are comparable with the DOS obtained[26] near 0.16 eV ($\sim 10^{20}$ eV^{-1} cm^{-3}) and 0.60 eV ($\simeq 10^{16} - 10^{17}$ eV^{-1} cm^{-3}), they may not represent true DOS due to uncertainties involved in the constants A and B.

ν is obtained only for slow retrapping case. $\nu \gtrsim 10^5$ s^{-1} for low T TSC peak and is quite small as compared to value normally encountered in crystalline semiconductors[14] ($\approx 10^8 - 10^{15}$ s^{-1}). Therefore, the application of slow retrapping for analysing TSC peak $\gtrsim$ 120 K may not be justified and it appears that, at the low temperature, retrapping is quite significant in TSC in a-Si:H. ν obtained for 300 K TSC peak $\gtrsim 10^9$ s^{-1} and falls in the range of values observed in crystalline semiconductors. Thus, the application of slow retrapping for analysing 300 K TSC peak may be reasonable. It may be noted that ν_s obtained using Simmons' formula is comparable with ν obtained from single peak analysis within 1-2 order of magnitude.

4.5.3 Origin of the Structure in TSC in a-Si:H

Although a structure in TSC in the form of peaks in

a-Si:H have been reported by various authors[18-22], its origin is not yet fully understood. Fuhs and Milleville[18] have attributed it to the structure in DOS reported by Spear and LeComber.[26] The TSC peak $\approx$ 150 K is ascribed by them to a peak observed near 0.4 eV below E_c in DOS[26] and the peak at 250 K to the structure in DOS near $\approx$ 0.6 eV below E_c.[27] Chenevas-Paule and Dijon[19] also find two TSC peaks one near $\approx$ 130 K and the other at $\approx$ 260 K. They have attributed them to the presence of quasi discrete levels in the gap. Yamaguchi[20] has observed only one peak near $\approx$ 100 K and argued that the peak at $\approx$ 240 K is caused by adsorbates. Yamaguchi has attributed the peak at $\approx$ 100 K to the presence of a hole trap level near $\approx$ 0.2 eV above the valence band. Ibaraki and Fritzsche[21] observed a pronounced structure near $\approx$ 160 K and explain their results in terms of the multiple trapping theory.[28] They have concluded that the structure in TSC does not signify a structure in DOS. All authors have observed a strong decrease in TSC after light induced changes (S-W effect), however, no satisfactory explanation has been offered for this.

TSC in the present case shows two peaks; one at $\approx$ 120 K and the other at $\approx$ 300 K. The low temperature peak in our opinion is the same as the one reported by others.[18-21] The peak near $\approx$ 300 K (which has been observed by us) is probably present in all the other studies also, but might not have been seen due to a large dark current near this temperature.

The appearance of a peak near 300 K which corresponds to states near Fermi level is understandable. However, the origin of low T peak is not clear. It does not correspond directly[18] to the structure in DOS reported by Spear and Lecomber[26] since the energy of the localized states responsible for this peak is $\simeq 0.16$ eV below E_c, whereas the structure in DOS is $\simeq 0.4$ eV below E_c. The low T peak can also not be related to the presence of quasi discrete levels[19] because the step heating analysis (section 4.5.1) shows that there is a continuous distribution of traps. The possibility that the peak at low T arises from the contribution of surface states to TSC is ruled out by the wavelength dependence, as explained in section 4.4.2. In section 4.3.3, it has been pointed out that in a material which has a continuous distribution of states (e.g., a-Si:H), the observed TSC is expected to be a direct reflection of the initially occupied DOS in the excited state. This result although obtained by Simmons et al[23] in the limit of no retrapping, seems to hold qualitatively in the fast retrapping case also.[29] Thus if there is peak in the initially occupied DOS, corresponding TSC peak is expected eventhough there is no peak in DOS. We show below that the product of a fast rising DOS and an exponentially decaying occupation function $f_o(E)$ might be responsible for the low T peak. Neglecting the hole contribution, the electron occupancy function $f_o(E)$ above E_F is given by[30]

$$f_o(E) = \frac{Rn}{Rn+p}\left[1 + \exp(E-E_{fn})/kT\right]^{-1} \quad (32)$$

where R is ratio of electron to hole capture cross section ($R = S_n/S_p$) and E_{fn} is quasi Fermi level for electrons after excitation at low temperature. Fig. 4.16(a) shows $f_o(E)$ for $E_{fn} = 0.17$ eV, T = 30 K (curve I), $E_{fn} = 0.21$ eV, T = 80 K (curve II) and $E_{fn} = 0.48$ eV, T = 200 K curve (III). Taking the DOS g(E) (Fig. 4.16(b) full curve) which is identical to the Spear and LeComber plot,[26] between E_F and 0.2 eV and is slightly modified in the region closer to E_c, the corresponding density of occupied states $f_o(E)g(E)$ is obtained (Fig. 4.16(b), dashed lines I, II and III). It shows in addition to the peak at 0.4 eV corresponding to the peak in g(E), another peak near 0.16 eV. Since g(E) increases rapidly and $f_o(E)$ decays exponentially as a function of E in this region, the product $f_o(E)g(E)$ has a peak $\approx$ 0.16 eV although g(E) does not have a peak at this energy. Thus according to Eq. (28), a corresponding peak is expected in TSC.

It should be noted that the position of this peak should not depend upon E_{fn} (see Fig. 4.16(b) so long as $|E_c-E_{fn}| > 0.16$ eV. E_{fn} is changed by chaning the intensity of excitation and is found that this results in a lower TSC peak but its position is unchanged as expected (see Fig. 4.6). However, no TSC peak corresponding to

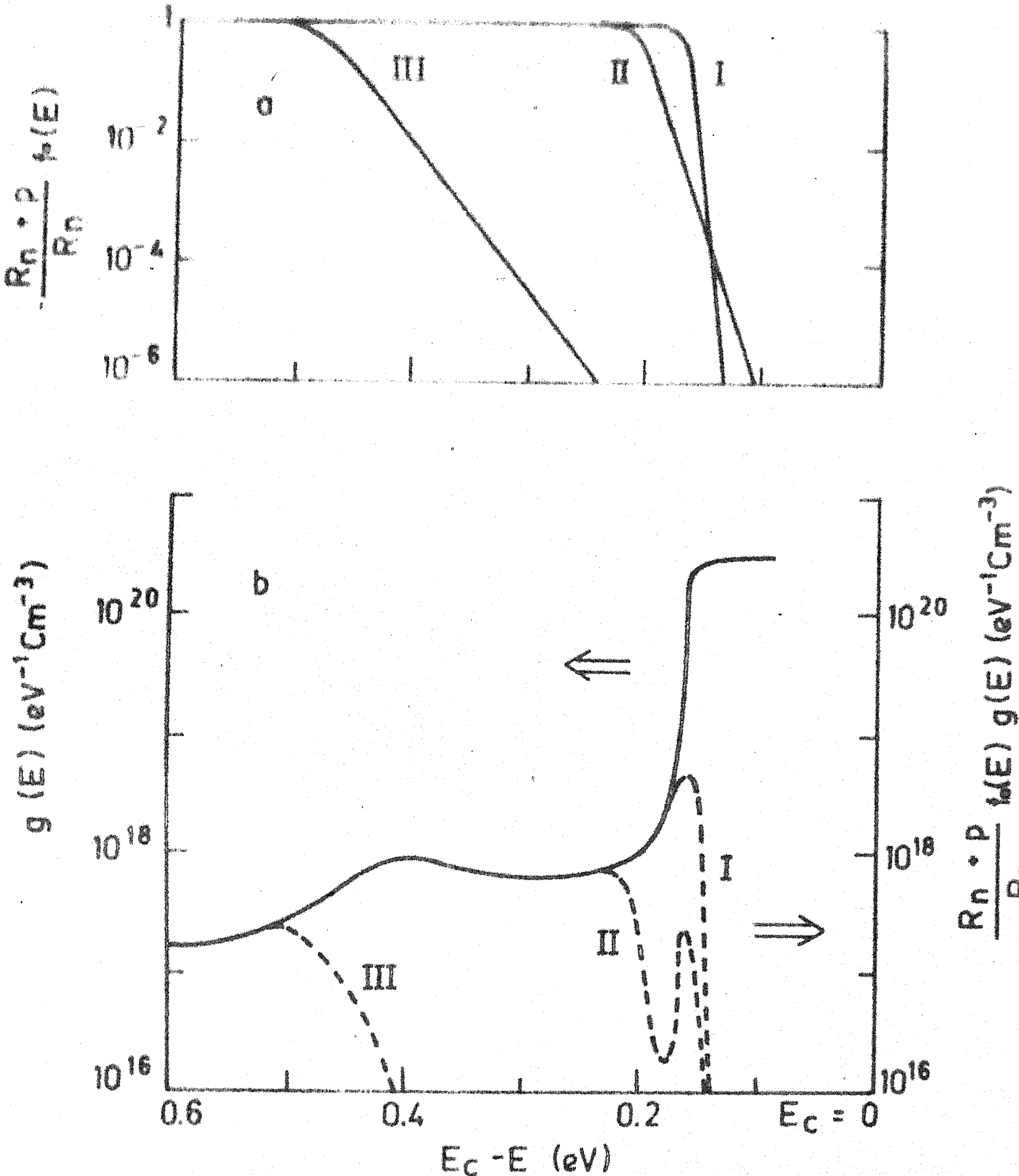

Fig.4.16(a) : The occupation function ($f_o(E)$) in a-Si:H(I)
(I) E_{fn} = 0.17 eV, T = 30 K (II) E_{fn} = 0.21 eV, T = 80 K
and (III) E_{fn} = 0.48 eV, T = 200 K

Fig.4.16(b) : Solid curve shows g(E) (scale on the lift) an[d] the dashed curves (I, II and III, scale on the right) show the density of occupied states $f_o(E)g(E)$, for different $f_e(E)$ as in Fig.4.16(a)

0.4 eV peak in g(E), is observed. Further, it is possible that S-W effect may decrease the sharpness in g(E) by creating more states in the gap. Since the low T peak might arise because of sharply rising DOS near band tails, the decrease in sharpness may give a smaller peak or no peak at all.

REFERENCES

1. Thermally Stimulated Relaxation in Solids; Topics in Applied Physics Series, ed. P. Braunlich 37 (Springer, Heidelberg 1979), see chapter 2 by P. Braunlich, P. Kelly and J.P. Fillard.

2. R.H. Bube, Phys. Rev. 83 (1951) 393

3. R.H. Bube, J. of Chem. Phys. 23 (1955) 181

4. G.A. Dussel and R.H. Bube, Phys. Rev. 155 (1967) 764

5. L.I. Grossweiner, J. Appl. Phys. 24 (1953) 1306

6. A review of different methods of analysis of data is by K.H. Nicholas and J. Woods, Brit. J. Appl. Phys. 15 (1964) 783

7. A.H. Booth, Can. J. Chem. 32 (1954) 214

8. R.R. Haering and E.N. Adams, Phys. Rev. 117 (1960) 451

9. C.F.J. Garlick and A.F. Gibson, Proc. Phys. Soc. 60 (1948) 574

10. P.J. Kelly and M.J. Laubitz, Can. J. Phys. 45 (1967) 311

11. Lushchik, Dokl. Akad. Na k, SSR 101 (1955) 641

12. R.A. Street and A.D. Yoffe, Thin Solid Films 11 (1972) 161

13. F.A. Fagen and H. Fritzsche, J. Non Cryst. Solids 2 (1970) 180

14. S.C. Agarwal and H. Fritzsche, Phys. Rev. B10 (1974) 4351

15. P. Muller, Phys. Stat. Solidi (a) 23 (1974) 165, 395

16. S.C. Agarwal, Phys. Rev. B10 (1974) 4340

17. H. Fritzsche and S. Chandra, Proc. of the Symposium on Thermal and Photostimulated Currents in Insulators ed. D.M. Smyth, Electrochem. Society (1976) p-105

18. W. Fuhs and H. Milleville, Phys. Stat. Solidi, (b) 98 (1980) K 29

19. A-Chenevas-Paule and J. Dijon, J. Phys. (Paris) 42 (1981) C4-605

20. M. Yamaguchi, J. Non Cryst. Solids 59,60 (1983) 425

21. N. Ibaraki and H. Fritzsche, Int. Conf. on Transport and Defects in Amorphous Semiconductors 22-24 March 1984, Bloomfield Hills MI.

22. D.S. Misra, A. Kumar and S.C. Agarwal (Accepted in Phil. Mag.)

23. J.G. Simmons, G.W. Taylor and M.C. Tam, Phys. Rev. 7 (1973) 3715

24. D. Adler, Solar Cells, 9 (1983) 133

25. C.R. Wronski and R.E. Daniel, Phys. Rev. 23 (1981) 794

26. W.E. Spear and P.G. LeComber, Phil. Mag. 33 (1976) 935

27. W.E. Spear, Proc. of Fifth Int. Conf. on Amorphous and Liquid Semiconductors (1973) Garmisch-Partenkircheh FDR ed. J. Stuke and W. Brenig, Taylor and Francis, London, 1974 p-1

28. M.A. Kastner and D. Monroe, Solar Energy Mater. 8 (1982) 41

29. A preliminary calculation including retrapping in Simmons formulation has been done by us and will be published shortly.

30. J.G. Simmons and G.W. Taylor, Phys. Rev. B4 (1971) 502

CHAPTER 5

PHOTOCONDUCTIVITY IN a-Si:H

5.1 INTRODUCTION

Photoconductivity measurements give the information about the recombination kinetics in semiconductors and have been considered an important tool for the characterization of thin films of a-Si:H. Steady state and transient photoconductivity (SPC and TPC) measurements have been done and give a lot of insight into a-Si:H[1,2]. The present investigation concentrates on SPC measurements and therefore, only these are discussed in details.

Spear et al[3] reported the spectral (λ), intensity (F) and temperature (T) dependence of photoconductivity (σ_{ph}) in a-Si:H. In the spectral dependence, the samples show maximum photoresponse for photon energies between 1.8 eV and 2.0 eV. σ_{ph} is found to be proportional[3] to F, i.e., $\sigma_{ph} \propto F^{\gamma}$ with γ (slope of log σ_{ph} vs log F curve) values ranging between 0.6 and 0.9 depending upon F and T . The dependence of σ_{ph} on T is divided in three regions[3] (I, 300 K $\leqslant$ T $\leqslant$ 450 K, II, 250 K $\leqslant$ T $\leqslant$ 300 K and III, T $<$ 250 K). In region I and II the activation energy ($\Delta E_{\sigma_{ph}}$) of σ_{ph} is found to be the same and in the region III it has a lower value. The transition from region II to III takes place around T 250 K. On the basis of these results Spear and LeComber[4] propose a model and conclude that the values of

$\Delta E_{\sigma_{ph}}$ can be explained by considering the recombination of electrons near E_A to the holes trapped near E_Y (Chapter 1, see Fig. 1.2). Further, it is argued that $\Delta E_{\sigma_{ph}}$ is lower at low T (region III) because the dominant conduction mechanism in this temperature range is hopping of electrons in localized states near E_A. On the other hand the results from the other laboratories are in agreement only qualitatively and the interpretations differ from those by Spear et al[5,6]. For instance, Wronski and Daniel[5] who observe that $\sigma_{ph} \propto F^{\gamma}$ report that $\Delta E_{\sigma_{ph}}$ in their samples is greater in region III as compared to region II. They explain their results by a model given by Rose[7] and find no evidence for a peak in DOS near E_x (i.e., 0.4 eV below E_c, see Fig. 1.2, Chapter 1). Fuhs et al[6] on the basis of the detailed measurements of SPC and TPC conclude that there is no evidence for a change from band conduction to hopping conduction in the temperature range (100 K $\lesssim$ T $\leqslant$ 500 K) investigated.

Vanier et al[8] and Persans and Fritzsche[9] have observed some new features in σ_{ph} of a-Si:H films. These are ascribed to what are known as the thermal and infrared quenching which have been observed in crystalline semiconductors also[10,11]. In thermal quenching, a broad peak is observed in $\sigma_{ph}(T)$ at low temperatures (T $\approx$ 125 K) and γ attains a value greater than unity in this range of T. In infrared quenching an enhancement or a reduction in σ_{ph} of

the sample, which is illuminated by a dc light with $h\nu > 1.5$ eV, is observed when a chopped beam of infrared photons $0.6 \text{ eV} \leqslant h\nu \leqslant 1.4$ eV is shone. Vanier et al[8] have found that changing the position of E_F towards one of the bandedges by doping with PH_3, B_2H_6, O_2, N_2 and air results in the elimination of these effects. This is in agreement with the conclusions of Persans also[9]. Thus, the quenching effects are observed only when the dark Fermi level (E_F) lies near midgap.

Recently Huang et al[12] have reported SPC and TPC measurements at different temperatures and have deduced the DOS in the upper half of the band gap from these data.

Moreover, all these authors have done measurements only down to the liquid nitrogen temperature (≈ 77 K). Recently, Hoheisel et al[13] have reported the measurements of σ_{ph} down to 4 K. They report that σ_{ph} becomes constant and γ approaches unity for $T < 50$ K.

In the present investigation, SPC measurements (section 5.2) are done for the intensities $10^{-2}F_o \leqslant F \leqslant 10^{0}F_o$ ($F_o \approx 10^{15}$ photons $cm^{-2}s^{-1}$) and temperatures $15 \text{ K} \leqslant T \leqslant 330$ K in the heat dried (A) as well as the light soaked (S-W effect, B) states. The results are reported in section 5.3.

In section 5.4 the interpretations of the results is discussed and the DOS distribution is calculated following Huang et al[12].

5.2 EXPERIMENTAL

Undoped samples of a-Si:H with nichrome electrodes in a coplanar configuration (see Chapter 2) are used. For the measurements of σ_{ph} at low temperatures, the samples are mounted on the cold finger of a closed cycle He refrigerator (see Fig. 4.1). The high temperature σ_{ph} measurements are done in the cryostat described in Chapter 2 (Fig. 2.6). σ_{ph} is measured for the band gap light ($\lambda \simeq 670$ nm) which is shone from an Oriel monochromator. The intensity of light is varied using neutral density filters. All the measurements are done in a vacuum $\sim 10^{-6}$ torr.

5.3 RESULTS

The samples exhibit ohmic characteristics in presence of light upto the electric field $\lesssim 10^{3}$ V/cm in states A and B for the temperatures ranging from 330 K to 15 K. The electrical parameters of the samples are shown in Table 2.4 (# 183, 186 and 190).

Variation of σ_{ph} with temperature for a-Si:H is shown in Fig. 5.1 in the states A (A1, A2 and A3 for # 190, 186 and 183, respectively) and B (B1, B2 and B3 for # 190, 186 and 183 respectively). σ_{ph} in states A and B, decreases monotonically with decreasing T, in agreement with others[3,5,6,13]. σ_{ph} for all the samples, irrespective of whether they are in state A or B, becomes constant below $T \approx 25$ K. In

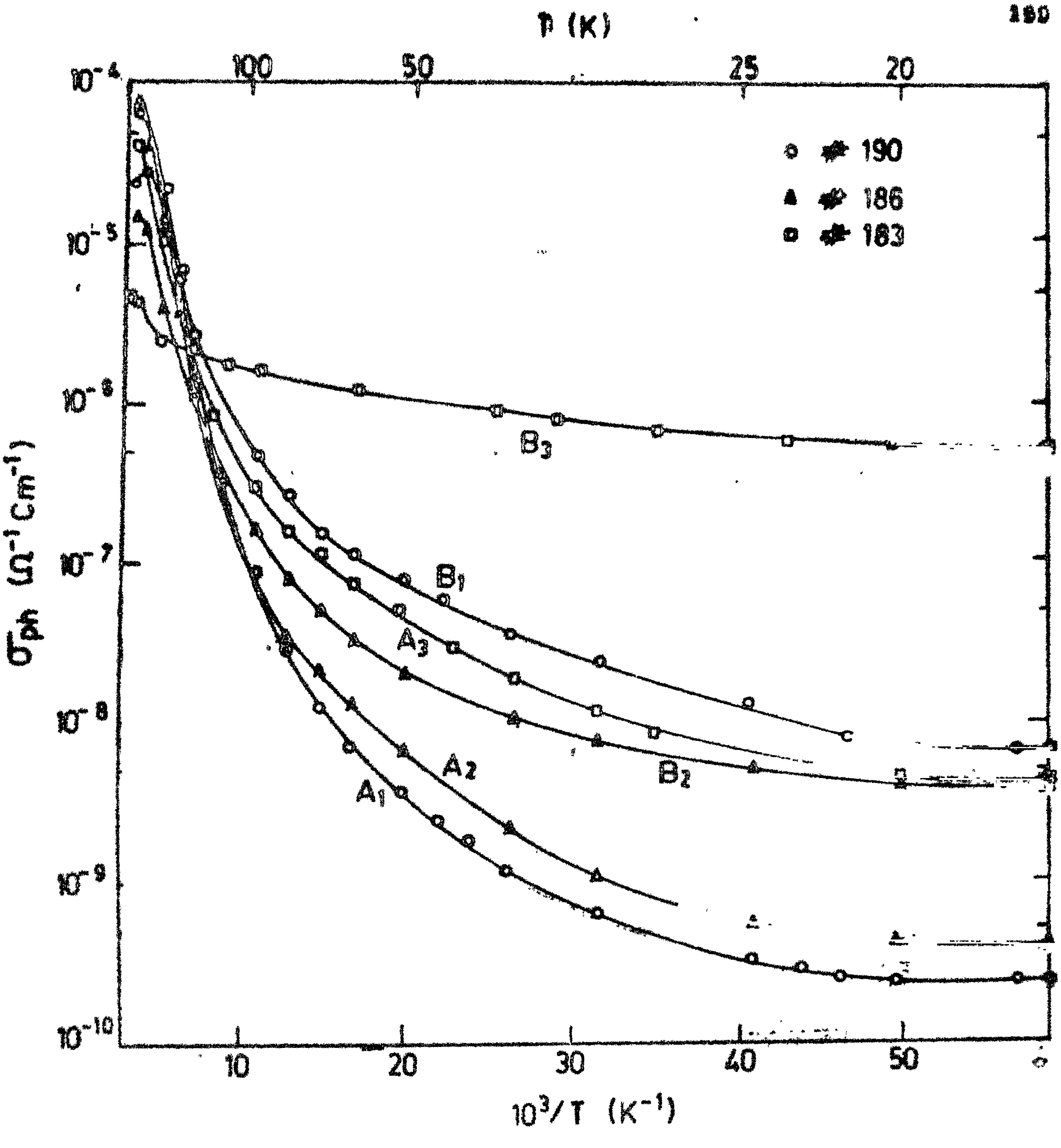

Fig.5.1 : Plots of ln σ_{ph} vs $10^3/T$ of 3 a-Si:H samples (# 190, # 186 and # 183) in heat dried (curves A_1 (# 190), A_2 (# 186) and A_3 (183)) and light soaked (curves B_1(# 190), B_2(# 186) and B_3(# 183)) states

contrast with Wronski and Daniel[5], and in agreement with Spear et al[3], $\Delta E\ \sigma_{ph}$ in our case is highest ($\simeq$ 0.12 eV) in temperature range II (250 K $\leqslant$ T $\leqslant$ 330 K) (Fig. 5.2) and then decreases continuously in state A. $\Delta E\ \sigma_{ph}$ and σ_{ph} in state B are found to be smaller for 250 K $\leqslant$ T $\leqslant$ 330 K. However, σ_{ph} in state B is greater than that in state A for all the samples below T $\sim$ 125 K. It may be mentioned that the thermal quenching effects[8,9] are not visible in the entire temperature range.

The intensity (F) dependence of a typical sample (#186) at different temperatures for intensities ranging from $10^{-2}F_o$ to F_o is shown in Fig. 5.3 and 5.4 for states A and B respectively. The temperature dependence of γ is shown in Fig. 5.5. γ is $\approx$ 0.72 and 0.80 for states A and B respectively near 300 K. It first decreases with a decrease in temperature then increases and becomes constant (0.85 for state A and 0.75 for state B) in the region (T 25 K) where σ_{ph} is independent of temperature. These results are in agreement with others.[12,13]

5.4 DISCUSSION

Our results of temperature and intensity dependence can be explained qualitatively by Spear and LeComber model[4] in a limited temperature range (150 K $\leqslant$ T $\leqslant$ 330 K). $\Delta E\ \sigma_{ph}$ in the region I (150 K $\leqslant$ T $\leqslant$ 330 K) is $\simeq$ 0.12 eV (see Fig. 5.6) which should be compared with that predicted by

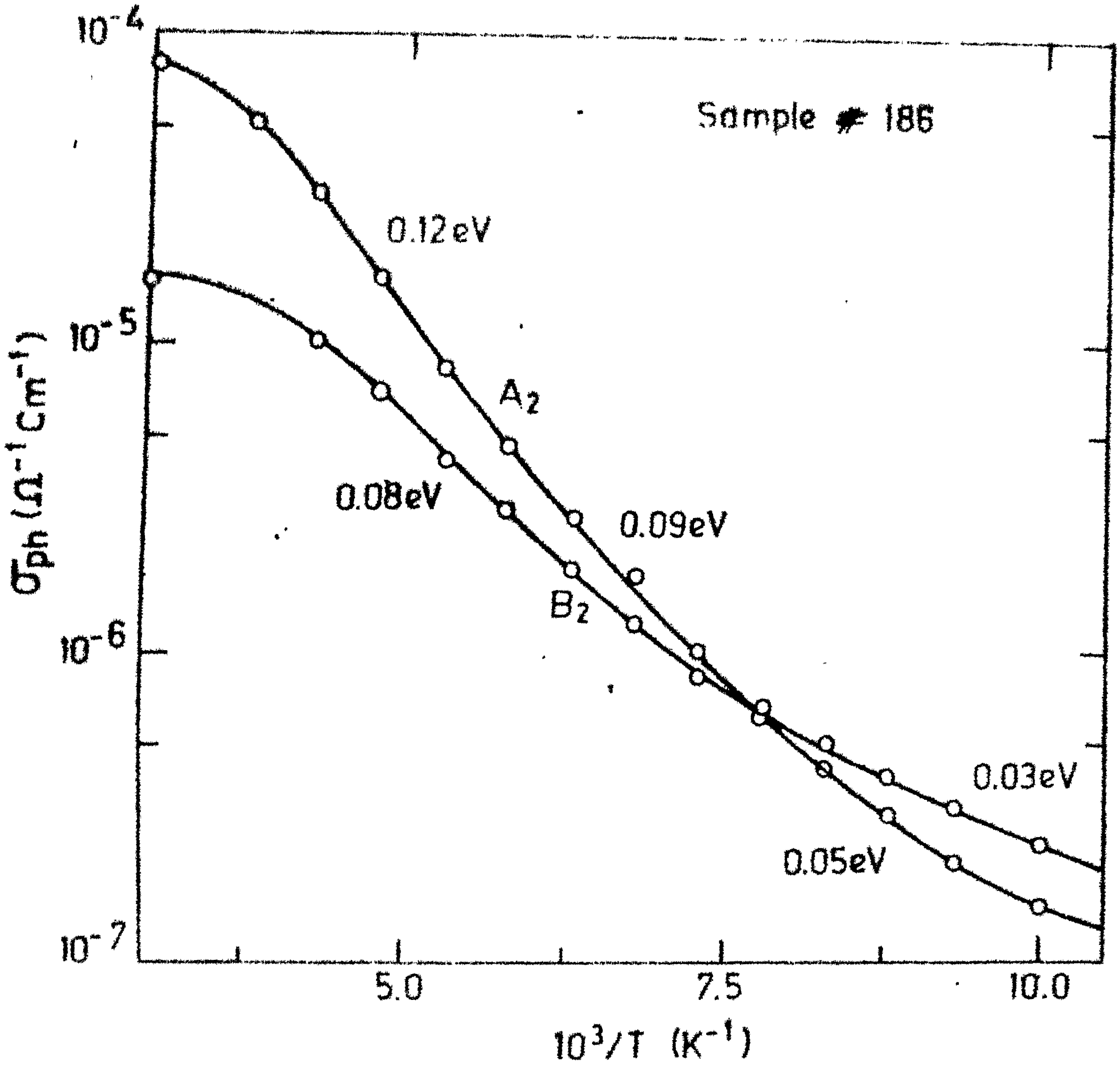

Fig.6.2 : Plots of ln σ_{ph} vs $10^3/T$ for sample # 186 in heat dried state (curve A_2) and in light soaked state (curve B_2). The slopes of straight lines fitted in different temperature ranges give activation energy of photoconductivity ($\Delta E_{\sigma_{ph}}$), as indicated

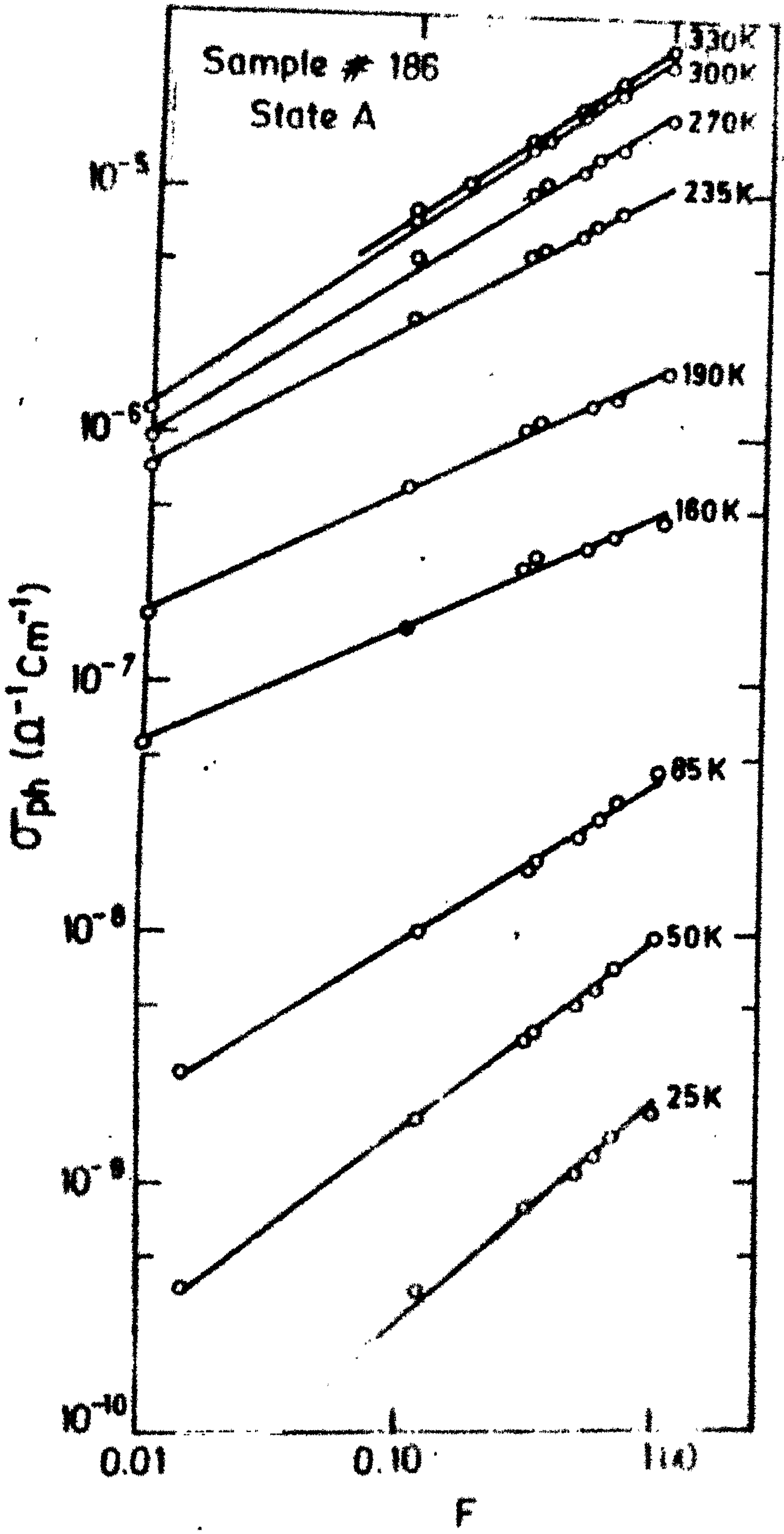

Fig. 4.3 : Intensity (F) dependence of σ_{ph} in a-Si:H (# 186) in heat dried state (A) at different temperatures, as indicated

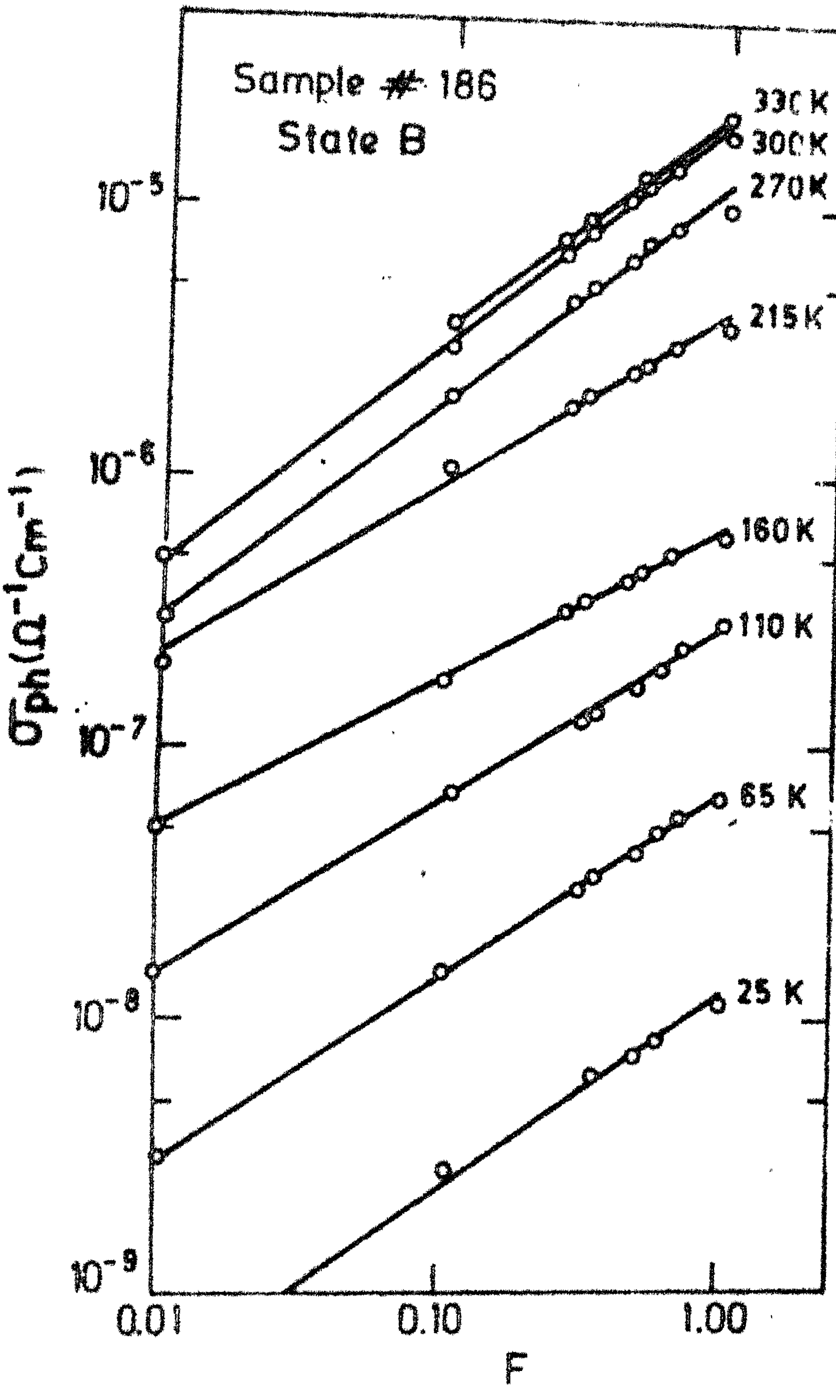

Fig.5.4 : Intensity (F) dependence of σ_{ph} in a-Si:H (# 186) in light soaked state (B) at different temperatures, as indicated

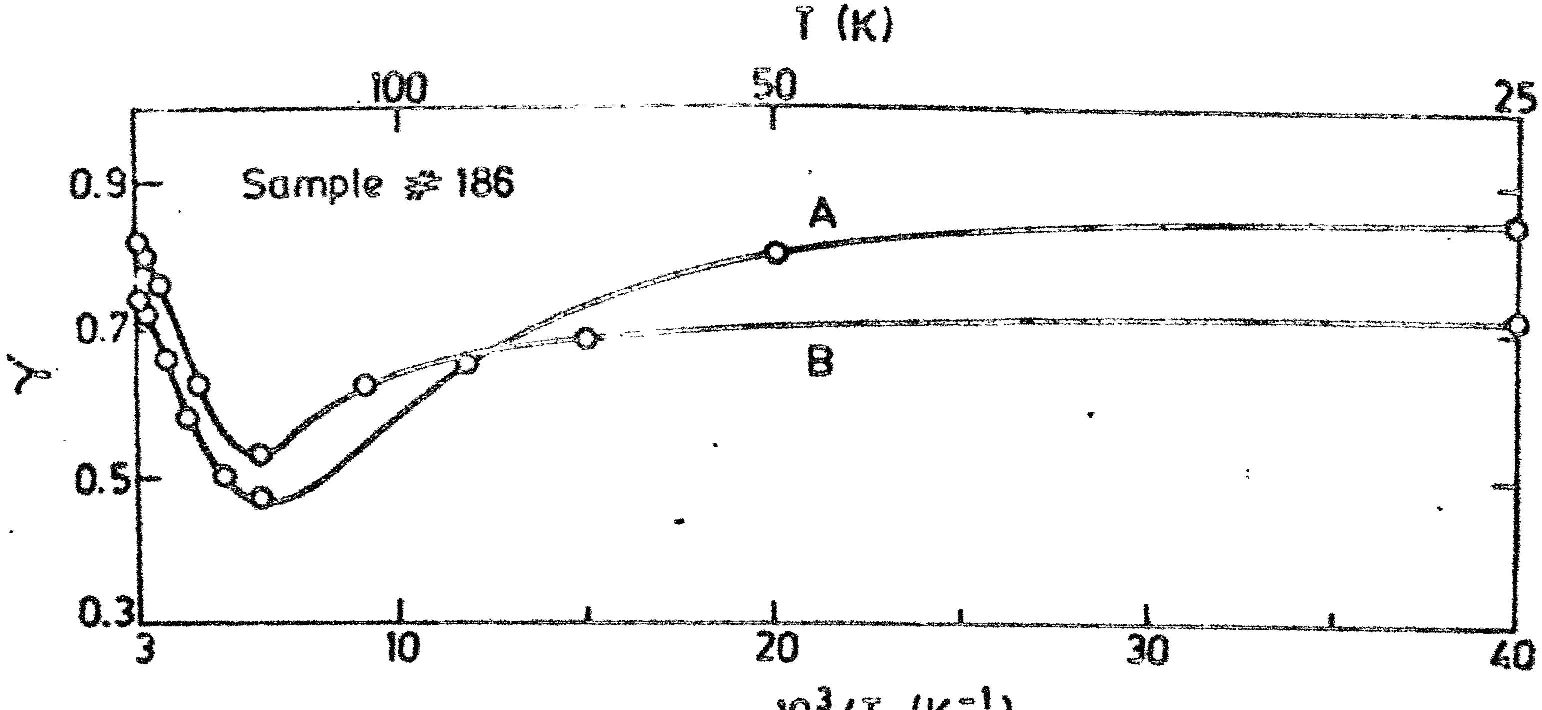

Fig.5.5 : Temperature dependence of γ (slope of ln σ_{ph} vs F curves in Fig.5.4) in a-Si:H (#186) in heat dried state (A) and in light soaked state (B)

the model ($\approx$ 0.20 eV). Similarly the model predicts a square root intensity dependence (i.e., $\gamma = 0.50$) while, we find that $\gamma = 0.60$ in temperature range II. Paul and Anderson[2] have, however, argued that the recombination path suggested by Spear and LeComber[4] need not be an unique explanation. Other paths (i.e., E_c to E_y, E_A to E_F see Fig. 1.2) may match the experimentally observed values of $\Delta E\,\sigma_{ph}$ and γ, as well.

However, the results of σ_{ph} at low temperatures are more difficult to explain. Spear and LeComber[4] suggest that for all T < 250 K, σ_{ph} is controlled by hopping of electrons near E_A and therefore $\Delta E\,\sigma_{ph}$ is $\approx$ 0.08 eV. Although in the temperature range 150 K $\leqslant$ T $\leqslant$ 250 K, $\Delta E\,\sigma_{ph}$ in the present case is $\approx$ 0.08 eV (see Fig. 5.2), for T < 150 K it is much smaller and then at T $\simeq$ 25 K it becomes almost zero.

Hoheisel et al[13] have explained their σ_{ph} results at low temperatures (4 K $\leqslant$ T $\leqslant$ 500 K) by suggesting that below 30 K, σ_{ph} arises from the thermalization of photo-excited carriers in the states above the mobility edges before they are localized in tail states and therefore, the thermalization time (τ_{th}) rather than the trapping or recombination time determines the value of σ_{ph}. Since τ_{th} is independent of the carrier density, σ_{ph} becomes constant below 30 K and γ approaches unity. Furthermore, τ_{th} does not depend upon the density of defects but is an

intrinsic property of the amorphous silicon network, being determined by the density of states near mobility edges. In the present case also, the value of γ is found to be approaching unity (see Fig. 5.5) at low temperatures (where σ_{ph} becomes constant) irrespective of whether the sample is in state A or B. Thus it seems likely that the thermalization of carriers is responsible for the observed behaviour of σ_{ph} at low temperatures.

The increase in σ_{ph} below $\approx$ 125 K in state B (S-W effect) shown in Figs. 5.1 and 5.2 may be related to the possibility that after S-W effect, the Fermi level has moved towards the midgap and is in a position so that the thermal quenching[8,9] effects start becoming visible. This argument is strengthened by the fact that the temperature ($\approx$ 125), where σ_{ph} in state B starts becoming higher than that in A (Fig. 5.2), is about the same where a broad peak due to thermal quenching in $\sigma_{ph}(T)$ is observed by others.[8,9] Alternatively, it may be that the S-W effect has created more states in the gap in such a way that the recombination paths, in this range of temperature, are different in states A and B. Another possibility may be that the thermalization time of carriers is changed in state B, since the light induced effects may increase the DOS near mobility edges (see also section 4.5.4). However, such an increase in DOS near mobility edges would decrease the τ_{th} and therefore, a decrease in σ_{ph}, but not an increase, is expected.

5.4.1 DOS Distribution From SPC Measurements

Even though we find that the Spear and Lecomber model[4] can qualitatively explain our results in a limited temperature range, it does not necessarily imply that the DOS distribution in our case has a structure in the form of peaks near E_x or E_y (Fig. 1.2). This argument is favoured when we find that in agreement with Huang et al[12] the intensity dependence of σ_{ph} at different temperatures can be fitted to the DOS distribution which is sum of two exponentials without any structure. The two exponentials are fitted in different regions of mobility gap, i.e., (i) near the dark Fermi level and (ii) near conduction band edge (E_c).

It may be noted that the exponential DOS is only one of the several trap distributions for which $\sigma_{ph} \propto F^{\gamma}$. The others are gaussian, a sum of two exponentials etc.

If we take

$$g(E) = g_o \exp\left\{-\frac{(E_c-E)}{kT_o}\right\} \tag{1}$$

where T_o is related to γ as

$$\gamma = \frac{T_o}{T+T_o} \tag{2}$$

then γ determines the trap distribution in the vicinity of the quasi Fermi level for traps (E_{ft}). This is close to the quasi Fermi level for free electrons (E_{fn}) in a-Si:H[12].

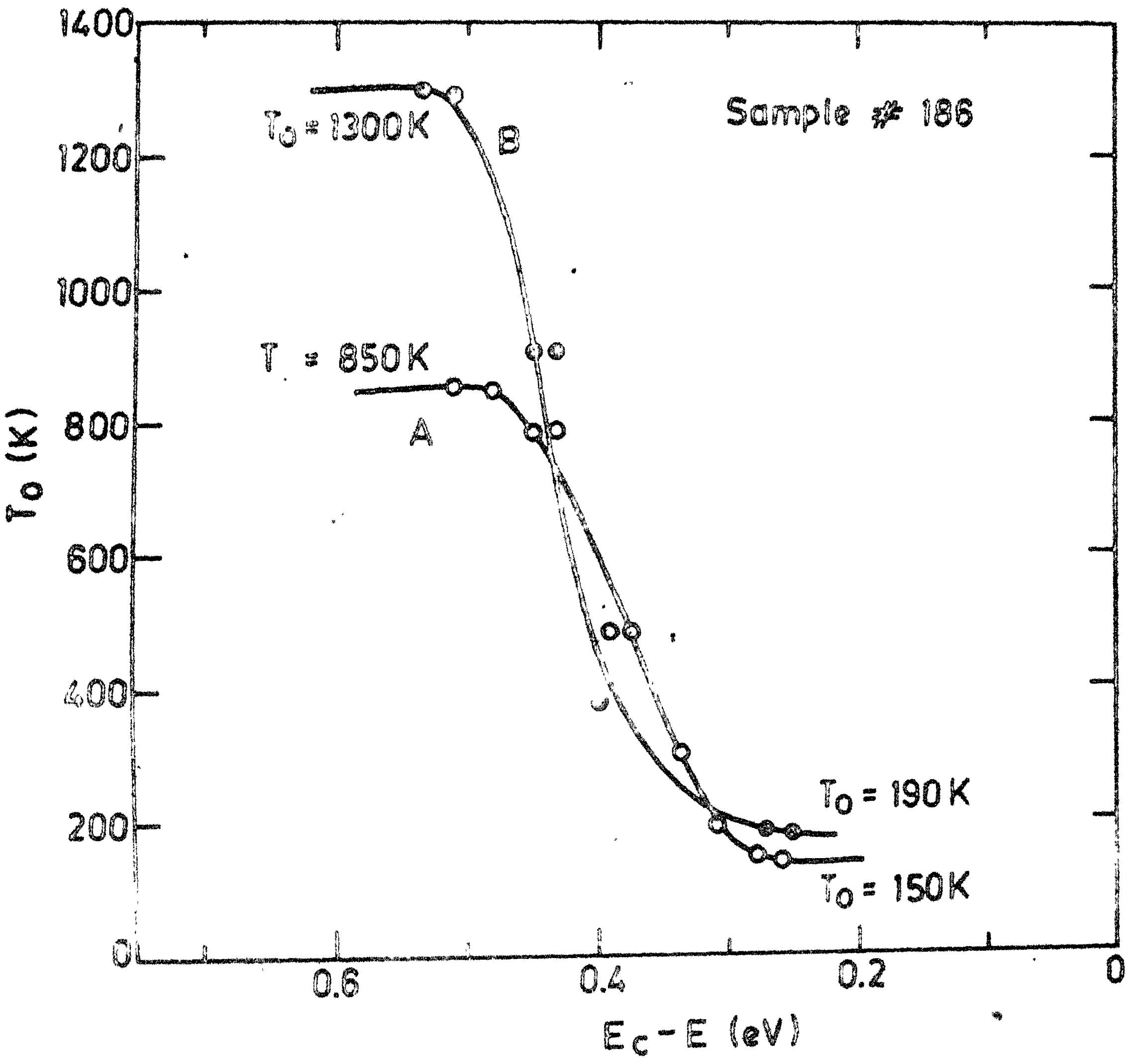

Fig.5.6 : Plots of T_0 vs E_c-E in a-Si:H (# 186) in heat dried (A) and in light soaked (B) states

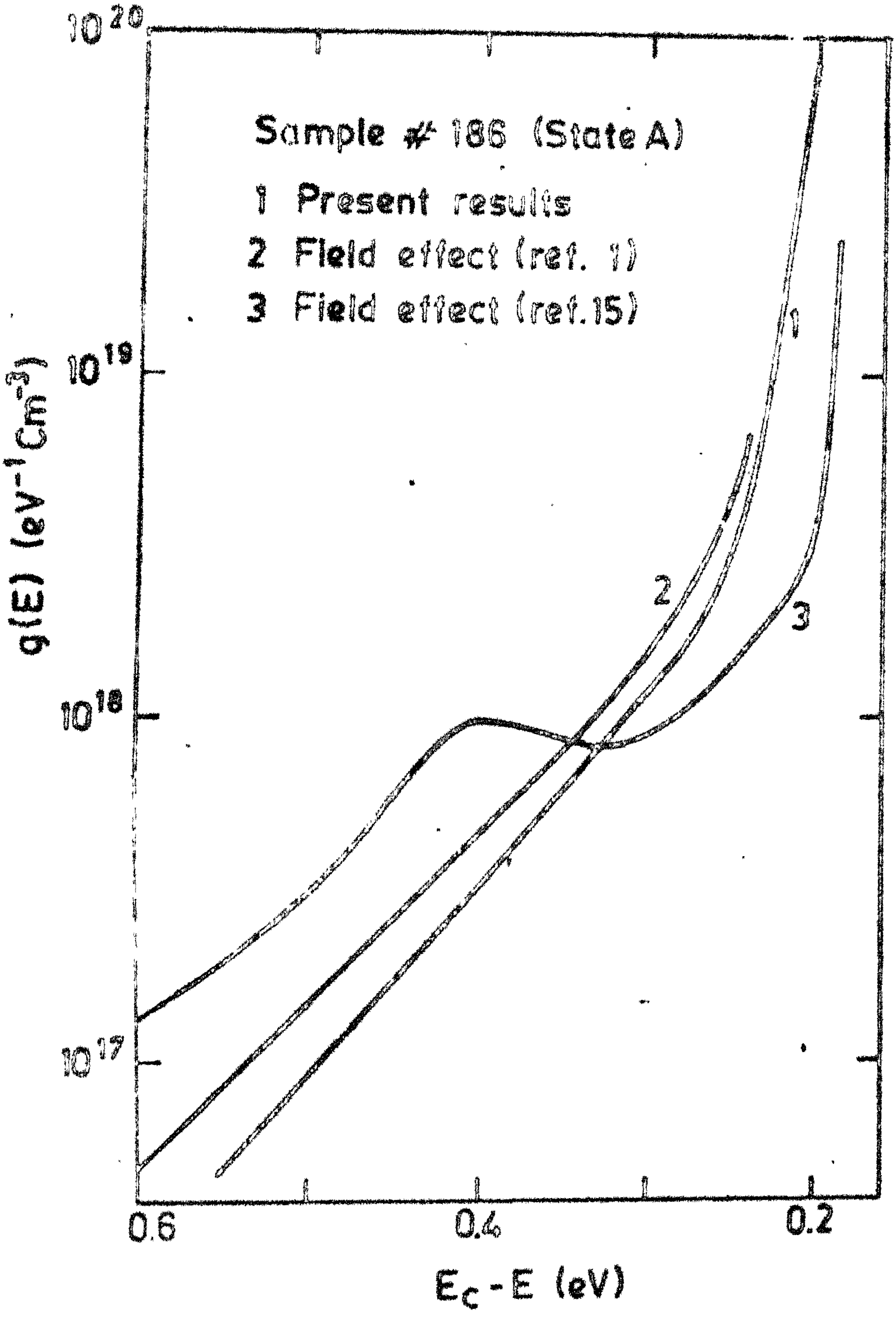

Fig.5.7 : DOS distribution obtained by fitting T_0 vs E_c-E data (Fig.5.6) to exponential distribution of states in different portions of mobility gap (i) near dark Fermi level (E_F) (ii) near conduction band edge (E_c); curves 2 and 3 are results of field effect experiment reported by others, as indicated

(Fig. 5.6), g_o (Eq. 2) is obtained by using DOS at $E_F \simeq 5 \times 10^{16}$ eV^{-1} cm^{-3} (Chapter 3).

5.5 SUMMARY AND CONCLUSIONS

We thus conclude that in our case the dependence of σ_{ph} on F and T appears to be governed by two processes in two different temperature ranges (i) recombination model suggested by Spear and Lecomber[4] for higher T (T > 150 K) (ii) thermalization of carriers suggested by Hoheisel et al[13] for low T (T < 150 K). From the temperature dependence of γ (Fig. 5.5) the transition from recombination limited process to thermalization process seems to be taking place around $T \simeq 130$ K where γ starts increasing with temperature.

We have suggested two possible explanations for a larger σ_{ph} for T < 125 K in state B as compared to that in state A. These are (i) shift of Fermi level towards mid gap after S-W effect (ii) a change in recombination path due to S-W effect in this range of T. However, at present it is not possible to point out specificly which of these is responsible for the observed behaviour.

Finally, the DOS distribution has been fitted to an exponential distribution. For comparison we have also plotted the DOS distribution obtained using field effect technique by others[1,15] (Fig. 5.7). However, it has been noted that a gaussian and a sum of exponentials[14] also predict that $\sigma_{ph} \propto F^{\gamma}$. Thus a distinction in the type of distribution on the basis of intensity and temperature dependence of σ_{ph} may not be possible. It can, however,

be said that the assumption of presence of a structure in the form of a peak near 0.4 eV below E_c (see Fig. 1.2) does not appear to be necessary for fitting the data.

REFERENCES

1. See for a review, H. Fritzsche, Solar Energy Mater., 3 (1980) 447

2. See also, W. Paul and D.A. Anderson, Solar Energy Mater. 5 (1981) 229

3. W.E. Spear, R.J. Loveland and A. Al-Sharbaty, J. Non Cryst. Solids 15 (1974) 410

4. Photoconductivity and Related Phenomenon, eds. J. Mort and D.M. Pai (Elsevier, New York 1976), see Spear and LeComber Chapter-5

5. C.R. Wronski and R.E. Daniel, Phys. Rev. 23 (1981) 794

6. W. Fuhs, M. Milleville and J. Stuke, Phys. Stat. Solidi (b) 89 (1978) 495

7. Concepts in Photoconductivity and Allied Problems, A. Rose (Kreiger, New York 1978)

8. P.E. Vanier, A.E. Delahoy and R.W. Griffith, J. Appl. Phys. 52 (1981) 5235

9. P. Persans and H. Fritzsche, J. Phys. (Paris) 42 (1981) C4-597, P. Persans, Solid State Comm. 36 (1980) 851, Phil. Mag. 46 (1982) 435

10. R.H. Bube, J. Phys. Chem. Sol. 1 (1957) 234

11. R. Newman, H.H. Woodbury and W.W. Tyler, Phys. Rev. 102 (1956) 613

12. C.Y. Huang, S. Guha and S.J. Hudgens, Phys. Rev. B 27 (1983) 7460

13. M. Hoheisel, R. Carius and W. Fuhs, J. Non Cryst. Solids, 59,60 (1983) 457

14. E. Bhattacharya and K.L. Narasimhan, (Preprint)

15. W.E. Spear and P.G. Lecomber, Phil. Mag. 33 (1976) 935

CHAPTER 6

SUMMARY AND CONCLUSIONS

A dc glow discharge system has been designed and fabricated. a-Si:H samples prepared by the glow discharge of SiH_4 mixed with Ar at $T_s \approx 580$ K are found to be amorphous in nature and contain hydrogen mostly as monohydride. The samples show $\sigma_{dc}(300\ K) \approx 5\times10^{-8}\ \Omega^{-1}cm^{-1}$ with $\Delta E_{\sigma} \approx 0.6$ eV and $\sigma_0 \approx 10^3\ \Omega^{-1}\ cm^{-1}$ (see Table 2.5). The optical gap is 1.7 - 1.9 eV and $\sigma_{ph}(300\ K) \approx 1\text{-}5\times10^{-4}\Omega^{-1}cm^{-1}$. The light induced changes in dark conductivity (S-W effect) in our samples are smaller than those reported by others in samples prepared using SiH_4+Ar mixture.[1] Guha et al who prepare their samples using SiH_4+H_2 mixture also find a small S-W effect which is about the same in magnitude as observed by us. Thus, it appears that the gas composition does not play an important role in determining the magnitude of the light induced changes. The electrical, optical and structural characterizations show that the a-Si:H films prepared in our glow discharge system are of the quality which compares favourably with those reported by other laboratories.

The density of states (DOS) obtained by SCLC, C(V), C(ω) and ICTS measurements on well characterized a-Si:H/Pd Schottky diodes are shown in Table 3.1 (for the characterization of these diodes see Table 2.6 Chapter 2). Clearly, no

serious discrepancy exists between the DOS obtained by the different methods on various diodes and we conclude that the DOS near Fermi level in our sample lies between 10^{16}-10^{17} eV^{-1} cm^{-3}. In view of the limitations and assumptions involved in obtaining the DOS by each of the technique, this agreement seems a bit suprising. In this context following comments may be relevant.

As argued by other authors, most of the steady state measurements are affected by the presence of surface/interface states, the only notable exception being the method of SCLC.[3] Further, it has been argued that the transient measurements, e.g., DLTS, TSCAP (Thermally Stimulated Capacitance), ICTS etc. are not influenced by the properties of surface/interface.[4] Thus it is generally felt that the DOS obtained by the SCLC and transient measurements give the true bulk DOS. Let us examine this a bit more closely.

SCLC measurements have been performed on n^+-i-n^+ structures,[3,5,6] as well as Schottky diodes[7] and can also be done on pin diodes. We have used the Schottky diode since this allows us to compare the DOS measured by SCLC method with the other experiments which can not be done on n^+-i-n^+ structures. denBoer et al[8] have argued that n^+-i-n^+ structures are preferable, since in this case the n^+ contact is injecting for electrons and simultaneously blocking for holes. Thus in the case of n^+-i-n^+ sandwiches, the contributions to SCLC come only from the electrons, whereas in Schottky barriers both electrons and holes can contribute to SCLC.

Although, stricity speaking, the contribution of holes to SCLC should also be considered while analysing the data obtained on Schottky diode, this may not cause much error in intrinsic a-Si:H, where the holes are minority carriers. But, a problem which is common to all the structures is that the SCLC data is analysed under a drift approximation which needs justification.[9] The drift approximation neglects any diffusion wings which may be established near the contacts, where the currents due to drift and diffusion cancel each other. The establishment of such wings will make the effective thickness of the sample smaller than the one used for actual calculation. This will affect the results most in the case of thin samples. Although the use of drift approximation is justified by observation of scaling rule.[3] $I/d = f(V/d^2)$, where d is the thickness and V is voltage, a complete SCLC model involving drift and diffusion will be more desirable.

Finally, the analysis ignores the heterogeneities in the material in neglecting the spatial variation of the DOS. This is true for all the other experiments as well and in our opinion, may be the most serious source of error in the DOS calculated from SCLC, because in this measurements the whole thickness of the sample is probed. The heterogeneities may also result in non uniform distribution of applied electric field.

In the experiments reported here nichrome has been used as the material for the back contact, which does not always yield an ohmic contact. Although, care has been taken to use only those samples which have an ohmic contact at the back, whether it is truley ohmic may be open to question. Thus, it appears that the experiments performed under reverse bias might be preferred, which makes the back contact barrier, if any, inoperative, since it is forward biased in this configuration. However, the analysis of the capacitance data, described in Chapter 3 (section 3.4), is based on the assumption that the Fermi level remains flat throughout the depletion region, even in the presence of a reverse bias. This assumption is not likely to hold. But, Cohen and Lang[10] have done the analysis for a case in which the Fermi level is assumed flat only in the tail of the space charge region and then remains at the middle of the gap and follows the edge of the conduction band upto the surface. The results obtained by them are not much different from those obtained by assuming Fermi level flat throughout the depletion region. Thus, it appears that the assumption of a flat Fermi level does not lead to much error in the DOS. Moreover, the results obtained by C-T measurements, which are done in reverse bias configuration, are same as those obtained by C-ω measurements, which are done at zero bias. Thus, it seems that if there is a barrier at the back it may not be effective.

Apart from this, the steady state capacitance measurements are influenced by the surface conditions. This may be quite serious, since Pd, which makes the Schottky barrier, is known to form a silicide near the surface.[11] However, in the present case the silicide formation appears to be small (section 2. 9). Further, the analysis of the temperature dependence of the capacitance, C(T) data, assumes that the various parameters of the Schottky barriers, e.g., barrier height etc. do not depend on temperature.

On the other hand, the isothermal transient capacitance (ICTS) measurements Chapter 3, (section 3.5) are free from these objections. But, here, it is not possible to get the DOS close to Fermi level[12]. Also at other energies, in order to fix the energy scale (E_c-E) one needs to know the parameter ν (attempt to escape frequency). This is not known with any precision and its value has been chosen rather arbitrarily between 10^{13} - $5x10^{14}$ s^{-1} by various authors. From the TSC measurements (Chapter 4, section 4.4), it appears that ν can be lower by several orders of magnitude. An order of magnitude error in ν will shift the energy scale by as much as 2 kT. An additional uncertainty arises from the difficulty in fixing the position of Fermi level with respect to the conduction band edge. As discussed in Chapter 2 (section 2.8) we estimate it by measuring the slope of the ln σ_{dc} plotted as a function of 1/T and correcting the obtained slope for finite temperature using the

temperature dependence of the optical gap. There are two objections to this procedure. First, the temperature dependence of the optical gap need not reflect the temperature dependence of the position of Fermi level. Secondly, any temperature dependence in the prefactor (e.g. mobility) is being ignored, which will change the slope of the $\ln \sigma_{dc}$ vs $1/T$ plot, especially if the prefactor varies exponentially with $1/T$.

Finally, we compare the DOS obtained by these methods with those obtained by the other transient methods e.g. DLTS, TSCAP and TCUR (Transient current). The DLTS measurements in doped samples give a DOS which is an order or two in magnitude lower than those obtained by other measurements. In addition DLTS also gives a minimum in the DOS $\approx$ 0.45 eV below the conduction band, whereas the other methods do not show any such minimum in the undoped samples. One may wonder whether the uncertainty in fixing the energy scales, referred to above, is responsible for this disagreement. However, the values of ν used by Lang et al[4] for the analysis of their DLTS data is quite high (5×10^{14} s^{-1}), and it is unlikely that ν is higher than this value. A lower value of ν will push the minimum towards the conduction band, thus making the agreement with other data even worse.

Okushi et al[13] suggested that the difference between DLTS and SCLC results may be due to a positive correlation

energy, at the dangling bond level (i.e. near E_C-0.5 eV) which may cause an increase of the effective density of occupied states in SCLC measurements. Recently, however, Kocka et al[14] found that the spectral dependence of absorption coefficient, measured on a Schottky diode in forward bias, does not depend on the applied bias. Thus, they have concluded that the suggestion by Okushi et al[13] may not be true.

We note that the DLTS experiments have been done only on doped samples. This is because in the intrinsic samples the Fermi level is too close to the dark Fermi level and does not change much after excitation, thus making it difficult to make DLTS measurements in such samples.[4] We feel that doping changes the DOS in a-Si:H significantly. Recently, the transient current (TCUR) and transient capacitance measurements on a-Si:H doped with Phosphorus have been reported by Beichler et al[12] which show the same general behaviour of DOS, as that obtained by Lang et al[4] from the DLTS measurements. Glade et al[15] measured the frequency and temperature dependence of the space charge capacitance and found that the DOS curve agreed with that obtained for DLTS measurements, for lightly doped samples. They, however, note that for moderately doped samples with $|E_C-E_F| < 0.5$ eV, there is a strong statistical shift of E_F with temperature, and this might affect the results obtained by DLTS measurements. Thus it appears that

one may not be justified in comparing the results of DLTS on doped specimens with those obtained by the other methods on the undoped ones.

It may be worthwhile pointing out that the DOS obtained by Lang et al[4] on the undoped a-Si:H by C(T) measurements is also lower than that obtained by the others. It is in this context, one may ask the question whether the samples prepared in different laboratories are alike. The answer can be given only by doing the many measurements and the DOS obtained, on one and the same sample as in the present study.

Although the analysis of each experiment has its own assumptions, the DOS, obtained by us from different measurements, are quite in agreement with each other. This does not necessarily imply that these assumptions are wholly justified. It may be that the calculated DOS are not affected much by these assumptions when the DOS is of the order of 10^{16} - 10^{17} eV^{-1} cm^{-3} at Fermi level, as in our sample. It has recently been brought to our notice[16] that the differences in DOS obtained by some of these methods start differing more markedly for samples having DOS at Fermi level less than 10^{15} eV^{-1} cm^{-3}.

In order to obtain the DOS in a-Si:H away from E_F and to see whether the peaks in DOS reported by Spear and Lecomber can be observed by some other method, thermally

stimulated currents (TSC) have been measured. These show two peaks; one at $\approx$ 120 K and the other near $\approx$ 300 K. By doing heat rate analysis, it is found that they arise from the states near 0.16 eV, and 0.60 eV respectively. The step heating analysis shows that a-Si:H has a continuous distribution of traps without any evidence of discrete levels. The analysis of Simmons et al[17] for a continuous distribution of traps in the limit of no retrapping is used to explain the origin of the observed structure in TSC. Although, the analysis is for no retrapping, it is found by preliminary calculations that the general features of TSC will be preserved if retrapping is included in Simmons formulation. Simmons et al[17] point out that the TSC in case of a sample having continuous distribution of traps reflects the density of initially occupied states. In view of this, it is shown that the TSC peak near $\approx$ 120 K may arise from the product of a rapidly increasing DOS (g(E)) near band tails and exponentially decaying occupancy function (f(E)). Therefore, this peak does not necessarily correspond to a structure near $\approx$ 0.16 eV. It is suggested that a decrease in sharpness of g(E) near band tails due to light induced defects (S-W effect) may result in a lower TSC peak or no peak at all near $\approx$ 120 K.

While analysing TSC for a sample having a continuous distribution of traps (e.g., a-Si:H), Simmons et al[17] point out that it is those traps positioned within 2 kT of a

certain energy $E_{mn}(T)$ that contribute most significantly to the TSC at a given temperature T. This implies that each energy level in the gap with a halfwidth of $\approx$ 2 kT can be considered a single trap. Thus, using single trap level analysis the trap parameters associated with the observed TSC peaks have been calculated in the limits of fast and slow retrapping (see Table 4.2, Chapter 4) as a first approximation. The values of DOS obtained near 0.16 eV and 0.60 eV are somewhat smaller than those reported in the literature.[18] However, the uncertainties in DOS obtained from TSC data may be large because of the approximate nature of analysis and the large error involved in the determination of constants A and B (section 4.3.3, Chapter 4).

Further, no evidence for a TSC peak corresponding to the peak at 0.4 eV below E_c in g(E) (Fig. 1.2) is found. It should have appeared as a shoulder in TSC curve (Fig.4.16, Chapter 4). However, retrapping can possibly obligerate it. Retrapping seems to be quite significant in a-Si:H especially at low temperatures. In our opinion the unusually small values of the escape frequency (ν) (Table 4.2) obtained using slow retrapping analysis for the low temperature TSC peak is an indication for this. Furthermore, the shape of TSC peak depends on the initial excitation conditions (e.g., wavelength of excitation, intensity of excitation etc) which is also indicative of strong retrapping.[19] In addition the contribution from the surface states to TSC has also been

ignored. However, from the dependence of the low temperature TSC peak on the wavelength of excitation the contribution of the surface states to TSC appears to be small.

Finally, DOS distribution has been determined in the upper half of the band gap (from E_F to near E_c) by fitting the temperature (T) and intensity (F) dependence of σ_{ph} to exponential distributions of states in two different portions of mobility gap. However, it must be mentioned that a gaussian or a sum of exponential[20] also predict that $\sigma_{ph} \propto F^{\gamma}$. Thus the type of distribution (i.e., whether it is an exponential or a gaussian etc) can not be determined on the basis of dependence of σ_{ph} on F and T. This can, however, be concluded that the assumption of a peak at ≈ 0.4 eV below E_c (Fig. 1.2) is not necessary for fitting the data. It may also be stated that this analysis neglects the influence of surface states and heterogeneities.

Clearly, the most glaring approximations made in the analysis of all the experimental results in a-Si:H are the neglect of the effects of heterogeneities and the surface states. Further efforts are needed to develop a theory for a quantitative treatment of the effects of heterogeneities on the various properties of a-Si:H. Since the quantitative analysis for heterogeneities appears to be a difficult task, an alternative would be to try to improve the preparation techniques which give good quality homogeneous a-Si:H, with minimum or no heterogeneities. Similarly, there is a scope

and need for the characterization of the surface of a-Si:H, so that the effect of surface states in the analysis of various techniques can be taken into account. A correlation between the preparation conditions and the surface properties of a-Si:H samples would also be welcome.

Finally, the TSC measurements have been analysed qualitatively considering only one type of carriers and in the limit of no retrapping. For a more quantitative understanding, an analysis which takes retrapping into account is needed, which has not been worked out so far. Also, new experiments which can be analysed with less uncertainties should be designed and the results compared with the existing ones. We believe that such theoretical and experimental efforts will lead to a better understanding of the properties of a-Si:H.

REFERENCES

1. M. Tanielian, H. Fritzsche, C.C. Tsai and E. Symbalisty, Appl. Phys. Lett. 33 (1978) 353

2. S. Guha, K.L. Narasimhan and S.M. Pietruszko, J. Appl. Phys. 52 (1981) 859

3. K.D. Mackenzie, P.G. LeComber and W.E. Spear, Phil. Mag. 46 (1982) 377

4. D.V. Lang, J.D. Cohen and J.P. Harbison, Phys. Rev. B25 (1982) 5285

5. W. denBoer, J. Phys. (Paris) 42 (1981) C4-451

6. E. Bhattacharya, S. Guha, K.V. Krishna and D.R. Bapat, J. Appl. Phys. 53 (1982) 6285

7. S. Ashok, A. Lester and S.J. Fonash, IEEE Electron Dev. Lett. EDL-1 (1980) 200

8. W. denBoer, M.J. Geerts and M. Ondris, J. Non Cryst. Solids 59,60 (1983) 1183

9. H. Pfleiderer, W. Khruhler, M. Moller and R. Plattner, J. Non Cryst. Solids 59,60 (1983) 485

10. J.D. Cohen and D.V. Lang, Phys. Rev. B25 (1982) 5321

11. C.C. Tsai, M.J. Thompson and R.J. Nemanich, J. Phys. (Paris) 42 (1981) C4-1077

12. J.Beichler, H. Mell and K. Weber, J. Non Cryst. Solids 59,60 (1983) 257

13. H. Okushi, T. Takahama, Y. Tokumaru, S. Yamasaki, H. Oheda and K. Tanaka, Phys. Rev. B27 (1983) 5184

14. J. Kocka, M. Vanecek, Z. Kozisek, O. Stika and J. Beichler, J. Non Cryst. Solids 59,60 (1983) 293

15. A. Glade, W. Fuhs and H. Mell, J. Non Cryst. Solids 59,60 (1983) 269

16. W. Paul (Private communication)

17. J.G.Simmons, G.W.Taylor and M.C.Tam, Phys. Rev. 7 (1973) 3715

18. W.E. Spear and P.G. LeComber, Phil. Mag. 33 (1976) 935

19. C.F.J. Garlick and A.F. Gibson, Proc. Phys. Soc. 60(1948) 574

20. E. Bhattacharya and K.L. Narasimhan (Preprint)

PHY- 1984-D-MIS-DET